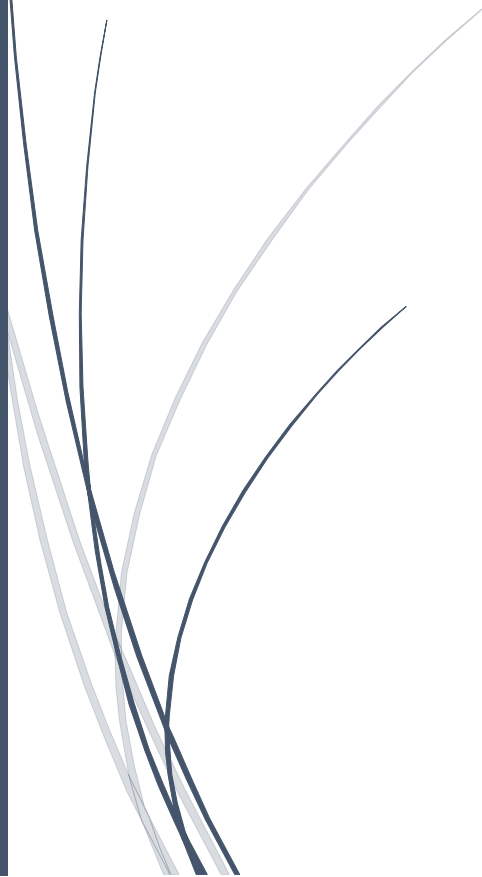




8/14/2021

A Novel Random Access Parallel Microscopy System for Bioimaging

Supervised by: Dr. Gil Bub



Kiamehr Rahemipour
MCGILL UNIVERSITY

Table of Contents

Acknowledgments	- 5 -
Abstract	- 6 -
Résumé	- 7 -
Summary	- 8 -
1. Introduction	- 12 -
1.1 Introduction: Cardiac Physiology	- 12 -
1.1.1 - Cellular biology - Action Potentials:.....	- 13 -
1.1.2 - Cellular biology - Ion Channels:	- 14 -
1.1.3 - Cellular biology - Calcium:.....	- 15 -
1.1.4 - Cellular biology - Genetics:	- 16 -
1.1.5 - Cellular biology - Conduction:.....	- 16 -
1.1.6 - Cellular biology - Effects of the nervous system:	- 17 -
1.1.7 - Cellular biology - Effects of physical load:	- 19 -
1.1.8 - Arrhythmias:	- 20 -
1.1.9 - Rarity of arrhythmias:	- 23 -
1.1.10 - Animal models:	- 24 -
1.1.11 - Induced Pluripotent Stem Cells(iPSC):.....	- 25 -
1.1.12 - 3D Models:.....	- 27 -
1.1.13 – Section Summary:	- 27 -
1.2 Introduction: Current State of Image Acquisition	- 28 -
1.2.1 – Current state of High-Throughput devices:.....	- 28 -
1.2.2 - optoDyCE:.....	- 29 -
1.2.3 - Optogenetics:.....	- 30 -
1.2.4 - Combining high throughput and super resolution:.....	- 31 -
1.2.5 - Total Internal Reflection Fluorescence (TIRF):.....	- 31 -
1.2.6 - NonLinear Optical (NLO) High-Throughput Microscopy:	- 32 -
1.2.7 - Two photon microscopy:.....	- 33 -
1.2.8 - Confocal microscopy:	- 34 -
1.2.9 - Polarized microscopy:	- 35 -
1.2.10 - Differential Interference contrast and Phase Contrast microscopy:	- 36 -
1.2.11 - Spectral imaging:	- 37 -
1.2.12 - Fluorescence microscopy:.....	- 38 -
1.2.13 - Light sheet scanning:.....	- 39 -
1.2.14 - FRET:.....	- 40 -
1.2.15 - Microfluidics, Optofluidic, and image Flow Cytometry (IFC):.....	- 41 -
1.2.16 - Lens free:.....	- 41 -
1.2.17 - Smartphone camera microscopy:	- 42 -
1.2.18 - 3D imaging:.....	- 42 -
1.2.19 – Section Summary:	- 43 -
1.3 Introduction: Image correction, storage, and processing	- 44 -
1.3.1 - Aberrations, and aberration corrections in microscopy:	- 44 -
1.3.2 - Data sampling:	- 45 -
1.3.3 - Pixel analysis:.....	- 46 -
1.3.4 - Noise:	- 46 -

1.3.5 - Saturation:	- 47 -
1.3.6 - Overall image analysis:	- 47 -
1.3.7 – Section summary:	- 48 -
2. System Design	- 50 -
2.1 - System Design: Camera.....	- 50 -
2.2 - System Design: Lenses	- 52 -
2.2.1 - Our setup:	- 52 -
2.2.2 - Fundamental basics:	- 54 -
2.2.3 – Multi-lens setup:	- 57 -
2.2.4 - Aberrations:	- 58 -
2.2.5 - Other measurements:	- 58 -
2.3 - System Design: Dome	- 62 -
2.4 - System Design: Illumination.....	- 63 -
2.5 - System Design: Skeleton/frame.....	- 68 -
2.5.1 - Design choice:	- 68 -
2.5.2 - 3D printed parts:	- 68 -
2.5.3 - Metal components:	- 72 -
2.6 – System Design: Adjustability and focus	- 73 -
2.7 - System Design: Electronics	- 75 -
2.7.1 - Arduino Uno:	- 75 -
2.7.2 - LEDs:	- 76 -
2.8 - System Design: Cooling system.....	- 76 -
2.9 - System Design: Fluorescence.....	- 80 -
2.10 – System Design: Vibration isolation	- 80 -
2.11 – System Design: Assembly steps.....	- 82 -
3. Proof-of-concept experimental design:	- 87 -
3.1 - Overall Design:	- 87 -
3.2 - Cell preparations:	- 88 -
3.3 - Imaging Conditions:	- 88 -
3.4 - Electronics setup:	- 88 -
3.5 - Data processing:	- 88 -
4. Results.....	- 92 -
4.1 - Results: Focusing and image acquisition.....	- 92 -
4.2 – Results: Effect of confluency and time on cardiac monolayers.....	- 96 -

5. Discussion.....	- 111 -
5.1 – Discussion: Experimental design, statistical analysis and reducing variabilities	- 111 -
5.1.1 - Introduction:	- 111 -
5.1.2 - Experimental design:.....	- 111 -
5.1.3 - Type I and type II error:	- 112 -
5.1.4 - Post experimental analysis:	- 113 -
5.1.5 - Our device: How do these concepts apply to RAP?.....	- 113 -
5.2 – Discussion: The effect of concentration and time	- 117 -
5.3 - Discussion: Other Designs and potentials	- 118 -
5.3.1 - Design and alternative versions:	- 118 -
5.3.2 - Future versions:	- 118 -
5.3.3 - Other potentials:	- 118 -
5.4 Limitations.....	- 120 -
5.4.1 - General limitations for high-throughput microscopy:.....	- 120 -
5.4.2 - RAP specific limitations:	- 121 -
6. The business side.....	- 123 -
6.1 - Gap in the market:	- 123 -
6.2 - Marketing:	- 123 -
6.3 - Manufacturing and production:	- 123 -
6.4 - Patent:.....	- 124 -
6.5 - Recommended price:.....	- 124 -
7. Conclusion.....	- 125 -
8. References	- 126 -

Acknowledgments

I would like to thank first and foremost my parents, Behzad Rahemipour and Roya Bahrehmand, who have been the most loving and supporting guiding stars in my life. I would like to thank my brother Radmehr Rahemipour, who is as an amazing of a brother to me as he is a friend. I would like to thank my friends who have been with me every step of the way, supporting me through the thick and thin. And last but certainly not least, I would like to extend my deepest appreciations to my supervisor Dr. Gil Bub who has been both an amazing mentor, role model and a friend, guiding me with unbreakable support every step of the way.

Abstract

We have developed a new solid-state High-Throughput (HTP) imaging device, designed to capture sequence of images (Videos) of multiple live biological samples simultaneously under physiological conditions (inside an incubator). And at a price of approximately \$25000 USD, it is orders of magnitude less expensive than many other commercially available HTP devices costing 100s of thousands of dollars. Commercial HTP systems generally require robotic motion to either move the camera or the sample. Alternatively, they would utilize a single sensor with a wide field of view to simultaneously capture many samples that are close to each other. Robotic components introduce a range of limitations associated with motion, and wide field microscopy results in relatively lower resolution. At the same time, these devices are usually very expensive. Our proposed device uses a novel architecture consisting of a parabolic mirror, custom 3D printed parts, optomechanical components, a camera, lens arrays, and a microcontroller-controlled LED array to image multiple samples of cells and/or small model organisms in tandem without many of the aforementioned limitations of a conventional high-throughput systems. Furthermore, a novel cooling and a novel vibration dampening system allow the device to be placed directly inside an incubator and monitor multiple samples as they incubate. Images can then be sent in real-time to a computer outside the incubator which can utilize the data in diverse applications, ranging from simple monitoring, to broadcasting live experiments on YouTube. The proposed imaging system will make HTP microscopy accessible to smaller labs while at the same time enabling all scientists, from big or small labs alike, to answer experimental questions that require high-speed imaging of many samples (large n) simultaneously, such as studying the effects of various compounds or innervations of cardiac cells. In our lab the device is validated by measuring conduction patterns in cardiac monolayers which display a wide range of dynamics rare and temporally sporadic events, which benefit from a large sample size.

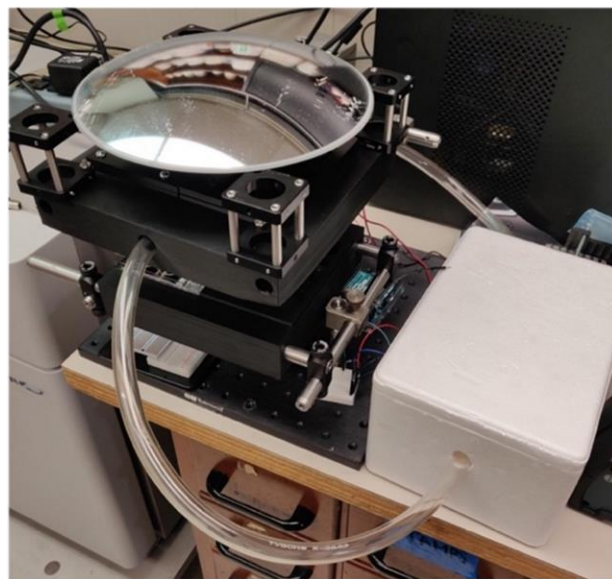


Figure 1 Overview of the overall RAP device sitting outside an incubator for demonstration purposes

Résumé

Nous avons développé un nouveau dispositif d'imagerie à haut débit (HTP) à l'état solide, conçu pour capter multiples séquences d'images (vidéos) simultanés de plusieurs échantillons biologiques vivants dans des conditions physiologiques (à l'intérieur d'une étuve). À un prix d'environ 25 000 \$ USD, il est beaucoup moins cher que de nombreux autres dispositifs HTP disponibles sur le marché, qui coûtent des centaines de milliers de dollars. Les systèmes HTP commerciaux nécessitent généralement un mouvement robotique pour manipuler la caméra ou l'échantillon. Alternativement, ils peuvent utiliser un seul capteur avec un champ visuel large pour enregistrer simultanément de nombreux échantillons proches les uns des autres. Les composants robotiques introduisent une variété de limitations associées au mouvement, et la microscopie à champ large donne une résolution relativement plus faible. En même temps, ces dispositifs sont généralement très coûteux. Le dispositif que nous proposons utilise une nouvelle architecture composée d'un miroir parabolique, de pièces personnalisées imprimées en 3D, de composants optomécaniques, d'une caméra, de mosaïques de lentilles et d'un réseau DEL contrôlé par un microcontrôleur, afin d'obtenir des images de plusieurs échantillons de cellules et/ou de petits organismes modèles en même temps, sans les nombreuses limitations susmentionnées des systèmes conventionnels à haut débit. De plus, un nouveau système de refroidissement et un nouveau système d'amortissement des vibrations permettent de placer le dispositif directement dans une étuve et de surveiller plusieurs échantillons pendant leur incubation. Les images peuvent ensuite être envoyées en temps réel à un ordinateur situé à l'extérieur de l'incubateur, qui peut utiliser les données dans diverses applications, partant de la simple surveillance jusqu'à la diffusion d'expériences en direct sur YouTube. Le système d'imagerie proposé rendra la microscopie HTP accessible aux laboratoires plus petits tout en permettant à tous les scientifiques, de laboratoires grands ou petits, de répondre à des questions expérimentales qui nécessitent l'enregistrement d'imagerie à grande vitesse de nombreux échantillons (grand n) simultanément. De tels questions peuvent inclure l'étude des effets de divers composés ou d'innervations des cellules cardiaques, par exemple. Dans notre laboratoire, le dispositif est validé en mesurant les schémas de conduction dans des monocouches cardiaques qui présentent un large éventail de phénomènes, des événements rares et temporellement sporadiques, qui bénéficient d'un échantillon à grande taille.

Summary

Increasing throughput for a given project refers to a decrease in processing time per unit entity. Stated in another way, increasing throughput refers to an increase in the data processed in a given amount of time. Throughput can be increased in three main ways: parallel processing, faster processing, and switching to a new workflow. These three ways can be explained with a simple example of a wheat farm. Parallel processing simply entails multiplying operation that are already underway. For example, a wheat farm run using manual labour that produces one ton of wheat a year can double the production by doubling the amount of land, workers, seeds, etc. In such a case, two farms are processed in parallel and provide twice the output. In the second approach, the processes underway are sped up. In our example of the wheat farm, we can increase the production of wheat by having workers work faster and for longer periods of time. The third way is coming up with new approaches and thinking beyond what is customary. Our farm for instance can use new technologies such as tractors, pesticides, genetic engineering, etc. to increase wheat production. It is important to mention that these three ways of increasing throughput are not mutually exclusive and can be employed in tandem. For example, the wheat farm can double the number of workers, land and supplies, have the employees work faster and for longer periods of time, and use new technologies, and in doing so improve wheat production more than any one method could have accomplished on its own. The incorporations of these new technologies and methods signify a new and improved workflow. The same concept applies in many different processes, including cell imaging. Most systems currently aim to increase throughput by the second aforementioned method, that is increasing the speed of an already existing workflow in one of three ways: by the movement of the sample to the plane of interest,³ ⁴ movement of the optical components to the plane of interest,^{5, 6} or use of widefield tracking^{7, 8}. In this project however we employ the third method and introduce a new way of thinking about cell imaging to increase throughput.

A good high throughput imaging system must have three main components: controlled light delivery and detection systems, suitable data storage, and methods for automation, which allow for increased throughput. Today most High Throughput (HTP) devices employ robotics for automation. Robotics can automate many aspects of microscopy from labeling the cells and other forms of sample preparation, to image analysis, data storage, data mining and modelling.⁹

Summary

Generally the aim of all these systems is to increase the amount of data collected per unit time while ensuring that the data is of high quality and consequently useful for making informed scientific decisions.¹⁰ These automated systems range in complexity. A simple high throughput system uses a motorized stage to move a small number of samples in two dimensions, whereas a more complicated system can move the light delivery and light detection systems as well as the samples. Even more complicated systems can move the sample from the incubator or have the incubator on the stage, image multiple plates and move the samples in multiple (x,y, and z) dimensions.¹¹

A fully automated system must consider many variables, such as sample climate, fluid delivery mechanisms, and sterilization,^{11, 12} in addition to the previously mentioned factors. Currently several advanced, yet very expensive, high-throughput systems are available with extensive and powerful optics. These devices primarily increase throughput by speeding up the workflow.¹⁰ Example of high-throughput systems include the Hamamatsu FDSS/ μ Cell system¹¹, Evotec's OPERA, Cellomics' CELLWORX,¹² and LaVision's TRIMSCOPE 64-spot multiplexer. These technologies are complex, sensitive to alignment issues, and have real restrictions on size, throughput and capacity of the overall set-up.¹² And while some systems are designed with the 96 well plate in mind and are HTP out of the box, others are more geared towards sample modification or image quality. As powerful as these systems are, they have two primary drawbacks: first is their high price, and second is the limitations and restrictions presented by the kinetic motion of robotic components, one of the most pertinent being the inability to increase throughput to the millisecond time scale. This limitation and others will be examined in depth throughout the thesis.

The case that I am presenting in brief is this: by using a novel solid state Newtonian optical setup, the presented device, named RAP for Random Access Parallel microscopy, can, at an affordable price and without the restrictions that are inherent in kinetic robotic movement, increase imaging throughput to make possible, near simultaneous in vitro and in-incubator recordings of multiple biological samples undergoing dynamic processes that are only milliseconds in duration, such as a cardiac contraction. This opens the door to many new physiological discoveries, including measurement of the arrhythmogenic properties of various compounds on cardiac monolayers which would have previously been

Summary

either impossible or extremely impractical. Two questions can then arise. Why do we want to measure arrhythmogenic properties of various compounds in cardiac monolayers? And if convinced of its importance, what advantaged does the RAP system provide that other imaging devices, including present high-throughput devices do not? To answer these questions, the next pages will discuss the physiology of cardiac rhythms and arrhythmias. Next, I will paint a macro picture of the microscopy world: what typical microscopy set-ups look like and what techniques are being used in the field; how the acquired images are collected and processed and highlight why they cannot be used to answer all HTP related questions; and in some cases, how these limitations have inspired the current system. The aim is to paint a picture of current major imaging technologies and where RAP fits in. I will then outline the design of RAP and follow with a proof-of-concept experiment that demonstrates the biological capabilities on cardiac monolayers imaged inside an incubator continue with the presentation and discussion of the results and the benefits, including statistical power, gained by using RAP, and end with a brief discussion of our venture into the business world followed by concluding remarks.

Chapter 1 – Introduction

To better appreciate the aim of this project, this chapter is dedicated to a macro scale overview of the mechanisms and phenomenon affecting cardiac physiology, rhythm, and arrhythmias. This chapter will then broadly describe the microscopy tools and techniques used in the life science, their advantages and disadvantages, and how they link together, so that we may gain a better insight as to how RAP integrates into that world. And as no optical scientific study can reach its full potential without post capture processing and analysis, this chapter will end with a broad overview of the most pertinent concepts related to such analysis.

1. Introduction

The delicate intricacies of the cardiac action potential, along with the many factors that affect its rhythm, make it susceptible to rare unpredictable arrhythmic patterns that may occur only over a short period of time, but can nonetheless have devastating consequences if they occur in an individual. The detection of these arrhythmic events is thus a crucial component to biological research.

Even though the detection of such events can be extremely valuable, the current microscopy systems used in the life sciences, although advanced, often lack the capabilities needed to capture rare cardiac events, or in cases where theoretically possible, they require such resources and prowess to capture the anomalies that it becomes very resource intensive and impractical, and for smaller labs, essentially impossible. The images captured using RAP however, combined with computational post-processing, enable such experiments and studies, even for labs with smaller budgets. These qualities are not necessarily exclusive to cardiac cells, other scenarios can present circumstances in which the detection of short duration events that occur may be beneficial. Here however, since our physiological proof-of-concept experiment is carried out using cardiac monolayers, we will focus on cardiac physiology.

The following pages will layout in further details the physiology of the cardiac action potential and rhythm, paint a broad view of the current world of microscopy, and touch on pertinent topics regarding the post processing of the recorded images and movies.

1.1 Introduction: Cardiac Physiology

Cardiovascular disease, ranging from genetic defects to physical strain, represents the most common cause of mortality in the developed world.¹³ Globally cardiovascular disease accounts for over 17.3 million death per year and in the US accounts for 1 in every 3 deaths.^{13, 14}

Arrhythmias and arrhythmogenic compounds are the focus of this chapter. To better understand arrhythmias, we must start with the most fundamental unit of rhythm in the cell, the cardiac action potential.

1.1 Introduction: Cardiac Physiology

1.1.1 - Cellular biology - Action Potentials: The beating of cardiac cells is primarily initiated by **Action Potentials (APs)** commencing from a group of specialized pacemaker cells that activate the heartbeat. More specifically, these APs start at the **SinoAtrial Node (SAN)**, and propagate through the heart via a cascade of ion flows. The cardiac action potential has many components, and many books exist to delve into the nuances. One example is a book titled *physiology of the heart* by Arnold Katz.¹⁵ In the next few paragraphs however, I will describe only the major components.

The direction of ion flow is determined by the electrochemical gradients of permeant ions.¹⁶ Within each AP, the flow of ions lead to four distinct phases. In each cell, once an AP is set in motion, there are 4 phases to the AP: phases 0, 1, 2, & 3. These phases refer to different

voltage differentials across a cell membrane and are dictated primarily by ion flow and gradients. At the beginning of phase 0 the cell is at the resting **Membrane Potential (MP)**.

The resting membrane potential is the voltage difference across a cell at the cell's resting state. The MP of a cardiomyocyte is biased

towards the potassium (K^+) equilibrium potential and is close to $-90mV$.¹⁶ During phase 0, the depolarizing stimulus from a neighboring cell changes the voltage across the cell membrane, leading to the opening of sodium (Na^{2+}) channels. The concentration of sodium is higher outside the cell than inside and consequently sodium flows in. The

inflow of Na^+ leads to the depolarization of the membrane and raises the voltage to about $+40mV$. During phase 1, the change in voltage seen in phase 0 results in the closing of the sodium channels and the subsequent opening of potassium channels, leading to a partial repolarization. In phase 2, the calcium (Ca^{2+}) channels open, and calcium enters the cell, along with sodium, but

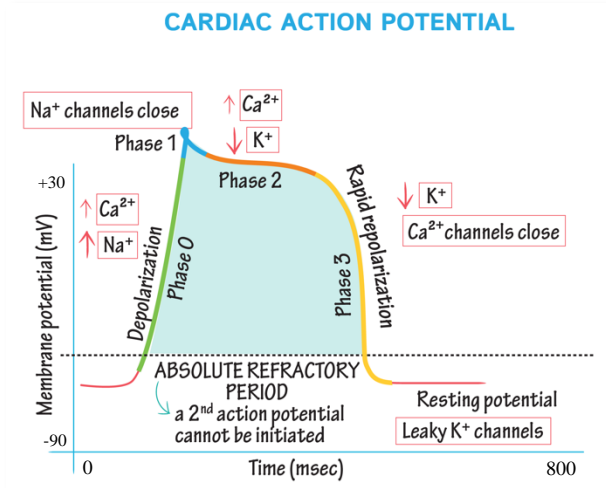


Figure 2 A typical Cardiac Action Potential curve showing the 4 phases. During phase 0, the depolarizing stimulus from a neighboring cell changes the voltage across the cell, leading to the opening of sodium channels (Na^{2+}). During phase 1, Na^{2+} channels close and K^+ channel open, leading to a partial repolarization. In phase 2, Ca^{2+} channels open. The inward movement of Ca^{2+} and Na^{2+} is mostly balanced by the outward movement of K^+ . During phase 3, Ca^{2+} deactivate and K^+ gradients repolarize the membrane.

Image modified from the following link:
<https://www.drawittoknowit.com/course/physiology/glossary/physiological-process/cardiac-muscle-action-potential>

1.1 Introduction: Cardiac Physiology

this is almost balanced by the outward movement of potassium, giving the AP its unique shape. In phase 3, the calcium channels eventually deactivate and the electrochemical gradient of potassium leads to a repolarization of the membrane.¹⁶ These phases are summarized in Figure 2. It is of note that specific regions can have varying action potential configuration and duration, such as the AP in atrium vs the ventricles.¹⁷

This variation can be caused by the acute responses of these myocytes to changes in rate, mutation, drug exposure, **Adenosine Triphosphate (ATP)** depletion, and stretch or muscarinic stimulation, and are generally due to changes in ion channel function that react to such stimuli.¹⁷ For example, the phase 1 notch and action potentials of Purkinje and midmyocardial cells are longer than those found in epicardium. These differences likely come from the variations in expression or function of ion channels and other proteins involved in cardiac ion currents. The exaggerations of these heterogeneities, or the diversity of various ion channels and proteins can also promote re-entrant excitation, which in turn is a common mechanism for many cardiac arrhythmias. The next section explores cardiac ion channels in greater depth.

1.1.2 - Cellular biology - Ion Channels: **Ion channels** are specialized membrane proteins that allow the flow of selected ions through a bilipid membrane. These channels play a vital key part in the generation of APs of cardiomyocytes.¹⁶ Examples of voltage gated channels include sodium, calcium and potassium channels.¹⁷ Ion channels usually have two main characteristics: **gating**, referring to their ability to open based on a specific stimuli or voltage; and **selectivity**, referring to their ability to only allow certain ions in once open.¹⁶ In cardiac cells, depolarizing inward currents are conducted by Na^{2+} and Ca^{2+} channels and outward currents by K^+ channels.¹⁶ Alterations in either the function or expression of these channels can alter with the normal behaviour of cardiac action potentials, leading to abnormal electrical activity and arrhythmias in the heart, which can consequently lead to cardiac death.¹⁶

The selectivity of ion channels come from their structural amino acid make up.¹⁷ This selectivity is mainly for **shape** and **voltage**. Variations in shape are due to stretch or volume changes which will be discussed later in the text, and variations in voltage naturally occur in the heart due to both internal and external factors, one of the most pertinent being the voltage changes of neighboring cells. Voltage sensitivity is a bigger influencer in dictating the cardiac action

1.1 Introduction: Cardiac Physiology

potential at the cellular level. Voltage channels primary operate by undergoing a conformational change once a voltage is applied.¹⁷ This conformational change can be localized to a specific domain of the protein. An example of a voltage sensor is the fourth membrane spanning segment of each six membrane spanning segment domain of a sodium channel that contains the positively charged amino acids arginine or lysine.¹⁷ These channels open upon sensing a propagating impulse (change in voltage) and result in a sodium influx and phase 0 of depolarization.¹⁷ Once open, two main mechanisms of inactivation, **N-type**(ball and chain model) and **C-type**, can be used to close the channel. In the ball and chain model a ball physically closes the pore and in C-type inactivation a rearrangement of residues in or near the pore takes place leading to the inability of ions to pass through.¹⁷ Generally, these ion properties are measured using the patch clamp technique, fluorescence microscopy and calcium or voltage sensitive dyes.¹⁶

1.1.3 - Cellular biology - Calcium: The next important factor in cardiac rhythm generation and propagation, is the role of calcium. The excitation-contraction coupling of the heart, the process connecting electrical excitation to the physical contraction of the heart is inseparably linked to calcium homeostasis.¹⁸ Calcium plays its crucial role in many signal transduction pathways to a large degree by a change in its concentration, varying between approximately 60-100 nmol/L to 600-1000 nmol/L.¹⁶ The major calcium currents in the heart are **L-type** and **T-type**, for long Lasting, and high Threshold, respectively. In brief, the role of calcium is two fold. First, it contributes inward current to sustain the long action potential in the heart. Second, calcium binds to **calmodulin**-the universal calcium sensor-¹⁸ and triggers the release of myofilament-activating calcium from the **sarcoplasmic reticulum (SR)** by binding to an SR surface protein called **RYanodine Receptor (RYR)**.¹⁷ The released calcium then triggers the release of even more calcium from the SR in a process known as calcium induced calcium release. This is primarily done through the activation of the **Ryanodine Receptor 2 (RYR2)** which acts nonlinearly and is a calcium receptor^{16, 19} and is generally controlled by precise calcium channels.¹⁹ In summary then, increases calcium leads to the release of even more calcium. However, this is until a certain point where a plateau is seen. The shape of this release is of sigmoid nature.¹⁹ And as previously mentioned, increased calcium concentration leads to myofilament activation which in turn lead to the physical movement of the cells and consequently the overall beating of the heart. Overall,

1.1 Introduction: Cardiac Physiology

due to its widespread function and role, calcium mis-regulations, such as spontaneously appearing calcium waves in cardiac myocytes, underlie a large range of cardiac arrhythmias.¹⁹

1.1.4 - Cellular biology - Genetics: Genetics is a significant factor in most forms of cardiovascular disease including both susceptibility to cardiac disease and its prognosis once afflicted. Most forms of cardiovascular disease stem from some form of genetic mutation.^{16, 20} As an example, two common genetic diseases are **Brugada Syndrome (BrS)** and **Catecholaminergic Polymorphic Ventricular Tachycardia (CPVT)**. BrS is an inherited disorder characterized by sudden cardiac death, occurring at a relatively young age and many of the sufferers are otherwise healthy.¹⁶ BrS can be caused by several different mutations, but ultimately they all lead to a general current imbalance in favor of repolarization.¹⁶ CPVT is characterized by abnormal intracellular Ca^{2+} handling and signaling from the SR. This is usually due to either a gain of function mutation in Ryanodine Receptor 2 (RYR2) gene or loss of function mutation in **calsequestrin**, which is an SR calcium buffering protein. This abnormal calcium release can cause delayed afterdepolarization which can in turn lead to triggered activity and ventricular tachyarrhythmias, a form of arrhythmia.¹⁶ These two examples illustrate a more general theme, that the genes that cause arrhythmias commonly interfere with the physiological mechanisms underlying action potential generation, conduction or the calcium cascade.

Clinically, gene targeting can be used for a more customized research and treatment. This technique enables the creation of cells and tissues that harbor cells with genetic variants specific to individual patients, which can be used to generate experimental models of these arrhythmias.²⁰ Yet, to this day, many questions remain. For example how can the same mutations have different effects on different arrhythmias in different people or even cause no symptoms at all.¹⁶ Such genetic studies, are another example of the type of questions that can benefit from the increased throughput and sample size afforded by RAP.

1.1.5 - Cellular biology - Conduction: Once an Action Potential is generated in one cell, the next criterion for a proper cardiac beat is the conduction of the AP throughout the **myocardium** (muscles of the heart). The myocardium is essentially a three-dimensional network of excitable cells that are all linked together, called a **syncytium**. The intricate mechanics of the cardiac rhythm depends on a precise conduction of the beating signal throughout this syncytium. **Gap**

1.1 Introduction: Cardiac Physiology

junctions, which in cardiac tissue are also a form of ion channels, are the fundamental carriers for impulses through the myocardium syncytium as well as exchange of signaling molecules between adjacent cells.²¹

Generally, a cardiomyocyte is a rod shaped cell that is connected to 11 other myocytes or fibroblasts, and the gap junctions are predominantly located at the intercalated discs at the end of these cells.²¹ The velocity and safety of the spread of signal is dependent on two factors, the active and passive properties of the individual elements as well as the connectivity of the network. As such, the time and voltage dependence of gap junctions is one of the primary features of signal conductance.²¹ Gap junctions ultimately are responsible for determining how much depolarizing current passes from one cell to the next, and thus are very important for the speed and safety of signal conduction.²¹ In homogeneous tissue, the uncoupling of gap junctions leads to a decrease in conduction velocity. In heterogeneous structures however this is not necessarily the case, where gap junction uncoupling could improve propagation by decreasing the influence of coupled myocytes that are spatially arranged in a way that dampens propagation.²¹ Signal transductions between cardiac cells are also transmitted by membrane soluble molecules, as well as the **extracellular matrix**, which, in addition to providing structural support, modulates biochemical and biophysical signals and facilitates intercellular signaling.¹³

1.1.6 - Cellular biology - Effects of the nervous system: The heart is innervated by a complex neural system called the intrinsic cardiac **Autonomic Nervous System (ANS)**, which controls the cardiac syncytium. The cardiac autonomic nervous system consists of autonomic neurons in the heart itself as well as in the large vessels in the thorax.²² The traffic within these neurons converge at discrete locations called **Ganglionic Plexi (GPs)**. These GPs are embedded in epicardial fat pads, and may contain hundreds to thousands of autonomic neurons.²² An imbalance of the ANS can play a pertinent role in the genesis of arrhythmias.²²

In general, the nervous system can be divided into two functional and structural types, **sympathetic**, which increases heart rate, and **parasympathetic** which slows down the rhythm. Sympathetic stimulation in a normal heart results in an increase in **chronotropy** (effects that change the heart rate), **ionotropy** (changes in myocyte contraction force), and **dromotropy** (changes in electrical impulse propagation). This sympathetic stimulation acts on both the atrial

1.1 Introduction: Cardiac Physiology

as well as the ventricular myocytes to activate channels among which are inward sodium current and delayed rectifier potassium as well as chloride currents.²³ Additionally, excess sympathetic innervations in cardiac cells can lead to arrhythmias as well as epileptic seizures and other chronic diseases such as hypertension and heart failure.²⁴ The parasympathetic nervous system has the opposite effect. Postganglionic parasympathetic axons innervate the atria and ventricles. These neurons can also change the activation, electrical conduction and effective refractoriness of atrial, nodal and ventricular myocytes. They do so via muscarinic acetylcholine receptors on myocytes.²³ Augmentation of the parasympathetic nervous system can increase refractory period and reduce ventricular tachycardia and ventricular fibrillation by lowering the dispersion of repolarization.²³ Both sympathetic and parasympathetic systems then, have a regulatory role in the heart, and thus, cardiac denervation can increase the risk of ventricular arrhythmias and arrhythmic death.²⁴

The sympathetic and parasympathetic pathways perform their actions by releasing certain **neurotransmitters**, which are chemicals released from nerve cell endings. Some examples are acetylcholine, catecholamines, angiotensin II and norepinephrine. Acetylcholine acts on nicotinic acetylcholine receptors on the efferent postganglionic intrinsic cardiac neurons. These neurons receive input from both the left and the right vagal trunks.²³ Sympathetic catecholamines lead to an increase in heart rate, and release of angiotensin II directly promotes ventricular arrhythmias due to the loss of urinary potassium and magnesium. Furthermore, animal studies have found that the degree of ventricular dilation is directly related to increased angiotensin converting enzyme activity in the ventricles.²³

Cardiac rhythm can be experimentally manipulated in vitro as well. This can be achieved by stimulating various nerves, or nerve groups. For example, parasympathetic stimulation is generally antiarrhythmic and vagal nerve stimulation improves survival in animal models of cardiac ischemia, if it is started at the time of the coronary artery occlusion.²³ Other examples include baroreceptors which can be targeted at the carotid sinus and stimulated to increase parasympathetic afferent activity to augment vagal tone, which then leads to a decrease in blood pressure and heart rate.²³ Another way of increasing vagal tone and decreasing sympathetic activation is by SCS or Spinal Cord Stimulation.²³ Atrial fibrillation can be induced by suprathreshold **vagal nerve stimulation (VNS)** or slowing the sinus rate or AV conduction.

1.1 Introduction: Cardiac Physiology

Hyperactivity of the cardiac ANS can also be shown to trigger **Atrial Fibrillations (AF)**.²² Modulating parasympathetic and sympathetic tone can be used as a means of controlling arrhythmias.²² Clinically, a novel form of treatment stemming from such studies is neuromodulation and autonomic denervation, however a lot more research is needed.²² These examples further highlight the potential human benefits of studying innervated cardiac tissues and have led to the development of in vitro model systems that look at neurally mediated arrhythmias in a controlled setting. Cardiac and neuron co-cultures are used to gain insights into how neurons modulate cardiac activity, however heterogeneities introduced by the cell culturing process results in variations in dynamics that complicates data interpretation. Since experimental variation can only be accounted for by increasing sample size, cardiac coculture systems are another experimental system that can greatly benefit from technical possibilities afforded by RAP.^{25, 26}

1.1.7 - Cellular biology - Effects of physical load: The next potent extracellular factor affecting a heart's rhythm is the effect of physical load on the heart. The heart's mechanical environment has a significant effect on its electrical behaviour and subsequently on its rate and rhythm. This effect is called the **MechanoElectric Feedback (MEF)**²⁷ and is an important part of the heart's electromechanical regulatory loop.²⁷ The mechanical environment can be impacted primarily in two ways: through the way the heart's contractile force itself interacts with the environment; and second, through external factors, such as obesity, and the load on the heart affecting the contraction force.^{14, 27, 28} These biophysical cues are sensed by cardio myocytes through **mechanosensors**. These sensors usually have membrane associated protein complexes and convert physical stimuli into biochemical signals.¹³ There are a variety of mechanosensors and they work in a variety of ways, two of the most pertinent are **stretch activated channels** and **volume activated channels**.

Stretch activated channels respond to mechanical stretch by an increase in the probability of ion channels being open.²⁷ Furthermore, stretch can induce the release of a number of molecules. For example, stretch results in the upregulation of the master cardiac gene regulator **myocardin** as well as the vasoconstrictor **angiotensin II**.^{29, 30} Additionally stretch leads to an increase in the affinity of **troponin C** for calcium which results in a higher calcium transient effect and higher force.²⁷ The overall effects of stretch on cardiac cells is a suppression of growth and

1.1 Introduction: Cardiac Physiology

proliferation, and an increase in cell death, but also an improvement in myogenic differentiation of stem cells, perhaps to help overcome the damages caused by stretch.^{29, 30} Additionally there is an enhancement of smooth muscle cells and an enhanced expression of EMC and adhesion molecules as well as an upregulation of gap junctions. Systolic stretch can also have different effects on action potential shape, including shortening, prolongation and crossover of repolarization.²⁷

Volume changes can also affect the heart rhythm. Volume activated channels are not directly affected by stretch or deformation but rather, as the name suggests, with volume changes. An example of this type of channel is the volume activated chloride (Cl⁻) channel. Volume activated channels play an important role in the regulation of osmosis events such as myocardial ischemia and reperfusion. It is important to note that cell volume changes can be a signal of underlying events such as inflation of intracellular organs, deformations of the cytoskeleton, changes in ion strength, and membrane curvature among other events. Thus the role of receptors that respond specifically to volume in the cells is critical.²⁷

To summarize, cardiac cells can sense their environment and accordingly adapt the amplitude and pattern of the load, its timing, the direction of the load and phase relative to action potential generation.²⁸ Some efforts have been made to study such dynamics in vitro. A common attempt is to apply mechanical pressure to cardiac cells by adhering them on an elastic membrane and stretching that membrane.²⁸ Fluorescent beads embedded in the substrate can also be used to monitor cardiac activity.²⁸ Overall however, it is significantly challenging to replicate the complex in vivo dynamics in vitro.²⁸

All of the components mentioned so far in the previous sections that are involved in the initiation, conduction and monitoring and regulating of the cardiac cycle can fail, and these malfunctions can result in arrhythmias.

1.1.8 - Arrhythmias: Arrhythmias are irregular rhythms of the heart. Arrhythmias can occur at any age, and last for various lengths of time.^{31, 32} As mentioned over the previous sections, under normal conditions, coordination of heart contraction and rhythm is controlled by a network of cardiac myocytes that communicate through voltage gated ion channels and gap junctions

1.1 Introduction: Cardiac Physiology

controlling both the internal and external ion flux. Generally only 1% of the myocytes are responsible for initiating a contraction and these cells are broadly called pacemaker cells.¹⁴ If these pacemaker cells malfunction or if other cells that do not regularly show automaticity, such as the Purkinje fibers, start automatically firing (abnormal automaticity), an ectopic heart beat can occur. The **SinoAtrial Node (SAN)** is the most pertinent of the pacemakers and sets the heart rate.¹⁶ In cases of disease however, other arrhythmogenic factors such as early and delayed afterdepolarization can occur in other areas of the heart and the premature depolarization can interfere with the regular AP of sinoatrial node and lead to arrhythmias.³³ The resulting arrhythmias are divided by how they affect the heart rate and also where they originate (ventricular and supraventricular).

Arrhythmias can be categorized based on the effect that they have on heart rate. The main types are bradycardia, which is slow heart rate, and tachycardia which is fast heart rate. Bradycardia is generally defined as a heart rate below 50-60 beats per minute. Its symptoms include transient dizziness or light-headedness, fatigue, **dyspnea** (difficulty breathing), **syncope** (a temporary loss of consciousness due to low blood pressure), and confusion.³⁴ Tachyarrhythmia is rapid heart rate, generally defined as over 100 beats per minute. It can be caused by genetic factors as well as electrical remodelling due to cardiac disease, pharmacological agents, and hypokalemia.³³ Life threatening bradyarrhythmia and tachyarrhythmia often come about as a result of intracellular abnormalities involving impaired function of ion currents, gap junctions, or calcium abnormalities or extracellularly when electrical stimulations is applied to vulnerable pacing sites, such as abnormal neuronal activity, or as a result of physical influences on the heart. Examples include early afterdepolarizations and delayed afterdepolarizations causing tachyarrhythmias when the amplitude of the afterdepolarization becomes sufficiently large.³³ Or bradycardia caused by factors that slow the rhythm of the heart such as a block in AV or sinus node dysfunction.³³

Arrhythmias can also be categorized based on the location of origin. **Ventricular arrhythmias**, as the name suggest start in the ventricles of the heart. The range of symptoms vary widely from no symptoms to full cardiac arrest and death.²³ These arrhythmias can occur as a result of myocardial injury or a scar due to myocardial infarction. The presence of these scars and fibroses can contribute to a remodeling of cardiac neurons and predispose the individual to ventricular

1.1 Introduction: Cardiac Physiology

tachycardia and ventricular fibrillation and long QT.²³ Other causes can be nonischemic cardiomyopathy and adult congenital heart disease as well as genetic factors.²³

In supraventricular

arrhythmias, arrhythmias originate from the atria or the upper chambers. Symptoms can last from a few minutes to a few days or be completely asymptomatic. They include, fluttering in the chest, shortness of breath, light-headedness, sweating, and fainting.

Similar factors that lead to ventricular arrhythmias can also lead to

supraventricular arrhythmias such as injury or genetic diseases that lead to an underlying change in cell and tissue physiology. Some types include atrial flutter, paroxysmal supraventricular tachycardia and atrial fibrillation. Atrial fibrillation increases both the heart rate and irregularities and are one of the most common types of supraventricular arrhythmias. These arrhythmias are often linked to underlying conditions more common in an older population, such as structural heart disease, hypertension, diabetes mellitus, and autonomic imbalance.¹⁶

Overall, the basis of most cardiac arrhythmias can generally be summarized as abnormalities in impulse generation, propagation, or the duration and configuration of individual action potentials.¹⁷ The main two categories of the mechanisms of arrhythmia generation are enhanced or abnormal impulse generation and improper impulse conduction, called **focal activity** and **re-entry** respectively.¹ Focal activity includes both **automaticity** (the ability of cardiac cells to initiate spontaneous APs) and **triggered activity**.¹⁶ Re-entry refers to the process of the same

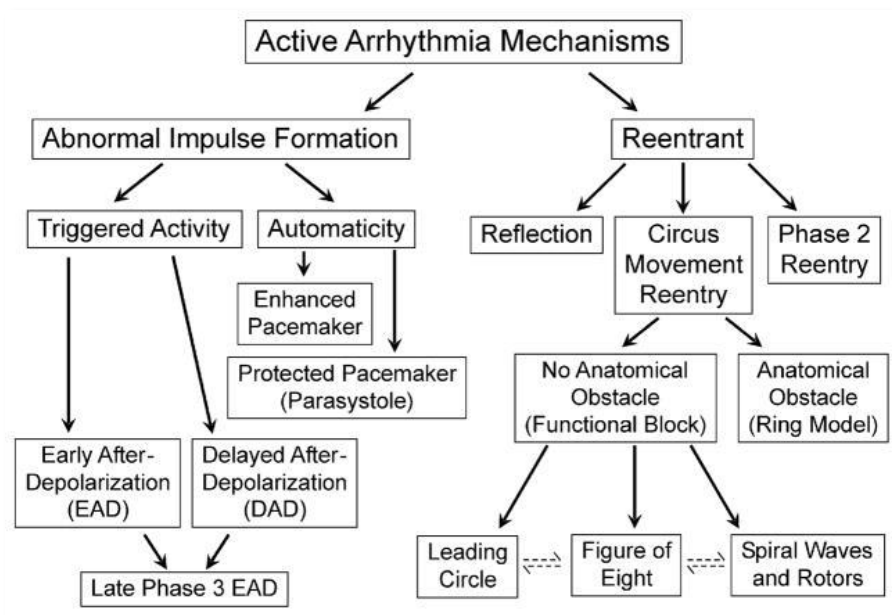


Figure 3 Table of common active arrhythmia mechanisms.¹ The main two mechanisms are Re-entrant and Abnormal Impulse Formation. Abnormal impulse formation refers to events where the generated cardiac beat is abnormal in nature and re-entry refers to one generated rhythm re-entering the same group of cells and causing another contraction, leading to abnormal rhythms.

1.1 Introduction: Cardiac Physiology

signal entering the same groups of cells again to initiate another cardiac beat. These are summarized in Figure 3.

Triggered focal activity can be caused by either **early or delayed afterdepolarization**, either in the atrial or ventricular myocytes. Early or delayed after depolarization refers to how quickly the depolarization phase of the cardiac action potential occurs following polarization. Both early and delayed afterdepolarization can generate enhanced and/or abnormal impulses.¹⁶ There are two proposed mechanisms for early afterdepolarization. The first proposes that the prolonged repolarization of the action potential increases the Action Potential Duration (APD), which allows recovery and reactivation of L-type Ca^{2+} current (I_{CaL}), resulting in enhanced inward I_{CaL} that further depolarizes the membrane. The second is that at threshold of calcium activation, but before complete repolarization takes place, spontaneous calcium release can activate sodium transporters which can depolarize the membrane.¹⁶ Delayed afterdepolarizations occur as a result of abnormal spontaneous calcium release from the sarcoplasmic reticulum into the cytoplasm.¹⁶

Re-entry, also known as **circus movement**, occurs when the same electrical impulse is allowed to re-enter the circuit and repetitively excite the same site of origin.³³ Re-entry can only be demonstrated in a multicellular environment and under certain conditions. First, the normal conduction should be interrupted by an obstacle which the activation front must propagate around. The blockade can be anatomical (e.g. a post infarction scar), or functional, (e.g. a region of refractory tissue). Second, the refractory period should be shorter than the impulse conduction time within the circuit, so that the impulse can return to the site of its origin and then start another circle.³³ If these conditions are met, the signal can re-enter the same site and generate an arrhythmia.

1.1.9 - Rarity of arrhythmias: Arrhythmias are rare events: while some arrhythmias are continuous (e.g. persistent atrial fibrillation) many arrhythmias (e.g. paroxysmal atrial fibrillation) consist of a brief, sporadic, and randomly distributed period of abnormal rhythm followed and preceded by a longer period of normal rhythms.^{24, 32, 35} This impacts experimental studies of cardiac arrhythmias as well. In one study for example studying the effect of IL-1 β on arrhythmia of diabetic mice, the authors looked for spontaneous cardiac events, **namely Neuron Specific**

1.1 Introduction: Cardiac Physiology

Enolase (NSE) for a continuous period of 10 min with an incubation period of 24 hours to quantify the effects of IL-1 β . They observed that mice treated with IL-1 β showed higher NSE overall. However, this was not a consistent observation. That is, not all samples showed a fixed increase all the time, and IL-1 β only increased the likelihood that NSE levels would be increased. Studies such as this can greatly benefit from the ability to image and monitor multiple samples simultaneously over a continuous period of time as this increases the sample number but just as importantly, decrease the variability caused by miscellaneous cofactors.³⁶ The effect of variability and sample size and its relevance to RAP is explained in greater detail in the discussion section.

Most of the information known to date regarding the physiology of the heart, cardiac rhythms as well as arrhythmias has been gathered from cardiac model systems. As experiments on the living human heart and human heart cells carries obvious restrictions, models are needed to study cardiac cells and tissues. Three main types of models exist: animal models, human pluripotent stem cells, and 3D models.¹³ Computational cardiac models³⁷ also valuable, however they are not in the scope of this thesis.³⁷ All of these models have their own advantages and disadvantages, and all are extremely important both for academic studies as well as industrial drug development. As an interesting fact, in the US, only 1 out of every 9 compounds that enter clinical trials end up being registered. Even after registration, up to a quarter of drugs can fail. And even further only 30% of drugs that do reach the market end up recovering the investment.³⁸ These statistics, in addition to the fact that most of our cardiac knowledge is dependent on the use of models, emphasizes their importance. In the following sections I will delve deeper into **animal models**, **iPSCs**, as well as recent advancements in the development of **3D tissue models**.

1.1.10 - Animal models: Biological models are models that are derived directly from living animals. These models have the advantage of being as natural as possible and a lot of what we know comes from such animal models.^{20, 38} One of the best such models, substituting an animal model mammalian heart for study, is the Langendorff perfused isolated mouse, rat, rabbit or guinea pig heart.³⁸ However, non-human myocytes express different ion channels and have different action potential properties compared to human myocytes, and the structure and

1.1 Introduction: Cardiac Physiology

geometry of these hearts can be very different from the human heart.^{16, 38} For example, the heart rate for mice is 8 times faster than humans and the AP is much shorter.¹⁶ Other differences include lipoprotein metabolism and the susceptibility to disorders of lipid metabolism.²⁰ Mammalian heart cells can be used in tissue culture preparations, however here a limitation to consider is that adjacent cell populations can give signaling cues for the sequential development stages in in-vivo heart cells which can be lacking in in-vitro studies, resulting in abnormal phenotypes.¹³ Overall, the limited predictive value as well as relatively high costs and lower availability of animal cardiac models for drug discovery is a primary reason for slow cardiac drug discovery. Induced Pluripotent Stem Cells (iPSCs) can help solve some of these limitations.³⁹

1.1.11 - Induced Pluripotent Stem Cells(iPSC): **Induced Pluripotent Stem Cells(iPSC)** are stem cells that have the ability to differentiate into many different cell types.⁴⁰ Recent discoveries have made it possible to reprogram somatic cells to iPSCs by introducing a few transcription factors which are linked to the pluripotency of these cells. These iPSCs can then be differentiated into cardiomyocytes.¹⁶ The reprogramming is straightforward however it is not very efficient.³⁸ At the moment HL-1 cardiomyocytes are the main model cell lines that can continuously divide, spontaneously contract and maintain a differentiated adult cardiac phenotype.⁴¹

There are many advantages to the use of iPSCs. Like human embryonic stem cells, iPSCs have the capacity for long term propagation and expansion, and are capable of differentiating into all somatic types.²⁰ More relevant to this thesis, they can differentiate into various forms of cardiac cells and are useful in studying disease pathophysiology.³⁹ They can proliferate for extended periods of time and more closely resemble cardiac cells including their ion channels, as well as signaling and contractile proteins needed for functional excitation – contraction coupling.³⁹ The existence of such cell lines, with the increased availability, specificity, and lower costs, and the ability to be immortalized, has provided researchers with valuable tools to probe the intricacies of cardiomyocytes.⁴¹ Two more practical advantages of iPSCs are the excess supply and the ability to use patient specific disease models.^{16, 40} These include but are not limited to, a more patient-specific study of ion channels, their disorders and channelopathies.¹³

1.1 Introduction: Cardiac Physiology

There are several methods for turning somatic cells into iPSCs and then from there to differentiate them again to different types, such as cardiomyocytes. Most protocols use a serum with a high-fetal calf concentration to differentiate stem cells to cardiomyocytes. Both iPSCs and embryonic stem cells spontaneously form embryoid bodies in the presence of this serum, which leads to the formation of **endo-, ecto-, and mesodermal cells**.⁴⁰ The most common protocols generate ventricular-like hiPSC-CMs.⁶ Additionally more specific players in the differentiation pathways can also be targeted. For example, inhibition of the GSK3/Wnt signaling pathways plays an important role in the differentiation of iPSCs to functional cardiomyocytes.⁴² Some of the first iPSCs were formed by an overexpression of various transcription factors.^{20, 40} Differentiation can be monitored, using **multielectrode arrays (MEA)**, which allow for studying the extracellular field potential signals from clusters and monolayers of hiPSC-CMs, in a non-invasive and nonterminal manner.⁶

Adult cardiac cells are terminally differentiated cells that cannot repair themselves. In this light iPSCs represent a renewable and scalable cell source that can potentially be useful for cardiac engineering applications.⁴² Although no clinical trials have been performed so far using iPSCs for cardiac regeneration,⁴⁰ in preclinical models, iPSC derived cardiomyocyte models have seen significant advancements.⁴⁰ The advancements in iPSCs now enable both the production of cardiomyocytes from healthy as well as diseased cardiac cells, offering the opportunity to study cardiac diseases in a dish.³⁹ Recently iPSCs have been explored for customized modeling of disease and drug development.³⁹ Some examples of are hypertrophy models, experiments on abnormalities in contractile function, arrhythmia models, models of congenital long QT syndrome, and models of myocardial infarction.³⁸

There are however some disadvantages to iPSCs. iPSCs still have some differences with normal cardiomyocytes in terms of protein expression and distribution, morphology, contractility and electrophysiology.⁴⁰ One important difference between human induces pluripotent stem cell cardiac myocytes is that cardiac myocytes, particularly in ventricular cells, do not demonstrate spontaneous beating, whereas stem cell derived cells do, because of the substantially reduced density of potassium channels and reduced expression of pacemaker current.¹⁶ Other problems with stem cell therapy is inappropriate differentiation, cellular uncoupling, formation of scars and accelerated apoptosis of transplanted cells.⁴³ Furthermore their incomplete maturation may

1.1 Introduction: Cardiac Physiology

reduce their predictive power.⁴⁴ Some examples of this immaturity is a lack of T-tubules, abnormal morphology, altered gene expression, and reduced sarcomere organization.¹⁶

1.1.12 - 3D Models: Although compared to 3D models, 2D models are easier to handle, better documented, cheaper and more readily available,^{43,44} these models can be limiting particularly when studying the effect of drugs, toxins, and signaling modifiers on tissue dynamics where the effect of the 3D environment is important. **3D cardiospheres** are 3D cell aggregates of heart cells,⁴³ which may overcome some of these limitations.¹⁴ There are a few ways to culture these cardiospheres. One method by which simple 3D-cultures have been made is by using non-adhesive surfaces and non-tissue culture treated plastic, or highly porous biodegradable polymers such as collagen, polyglycolic acid, gelatin, or alginate scaffolds. Other methods include cell sheet engineering using temperature sensitive substrates.⁴³ One study using dog heart cells showed that cardiospheres can be grown using poly-L-ornithine-coated surfaces in the presence of factors FGF-2 and EGF.^{43,44}

In vivo, cardiac tissue is embedded in extracellular matrix proteins, and exposed to many mechanical, electrical, biochemical and other types of stimuli that lead to their development.⁴⁴ They undergo cyclic deformation, have rapid calcium transients and electrical signals or simply experience shear stress from blood flow. Additionally, cardiac development pathways are affected by electrochemical stimulations. As these factors operate in a three dimensional space, the best way to study them is by using 3D models.⁴⁴ The technology for 3D cardiac models is still not mature and most 3D model systems are still at the proof-of-concept stage.

1.1.13 – Section Summary: The above pages highlighted the fundamentals of cardiac rhythms, the underlying mechanisms, and some of the most fundamental factors leading to irregular rhythms, otherwise known as arrhythmias. I then outlined the most common models for studying cardiac tissue. In the next section, I highlight some of the current imaging methods that are most commonly employed to study biological phenomenon including studying cardiac physiology.

1.2 Introduction: Current State of Image Acquisition

The multitude of factors that affect arrhythmias necessarily require various imaging techniques to study the different aspects of the process. In this thesis I propose a new RAP system, which aims to provide a new imaging tool for scientists. The natural question to ask then, is given the myriad of imaging techniques and devices available, what new capabilities does RAP introduce that are currently lacking in the market? What void does it fill? And what new discoveries does it enable? The short answer is that it enabled scientists to image multiple samples simultaneously for extended periods of time under biological, incubated conditions. For a more in-depth review however, we begin with a general exploration of some of the most common imaging systems and techniques, their advantages and limitations and how they have inspired our RAP system. Chapter 2 then explores the design of RAP and the need for its capabilities are discussed in greater detail in the discussion section. What follows in the next few pages is aimed to paint a macro picture of the world of microscopy today.

1.2.1 – Current state of High-Throughput devices: To this day increased throughput has primarily involved either the use of widefield microscopy or using robotics to speed up the workflow of the optical setup. There are numerous such devices on the market, each aiming to solve a particular shortcoming and each presenting different advantages and disadvantages at different price points. Some examples of high throughput devices include the IonWorks planar patch, the Fluorometric Imaging Plate Reader (FLIPR), Multichannel Electrode Arrays, xCELLigence, and FDSS/ μ Cell.³ While some HT systems capture data in parallel (e.g. MEA based systems or the FDSS/ μ Cell), they do so at low spatial resolution which poses some limits on the types of data that is collected. Other HT imaging systems (e.g. FLIPR) automate already existing workflows, setups and technologies and have not created an optical setup dedicated to high throughput from the ground up. Collectively then, these systems have a common shortcoming: they are either limited in spatial resolution or are unable to image samples in parallel, resulting in a loss of data. This is problematic in cardiac tissue, where spatial resolution is important and critical events occur faster than the rate by which robotic components can switch between samples. RAP however rethinks high-throughput imaging, and is setup around that concept. Yet our system still is inspired from the many phenomenal imaging technologies

1.2 Introduction: Current State of Image Acquisition

that exist. I start by discussing optoDYCE, a technology developed by one of our close collaborators which can also be used to study wave propagation in cardiac monolayers.

1.2.2 - optoDyCE: The all-optical dynamic cardiac electrophysiology framework (**OptoDyCE**) is a technique, developed by one of our close collaborators Dr. Entcheva, that allows the fast quantification of physiological phenomenon. As the system uses optogenetics to stimulate the tissue and fluorescent dyes to monitor the tissue, the overall system is said to be all optical, and contactless. Robotics are used to automate the system making it high throughput and the first all optical technique able to reach up to 10,000 cells a day - the threshold for being considered high-throughput in the industry.³ One of the biggest advantages of OptoDyCE is that it can be combined with already scalable HTP models, and used to analyse biological systems including stem cell-derived cardiomyocytes. Combining the High HTP capabilities of OptoDyCE with the efficiency of these biological models for drug screening can be very promising.³ Furthermore, this increased efficiency of detecting promising drugs before getting to more expensive phases, can increase the willingness of drug companies to pursue more “high-risk” drugs.³ A more specific example of use can be seen in arrhythmias in cardiac cells, where **optogenetic actuation** (optical pacing) via light sensitive channels is combined with dye free imaging of cardiac contractions.³ Other examples of optoDyCE include the study of the interrogation of neural influence on cardiac monolayers using optogenetic as well as optochemical stimulation.²⁵ Overall, OptoDyCE is intended to complement, and not replace comprehensive in vitro and in vivo testing.

optoDyCE is built around an inverted microscope set up, but the workflow is just as important, which combines optical actuation of cardiac cells (using opsins or spark cells) with robotic microscopy. **Opsins** are light sensitive molecules that can depolarize or hyperpolarize the cell’s membrane. The use of such proteins for cellular activation is part of a class of technologies collectively called **optogenetics**. **Spark cells** are tandem cell units throughout the sample which activate the neighbouring cells that are under observation. These simulations in turn can trigger a variety of signals including voltage calcium signals, action potentials (AP) and mechanical contractions. The effects are then measured with simultaneous optical sensing of voltage or intracellular calcium using synthetic red-shift dyes or even dye free methods.³ The samples can be from a variety of cell lines, for example neonatal rat ventricular myocytes or iPSC-CMs, from

1.2 Introduction: Current State of Image Acquisition

cell monolayers as well as 3D structures.³ The automation however still relies on robotics moving the sample to position each well under the optical path one by one, and recording each for 5-20 seconds. This again inherently impedes the throughput, and results in limitations of missing information from each well while the other wells are being recorded, which is discussed further in the text.

1.2.3 - Optogenetics: Optogenetics refers to techniques that aim to control or record from excitable cells using genetically coded actuators and sensors that are light-sensitive. The basic principle of optogenetics is relatively simple. Genetic engineering is used to insert light sensitive channels (opsins) into cell membranes. These opsins, and consequentially the cells, can then be controlled using light.⁴⁵ Channelrhodopsin-2 (**ChR2**) channels, are one of the primary opsins used in optogenetic experiments. Because of the specificity and speed of this technique, optogenetics can be beneficial both in improving spatial as well as **temporal resolution**. **Spatial resolution** has its own obvious advantages, and temporal resolution can be particularly important in cases where a process occurring over short periods of time is being investigated such as: calcium transient duration, beat rate, conduction velocity and pattern formation of cardiac cells. In most of these cases alternate, contact based methods, such as patch clamp and sharp electrode-based electrophysiology, can also be used.¹¹

Opsins can be delivered and integrated into the cells in two primary ways. The first is by genetically inserting the opsin genes inside the target cell. The second is non-permanent gene expression.¹¹ In both cases, once opsins have been inserted, the cells can be manipulated optically and imaged using conventional imaging techniques, two of the most popular being fluorescence and brightfield microscopy.¹¹

Optogenetics have recently shown significant promise in cardiac studies where optogenetics can control depolarization, hyperpolarization, refractoriness as well as the shape of the cardiac action potential, and can sustain these changes for relatively long periods of time.⁴⁵ The power and ease-of-use of the techniques can be compared to changing parameters of interest in computational models and can be used to provide new insight into pacemaking, arrhythmogenesis and suppression or cardioversion of various elements and factors.¹¹ At an organ level in animal studies, cardiac arrhythmias can also be stopped by either using inhibitory

1.2 Introduction: Current State of Image Acquisition

opsins and thus hyperpolarization or by applying a depolarizing optical perturbation at the global level.¹¹

Overall, the main benefits of optogenetics are its ability to enable real-time, reliable, repeatable and precise stimulation and feedback in excitable cells, at any scale from cells to the tissue level.^{11,45} Theoretically this technique can also be used in vivo, and at multiple locations of a sample, if light access could be provided.⁴⁵ This kind of all optical set up can also be much more easily automated.⁴⁵ Additionally, these tools can be brought inside an incubator so that experiments can be performed while the cells are in controlled environments.⁴⁵ Optogenetics has some limitations, namely sample preparation requires an extra step and the optical tools may not be readily available in some labs. Yet overall, these limitations are compensated for by the benefits of using contactless techniques, which result in less tissue damage than traditional electrodes.^{11,45} In summary, optogenetics then is a technique for fine detailed and fast biological manipulation. Implementing optogenetics in our RAP system is an important next goal for our lab.

1.2.4 - Combining high throughput and super resolution: Combining high throughput microscopy with super resolution microscopy is generally dependent on a new workflow that allows the samples to be rapidly scanned in a low resolution high throughput system, and once regions of interested have been identified, imaging those regions under a super resolution system. This workflow however does not produce high resolution images at high speeds, and furthermore requires the continuous repositioning of the samples which can create its own challenges such as feature space analysis which then necessitates the use of a coordinate system.⁴⁶ Problems such as repositioning the sample so that images can be overlapped are a good example of why it is very difficult to increase the throughput for techniques that require extreme focus, even though they can be very powerful in alleviating other shortcomings. An example of a system with very fine resolving power but low throughput is TIRF microscopy.

1.2.5 - Total Internal Reflection Fluorescence (TIRF): **TIRF** is an specialized technique that uses refractive properties of light to only image a thin section on the surface of a sample immediately adjacent to the lens.⁴⁷ In fact, many microscopes can be converted to a TIRF by adding a few components including a prism or condenser. The general mechanism works by using optics and

1.2 Introduction: Current State of Image Acquisition

special materials to take advantage of Snell's law and make sure that the beam of light totally internally reflects and thus only hits the surface of the specimen. The basic path is as follows: a gas, argon-ion, krypton, or helium-neon light source is used to excite the sample → light passes through glass → enters a metallic intermediate layer → reflects back from metal-water boundary → travels to the detector.⁴⁸ Although for simplicity we say that the light beam does not travel into the medium, in reality it does, but to a very small degree, usually a subwavelength which then generates a thin electromagnetic field, called an evanescent field, in the aqueous medium between the microscope and the sample. This field is then captured and recorded.

The high sensitivity of TIRF to distance can be used both to eliminate background noise and also to measure distance of objects from the surface,⁴⁸ while simultaneously significantly improving resolution.^{47, 49} This technique is also about 6-7 times faster than confocal microscopy when imaging a single sample but is slow when switching between samples. As a result TIRF is good for studying single-molecule dynamics for applications that have a time-resolution demand.⁴⁸ Furthermore, TIRF only minimally disturbs the cells with light.⁴⁸ Overall then, TIRF specializes in higher signal to noise ratios and focus, at the expense of simplicity, throughput and price, although some efforts have been made to increase throughput.⁵⁰ In one paper for example, the authors used a high refractive index contrast waveguide on a photonic chip platform. The authors explain that the key aspect of this platform is that an evanescent field is generated at the surface of the waveguide structure. This platform can then be used to both hold the cells and illuminate them. By decoupling the light collection and excitation path, this method allows for brighter images of larger areas. This method however, although improves upon the speed of TIRF can still only image one sample at a time, and therefore does not address the need for near simultaneous recording of multiple samples, or the extremely fast switch times between samples addressed by RAP.⁵⁰

The main advantage of TIRF is also its primary disadvantage, that it can only image the surface of the specimen. Other systems exist that allow much deeper penetration, particularly NLO and confocal microscopy.

1.2.6 - NonLinear Optical (NLO) High-Throughput Microscopy: NonLinear Optical (NLO)

microscopy is a class of techniques used to measure nonlinear optical characteristic of the sample

1.2 Introduction: Current State of Image Acquisition

that can be observed when a high intensity light, such as a laser, illuminates them.⁵¹ Some examples of nonlinear properties include the chemical structure, fluorescence, two-photon excitation fluorescence, second harmonic generation, third harmonic generation, vibrational sum frequency generation, spontaneous Raman scattering, stimulated Raman scattering, and coherent anti-Stokes Raman scattering.⁵¹ Some of these nonlinear techniques, such as two-photon microscopy, are discussed further in the following pages.

There are several benefits to NLO microscopy: it has a good depth discrimination; especially into turbid specimens; the interaction between molecules as well as ultrafast light pulses generate a contrast that can be used in a broad spectrum of high resolution imaging modalities;⁵² NLO typically uses long wavelengths (infrared) for illumination, which means less tissue scattering and absorption, less photodamage and photobleaching as well as being localized to the excitation volume; and finally, biophysical and biochemical states of specimens can be addressed by quantifying the geometry, the vibronic and electronic states and the aggregation of probe molecules using NLO.⁵² The main disadvantage of nonlinear optical methods is the complicated set up, cost, and low throughput, which again highlights the necessity of trade-offs in microscopy.

1.2.7 - Two photon microscopy: In brief, as the name implies, **two-photon microscopy** uses two photons to excite a **fluorophore**. If and only if two photons arrive at the same location at the same time, does the fluorophore receive enough energy to be excited.⁵³ This ensures that only fluorophores at that specific location where the two photons meet are excited, thus only the intensity needs to be recorded, because the location of light can be deduced to have come from the single point where the two photons met.^{53,54} Images are collected by scanning the image point by point⁵³ and then amplifying the signal using a high sensitivity detector such as a **Photo Multiplier Tube (PMT)**. Pulsed lasers are used to introduce high intensity photons without having a continuous flow of high energy into the sample.⁵³

The main advantages of two photon microscopy are the precision by which the fluorophores can be excited and the lack of any out of focus light⁵³ as all the emitted light is known to have been emitted by just one point.⁵⁴ Two additional advantages are the penetration depth⁵⁴ and the ability for the same excitation light to excite multiple indicators with different releasing

1.2 Introduction: Current State of Image Acquisition

wavelength simultaneously.⁵⁴ Three potential downsides to two photon microscopy are the damage that can occur to the sample by the laser, the relatively high cost of the system, and the relatively low throughput.⁵⁴ Efforts have been made to increase the throughput. However, these efforts again do not address the gaps in the microscopy world addressed by RAP. In one paper for example the authored used two photon microscopy to image High-Density well plates. While their results demonstrating the possibility of using two-photon microscopy in a multi-well plate is promising, the need for movement of the samples and their sequential recording still remain.⁵⁵

In recent years, in addition to two photon microscopy, some new approaches have arisen using three photons to excite the cells with either point scanning or temporal focusing. This technique uses light scanning and an additional photon for excitation purposes, which reduces the effects of light scattering, and increases penetration depth of the illumination beam into the sample,⁵⁶ as well as reducing the out of focus light areas even further. This however also increases the price. A cheaper method for increasing penetration depth and increasing focus is confocal microscopy.

1.2.8 - Confocal microscopy: **Confocal microscopy** is similar to a traditional microscope set up but uses a **pinhole** structure to block all out-of-focus light, and a photomultiplier detector combined with a scanning system instead of a camera to produce an image.⁵⁷ The pinhole is the main distinguishing aspect of confocal microscopy. An image is produced by moving the confocal point (pinhole) across the sample, using oscillating mirrors, pixel by pixel and compiling the data into one single image. Since primarily photomultiplier tubes which only detect the intensity of light and no spatial information are used as detectors, the spatial resolution comes from the knowledge of where on the sample the pinhole was focused on.⁵⁸ The smaller the pinhole the better it is at blocking out-of-focus light but at the same time the less photons that pass through it, leading to either slower acquisition or poorer quality photos.⁵⁴ As an example, scanning point confocal microscopes are about 200 times less efficient at collecting and detecting fluorescence from specimen as compared to wide-field microscopy, but improve focus.⁴⁷ Furthermore confocal microscopy takes longer when compared to camera based techniques, which can be problematic especially in dynamic samples.

Methods have been developed to increase the speed. For example, in **spinning disk confocal microscopy**, a single pinhole is replaced with a spinning disk full of spirally arranged pinholes

1.2 Introduction: Current State of Image Acquisition

and the PMT tube is replaced with a **Charged Coupled Device (CCD)** detector which leads to significantly faster acquisition.⁵⁸ Other methods concentrate on improved workflows around more highly dense plate setups,⁵⁷ or novel ideas to tackle more specific challenges. For example, one scientific group discovered that a lower sample volume while testing the effect of drugs on cellular assays could still be efficient in providing useful data. This allowed for more drugs to be screened using confocal microscopy and consumed less of the necessary but expensive reagents. They thus used femto-liter-sized samples to be able to image more samples without an extensive decrease in data quality.⁵⁹ There are some further disadvantages to confocal microscopy, including loss of resolution and limitations in zoom when compared to some other microscopy techniques, and incompatibility with spectral imaging or two photon microscopy.^{54, 60}

Confocal microscopy highlights, yet again, the common theme of trade-offs in microscopy between focus, light collection and speed, in a traditional approach to microscopy. Other simpler methods also exist to take advantage of inherent optical properties of the specimen to capture images. One example is polarized microscopy.

1.2.9 - Polarized microscopy: At the most fundamental level, **polarized microscopy** utilizes the fact that all proteins maintain some degree of orientation with respect to the membrane plane,⁶¹ and therefore bend polarized light. This property can be used to analyze refraction and absorption (**anisotropy properties**), orientation, magnitude of the specimen birefringence (often of hard tissue such as bones and extra cellular matrices that have strong birefringence) and allows us to get more information about the organization of endogenous molecules that make up a cell in a non-destructive way.⁶¹ In a polarized microscopy set up, without any sample, all the light that is passing through the polarizer will be blocked, but if a sample with birefringent properties is present, light will bend according to the polarizing properties of the sample so that some light will pass through, and structural information about the sample can be inferred.⁶¹ The main differences of a polarized light microscope and a standard trans-illuminating microscope is the polarizer and a compensator before the condenser, an analyzer behind the objective lens, as well as a graduated circular revolving stage.⁶¹ Theoretically, then, a conventional microscope can be turned into a polarizing microscope using add-ons that include the main components. An example of a modern version of the polarizing microscope is LC-PolScope.⁶¹

1.2 Introduction: Current State of Image Acquisition

The main advantage of polarized microscopy is the enhancement of contrast based on optical properties of the sample and is often used to monitor and analyze the early developmental stages of organisms.⁶¹ The main disadvantage is that quantitative observations are difficult in this set up and no significant improvement is gained in speed. Some efforts have been made in specific cases to utilize the advantages of polarized microscopy to increase throughput, but these advantages are case and study specific. Furthermore, they do not provide the ability to simultaneously record multiple samples or switch between multiple samples at an extremely fast rate.⁶² One example is a study conducted by Sugano and colleague where they modified the usual workflow of research concerning certain oral drugs. In the original workflow, drugs were dissolved in a DMSO compound. Sugano and colleague instead used a solid form of the drug precipitate to study the effects of the drug. This change provided a high-throughput method for investigating the solubility properties of the compounds, however it was specific to that case only.⁶² Another technique taking advantage of inherent optical properties of the specimen is DIC.

1.2.10 - Differential Interference contrast and Phase Contrast microscopy: Similar to polarized light microscopy, **Differential Interference contrast (DIC)** also takes advantage of light polarization and works by separating polarized light into two streams of polarized light that are orthogonal. The technique can be used for unstained and transparent solutions to increase the contrast, as many biological samples are transparent and thus hard to see. DIC is usually most ideal for undyed samples and IR light can be used, so that thicker tissues can be imaged more easily.^{63,64} DIC can be installed on most upright or inverted microscopes as long as the essential optical components can be installed.⁶⁵ This interference contrast can then be combined with phase contrast, in dark or bright field illuminations.⁶⁶ **Phase contrast** is a technique which converts phase shifts in light to brightness changes.^{8,66} Phase contrast can take advantage of **refractive index differences** (the differences between the structural details between the specimen and the background) to increase the image contrast. Phase contrast works because generally specimens with higher refractive index slow down light to a greater degree as compared to the background. In certain conditions, efforts have been made to increase throughput using phase contrast microscopy. In one study published in Nature communication by Taute and colleagues, a defocussing phase contract microscopy technique was used for 3D tracking of bacterial movement.⁸ In this technique the diameter of the largest observable diffraction ring is

1.2 Introduction: Current State of Image Acquisition

used to judge the distance in the Z plane. This measurement, complemented by comparing the measured diffraction patterns to an already existing database, allowed the scientists to collect 3D information regarding the movement of certain bacteria with a high-throughput. As powerful as the technique is however, it is still limited to studying bacteria, and is only operational when the needed prerequisite databases are available.⁸

The main disadvantages of DIC are the moderately increased costs, and potential issues related to exogenous dyes or other added compounds as they may affect the birefringence. A third method for using optical properties of a specimen for imaging is spectral imaging.

1.2.11 - Spectral imaging: **Spectral imaging** is a technique that uses multiple bands across the electromagnetic spectrum (which includes but is not necessarily limited to the visible spectrum)^{54, 67}, captures a series of images at different emission wavelengths and joins them together.⁵⁴ A typical camera in spectral imaging can measure 3-15 bands whereas some can image hundreds of bands.⁶⁷ The technique improves on the depth penetration of a conventional confocal microscope, as the latter is limited by the phenomenon of scattering light and light absorption.⁵⁴

There are three main ways of imaging these spectra: optical elements, CMOS sensor or continuous filters such as a filter wheel.⁶⁷ While using optical elements to separate the different wavelengths of light, the image passes through a prism separating the wavelengths which are then imaged.^{68, 69} This technique requires significant calibration. Alternatively, CMOS sensors can have filters in front of the sensor and thus require no optical parts. These sensors are much more affordable and easier to use.^{68, 69} And finally the last variation uses a filter wheel set up, where a filter wheel turns the desired filter to position for each wavelength of interest in the optical path. This however limits the speed of acquisition as the wheel must continually turn and be precisely positioned. Spectral cameras themselves are similar to RGB cameras, in that they have different pixels to detect different parts of the electromagnetic spectrum,^{68, 69} but different in that spectral cameras have more subpixels for different wavelengths, up to 16, and that in many setups these wavelengths which can be changed, and are not necessarily limited to red, green, and blue portions of the visible light.^{68, 69} In many cases, confocal or fluorescent microscopes can be converted for spectral imaging.⁷⁰ As powerful as spectral imaging can be, it is also limited by spatial resolution (when using a spectral camera) or speed (when using a filter

1.2 Introduction: Current State of Image Acquisition

wheel) , highlighting yet again the trade-offs in microscopy.⁵⁴ Similar to some of the previously mentioned techniques, attempts have been made to use the capabilities of spectral imaging to achieve higher throughput, however, again, similar to previous techniques, the increase in speed is primarily applicable only to certain settings. An example was demonstrated by one study where a special filter was used to image real-time fluorescence spectra from photoactivated silver clusters on a specialized silver plated film, called silver island film. This technique allowed scientists to distinguish different luminescent spots in a large area with sub-second accuracy. Although such techniques do not provide the same capabilities as RAP, it is possible that such a technique, along with a spectral camera be incorporated in RAP to provide a system with even greater capabilities.⁷¹

1.2.12 - Fluorescence microscopy: The basic concept of **fluorescence microscopy** involves the absorption of a photon by an indicator which has been attached to a component of a cell, followed by emission of a photon with a different energy (hence different wavelength) a few nanoseconds later, by that same indicator.⁵⁴ The primary goal is to only capture light emitted by the indicator, and block out any other light. This technique is quite versatile and can be applied to many optical setups. For example, dyes can be of many different forms, and different methods can be used to excite the dyes, and various methods can be used to detect the light, a property that is taken advantage of where colocalization of multiple proteins need to be examined. It is also possible for an indicator to absorb energy from multiple photons but emit only one photon.⁵⁴ Because of these qualities and flexibilities, fluorescence microscopy can provide specific and sensitive data regarding biochemical, biophysical and structural status of cells, and provide high levels of temporal and spatial resolution, including 3D, enhancement of contrast, and precise spatial resolution with reduced background noise.⁷²

Fluorescence can also be very useful in studying the interaction of cell components over time. This includes information regarding reaction kinetics, morphological changes of the cell, fluorophore movement itself, cell growth and division, etc. Additionally, fluorescence intensity measurements can provide protein concentration data and help with monitoring cell volume, as well as membrane fusion or fission events among cells and subcellular compartments. Furthermore, multicolor fluorescence sampling can show the relationship between different

1.2 Introduction: Current State of Image Acquisition

substrates, allowing us to measure protein conformational changes, binding, as well as aggregation.¹⁰

Advances in fluorescence microscopy are continuously being carried out and variants of fluorescence microscopy can be more specifically catered to specific needs, such as Forster Resonance Energy Transfer (FRET), which can provide high-resolution capabilities;⁷² (FLIM) fluorescence lifetime imaging microscopy for investigating protein-protein interactions in living specimens;⁷² second and third harmonic generation (SHG or THG)⁷²; and 2-photon and light sheet microscopy to study neuron dynamics in vivo.⁷² Several other approaches include PALM and STORM,⁵⁴ where the basis of these approaches is to obtain a series of sparsely spaced samples and combine them, increasing spatial resolution at the cost of temporal resolution.⁵⁴ Overall then, four important aspects of fluorescence microscopy are its high contrast, its quantitative nature, its high specificity and that it can be used in live cells⁷⁴. Fluorescence microscopy is currently one of the most popular microscopy techniques and is also used in some high-throughput applications such as the FLIPR system mentioned earlier in this text.

Like the previously discussed techniques, fluorescence microscopy, as versatile and useful as it is, has several limitations. First, it is labor intensive and requires trained personnel to prepare, load and handle the samples, as well as find and focus and properly image the samples. The second limitation is the high cost, and the third is that the steps needed to capture an image are generally linear and rely on one another. As a result, slower steps become a bottleneck to the speed of the overall process.¹⁰ A fourth problem is that the limited light that is emitted by the fluorophores can be hard to collect, especially that the inevitably needed filters further decrease the amount of light available due to imperfections in design and manufacturing of the filters. A fifth problem is that not all components of the cell can be fluorescently labelled, and in those that can be, **photobleaching** and out of focus light can introduce practical challenges. Light sheet microscopy attempts to alleviate the latter problem.

1.2.13 - Light sheet scanning: **Light sheet microscopy** improves upon conventional microscopy by illuminating only the plane of interest, primarily by separating the detection and illumination pathways.^{54, 73} The main advantage of light sheet scanning is eliminating a significant portion of the background fluorescence as well as reducing photobleaching, as only the plane being imaged

1.2 Introduction: Current State of Image Acquisition

is illuminated. **Optical sectioning** (using light sheets at different locations in the z-axis) can be achieved by illuminating successive planes. This can be done in various optical setups including confocal and multiphoton microscopy.⁵⁴ Additionally optical sectioning allows us to image large 3D organisms without physically deforming them, observe dynamic 3D processes over time, and freely position the sample in space.⁷³ Many variations of light sheet microscopy can be introduced to match the specific needs of the experiment.⁷⁴ In one variation, the illumination pathway uses a condensing lens to condense the light rays in one position.⁷⁴ Another method is the use of a lens, with either a high or low **Numerical Aperture (NA)**, depending on whether a thin sheet with a small field of view or a thicker sheet with a larger field of view is needed.⁷³ Light sheet microscopy can be very useful in cases where the sample is light sensitive and/or a high level of precision in illumination is needed. This technique however does carry certain limitations. One is the nonuniformity of the light sheet over longer distances,⁶⁰ and another is shadowing, which occurs when light hits more optically dense areas on its way creating shadows behind it.⁷⁵

1.2.14 - FRET: Forster Resonance Energy Transfer (FRET) is the measure of energy transfers *between* fluorescently lit molecules and is a measure of how many molecules in a given volume are interacting.⁷⁶⁻⁷⁹ This occurs when energy that is excited within a high energy fluorophore (**donor**) is transferred to an adjacent **acceptor** fluorophore radioactively.⁷⁶ The energy that is absorbed by the acceptor molecule causes the lifetime, intensity and anisotropy of the molecule to change. Because FRET measures the interaction between fluorophores, it is a powerful technique for studying biological processes within a complex cell.⁷⁶

Readouts are small however and as a result sensitive to high signal to noise ratios and FRET studies in living cells produce ample background signal.⁷⁶ As a result of this small signal to noise ratio, and to no lesser degree the large variability between and within cells, FRET is not a very common technique.⁷⁶ FRET is also expensive and is generally low-throughput, although in specific situations, the properties of FRET may be taken advantage of to increase the speed of data collection. One such example is a study by Song and colleagues where they used the capabilities of FRET to measure the dissociation constant (K_d) for certain protein interactions in a specific protein pathway (SUMOylation pathway). Because of the high sensitivity of FRET to energy transfer, the authors were able to study the dissociation constant in a high-throughput

1.2 Introduction: Current State of Image Acquisition

manner. Unfortunately, however, such cases do not easily generalize to many research applications.⁷⁹

1.2.15 - Microfluidics, Optofluidic, and image Flow Cytometry (IFC): Microfluidics, optofluidic, and flow cytometry, are all methods for obtaining similar data from cells as some imaging techniques but without generating a traditional image. **Microfluidics** is a system of directed fluid movement over small distances with capillary action as the main method of transport.

Optofluidics is governing the flow of fluids using light. And **flow cytometry** is a technique where a single cell is suspended in fluid and is passed through a laser, a cell at a time, and the characteristics of the cell are collected and analyzed. Using these techniques one can assess the composition of the cell using absorption measurements from inexpensive detectors, and still gain scientifically valuable information.⁸⁰ These methods are generally simple, efficient, and since multiple microfluidic systems can exist in the same device due to their small size, high throughput. Another such technique with similar characteristic is lens free imaging.

1.2.16 - Lens free: **Lens free** imaging is a new concept that uses shadows cast on a sensor to image the cells. Two different wavelengths of light are used to illuminate the sample with an angle of 45 degrees, the shadow that these two wavelengths generate is then put together electronically and used to construct a sample.⁸¹ The image is then processed digitally, using filters to reconstruct the image and filter out the noise.⁸¹ In one paper the authors used this technique to model the 3D trajectories of human sperm cells.⁸¹ In this experiment the authors were able to achieve a 3D field of view of over 17 mm² and depth of field of approximately 0.5-1 mm with submicron positioning accuracy.⁸¹ This technique can be used to track the motion of other organisms as well.⁸¹

The main advantage of the lens free method is that it allows for better 3D imaging, without the use of traditional equipment, including doing away with lenses. Although this system is fast, it does not form a traditional image, and thus cannot be analyzed in the same way. The system however is more similar to imaging than a technique like flow cytometry. Another system with true images at higher speeds but which compromises on quality is using a modified smartphone camera.

1.2 Introduction: Current State of Image Acquisition

1.2.17 - Smartphone camera microscopy: Smartphone camera microscopy is exactly as the name suggests: using the powers of a camera smartphone, and with some modifications using it as a microscope.⁸² In one paper, the authors compared an easy to build smartphone camera microscope set up to a conventional microscope to see how effective the design can be in practice. The authors used common household products to create a microscope from a generic smartphone camera. They obtained a piece of plastic from a folder and punched a hole through it to create the lens holder,⁸² and used tape and staples to hold the components together. They tested the efficacy of the microscope in identifying cancer cases. A microscopist with the smartphone camera was then given access to the same samples as a microscopist on a conventional camera and asked to make several diagnoses⁸² for BCC (basal cell carcinoma), SCC (squamous cell carcinoma), NMSCs nonmelanoma skin cancers, as well as melanoma.⁸² Out of 80 inflammatory samples, 73.8% were correctly diagnosed using the smartphone camera.⁸² The major advantage of this system is that the system as a whole is relatively cheap and portable, increasing accessibility. The main disadvantage is the low quality of images, and the requirement to image one sample at a time.

1.2.18 - 3D imaging: The modalities described above, and indeed most imaging modalities, primarily focus on 2D imaging. **3D imaging** is a relatively new concept in microscopy. The basic concept so far in science is to scan many 2D images at different z-planes and combine them to create a 3D model or use a point-source laser scanning method which can image 3D objects by having 3 moving mirrors, two that move faster for the X,Y plane and one for the z plane.⁵⁴ A third way is spectral imaging, combined with a form of image analysis technique called “**linear uncoupling**”.⁵⁴ In all of these techniques, it is important to ensure the time it takes to scan the image since if different layers of the 3D object are imaged at vastly different times, the overall 3D image would be very difficult to analyze. To increase the throughput then, two main methods are employed: first by speeding up each step and second by parallelizing image acquisition so that more voxels can be imaged at the same time.⁵² In one study for example, the authors combined the techniques of light-sheet microscopy along with a collection of microlenses to allow for faster imaging of samples in 3D. The cells however were part of the same sample vial. This setup is beneficial when fast 3D imaging of a single vial is needed, but does not provide significant advantages when multiple sample vials must be studied.

1.2 Introduction: Current State of Image Acquisition

Furthermore the workflow still revolves around an automatized and sequential flow, and as such cannot be used to image multiple samples simultaneously or switch between images at the sub-millisecond scale.⁸³ In general, the use of 3D imaging techniques in HTS application is a field still in its infancy.

1.2.19 – Section Summary: In this section the most fundamental microscopy techniques were highlighted. It is clear then that no one technique addresses all possible imaging needs and that trade-offs need to be made in all cases. Our RAP system, like any other imaging modality, presents trade-offs, however we propose that it presents a combination of features and trade-offs that can be of great value to the scientific community and a valuable addition to the already advanced field of microscopy.

Regardless of the microscopy set up or the throughput however, the images acquired from any system need to be processed so that scientifically useful results can be obtained. These images need to be corrected, stored, and analyzed using software and relevant knowledge of the field of study. In all cases there is a cost to data collection which should be balanced with the benefit that the data provides.¹⁰ The primary aim is primarily maximizing the information gathered by each sample and not necessarily the production of visually pleasing images.^{10, 47} The ideal image will produce the most amount of information, accurately and precisely, with the least amount of data to be processed.⁴⁷ Various techniques have been developed and are used to extract information from the images collected.¹⁰ Some of these techniques are explored next.

1.3 Introduction: Image correction, storage, and processing

In practice, imaging systems are less than ideal and suffer from practical limitations and physical constraints. Concepts such as aberrations, optimized data sampling frequencies, the concept of a pixel and the related concepts of signal, background, and noise, as well as the more quantitative image analysis techniques such as thresholding, filtering and Fourier analysis are all inevitable components of most microscopy workflows. Our RAP system and its associated workflow, like any other imaging system, must also take these concepts into account while analyzing and processing the images. This section describes some of the most common concepts that are drawn upon in the subsequent chapters of this thesis.

1.3.1 - Aberrations, and aberration corrections in microscopy: **Aberrations** in microscopy are predictable imperfections that are produced as a result of the imaging technique used. For example, a simple lens produces what is called **chromatic aberration**. This means that the lens will focus different colored rays of light at slightly different distances. Although this is in most cases undesirable, it is certainly predictable and thus can be corrected. This is in fact what happens in a more expensive chromatically corrected lens.⁸⁴ Based on the conditions, the samples and type of microscopy, different techniques can be used to correct aberrations. And it is important to note that simply increasing the resolving power of the microscope will not necessarily eliminate the aberrations.

Aberrations can be measured using the **Point Spread Function (PSF)**, which describes the response of an imaging device to a single point of light, the closer two point sources of light can be while being distinguishable as two separate points, the smaller the PSF.⁸⁴ PSF can then be used to identify **spherical aberrations**, **astigmatisms**, and **coma**, which have characteristic diffraction patterns.⁸⁴ PSF can also be used to measure resolution.⁸⁵

There are several go-to conventional methods available for correcting aberrations. These include the use of higher quality and corrected lenses, more robust equipment, and more stable optical setups. If those means prove insufficient, other more advanced and specialized techniques also exist. One such concept is **Adaptive Optical (AO)** microscopy. The idea is simple: if the degree

1.3 Introduction: Image correction, storage, and processing

and type of the aberrations is known, a wavefront modulator can be used to compensate by applying the opposite distortions, regardless of whether it is a simple or a complex aberration. The compensation can come from physical correction devices such as deformable mirrors and liquid crystal spatial light modulators.⁸⁴

This concept relates to the concept of the “guide star”. A “guide star” can be created by fluorescence excitation or back scattering of an excitation light. This guide star then accumulates aberrations while traversing the sample and instrument before reaching a **wavefront sensor** (A wavefront, is a physical concept referring to the peaks and troughs of wave patterns with the same origin).⁸⁴ At that point its wavefront can be measured and because its original wavefront was known, the measured wavefront can be compared against the original and expected wavefront. Direct wavefront sensing can be applied to a variety of applications such as cultured cells, transparent tissues, as well as opaque samples such as a mouse brain. In direct wavefront measurements a dedicated sensor is used to measure the wavefront directly. The applications of guide star apply in different microscopy formats from widefield to two-photon microscopy.⁸⁴ There are many other methods for correcting aberration, and many of these methods can be more specific to the type of microscopy in use.⁸⁴

1.3.2 - Data sampling: In science and more pertinently in microscopy, adding new samples is often beneficial, but costly at the same time, and the cost can sometimes come with diminishing returns. A balance then needs to be created between the cost associated with scanning more samples and the benefit of new information that can be collected. Imaging too many samples can damage the specimen without providing any additional data and be harder to process, and scanning too little can have its obvious problems.⁴⁷ Many factors need to be considered to obtain an optimal balance. Data acquisition rates, or the rate of **temporal sampling**, refers to the frequency of image acquisition. Temporal oversampling may lead to photobleaching before an event can occur which can result in rare events being missed.⁴⁷ On the other hand, in live cell imaging, if the scanning takes too long, and thus the specimen is temporally under sampled, important cellular events may be missed or moving components can appear distorted.⁴⁷ Other factors more specific to each experiment also need to be taken into consideration such as the capability of the system to record and store data, as well as the sensitivity of the sample to being imaged. In brief then, it is neither ideal to image too frequently, nor is it ideal to image

1.3 Introduction: Image correction, storage, and processing

unfrequently, but rather the right temporal sampling frequency should be used to match the needs of the sample being imaged and the experiment.

1.3.3 - Pixel analysis: The **pixel** is the basic unit of any digital image. In a black and white image, each pixel has two main numbers associated with it: its **intensity** and **pixel size**.⁴⁷ Pixel intensity is brightness associated with each pixel and is correlated to the strength of the light emitted from (in case of a displaying pixel) or light registered (in the case of a sensor pixel), up to the saturation point. Pixel size is a function of the physical dimensions of each pixel.⁴⁷ There may be other numbers such as time-lapse frequency, or spacing between z-stack associated with a pixel, but those numbers are not relevant to most imaging applications.⁴⁷ The numbers associated with each pixel, and the relationship of these numbers between each pixel can be utilized to analyze the picture at a more quantitative level.

Aggregating all the pixel values for each recorded picture or frame, the next three initial numbers in each image as a whole that need to be analyzed are signal, background and noise.⁴⁷ **Signal** is data that refers to the sample of interest, **background** is a constant level of signal that is generated from confounding factors such as the imaging equipment, and **noise** is random variation in pixel intensity that is either introduced from the camera electronics (read noise) or from statistical variations in photon number (shot noise). Usually, background and noise need to be subtracted from the image. In general, background is subtracted by calculating the background either locally and subtracting it from the values in that locality, or doing so globally.⁴⁷ **Noise** on the other hand is mostly a phenomenon of random variation and is more difficult to extract and more sophisticated algorithms can be employed. Once noise and background are suppressed, the true signal can be distinguished.

1.3.4 - Noise: Noise causes random variation in pixel intensity in adjacent pixels and is present with varying degrees in every digital image. This random variation increases uncertainty in the accuracy of the measurements and thus limits the precision of the collected quantitative microscopy data since any differences in the measurements that are within the expected variance of the noise cannot be attributed to the specimen.⁴⁷ This can then get to the point that the data would essentially become useless.⁸⁶ The connection between variability and the statistical power of an experiment are explained in greater depth in the discussion section of this text.

1.3 Introduction: Image correction, storage, and processing

While background, which is generally constant, can be measured and subtracted from the image, shot and read noise is more difficult to subtract because it is a random distribution and thus results in an overall decrease in precision.³⁵ This random distribution can be of varying shapes depending on the underlying cause generating the noise. For example, Poisson noise is always present when counting stochastic quantum events such as the arrival of emitted photons at the detector.^{47, 86} There are different ways of dealing with background noise. Some methods include: using a pipeline for illumination correction,⁸⁶ white referencing, also known as flat field correction, or shading correction - a microscopy method that is used to reduce the effect of uneven illumination by imaging a known uniform background and subsequently subtracting that from the images of interest,⁸⁶ improving the optical path - for example using a more uniform light source-, or simply reducing aberrations.⁸⁶ Another approach is **Illumination Correction Function (ICF)**, where all images for a particular channel and from a specific plate are averaged and smoothed using a median filter.⁸⁶ In high-throughput microscopy the presence of systematic noise can be exacerbated as the linear sequence of steps carry on and each step adds to the accumulated noise.⁸⁶

1.3.5 - Saturation: **Saturation** destroys the linear relationship between number of photons and the intensity values recorded by each pixel. This is because pixels cannot increase their output value after a certain point, and after that point no matter if the light intensity is 0.1% higher or 1000% higher, the value will simply be displayed as the maximum.⁵²

1.3.6 - Overall image analysis: Once all the data has been captured, it needs to be processed. There are myriad ways in which an image can be processed. But three of the most basic concepts are filters, thresholding, and Fourier Analysis. **Filters** apply a pre-set algorithm to an image and multiple filters can be applied to any image. One common filter is smoothing, where each pixel is replaced by the average of its neighbouring pixels, or smoothed using a Gaussian distribution.⁸⁷ Other types of filtering such as nonlinear filtering (eg. median filtering),⁸⁸ are also possible.

Thresholding refers to selecting and filtering out pixels based on whether they hit and/or exceed a certain value.⁸⁹ Thresholding is a dynamic analysis tool that can be applied in many different situations, from removing background to detecting edges. A good example of image analysis

1.3 Introduction: Image correction, storage, and processing

where thresholding is used is cell counting. **Cell Segmentation and Counting (CSC)**, is an unsupervised approach for segmenting and counting cells in high-throughput microscopy.⁹⁰ The image is divided into square patches, which undergoes a gray level clustering, and then an adaptive thresholding technique is used to determine what constitutes a cell. The cells are then labeled, by detecting the centers of the cell, and counted. In this technique then thresholding is used to set a series of predetermined criteria for what constitutes a cell in an experiment and if the image segments meet the criteria they are counted as cells or else they are not.⁹⁰

Thresholding can also be used as part of a more involved analysis techniques such as **Fourier analysis** (aka. **Fourier Transform**) of images which is one of the most powerful data processing techniques. These processes can be used to apply filters; compress digital files and folders; use signals from multiple lower resolution images to construct one higher quality image; extract specific information from data, such as identifying the content of an image; as well as reducing noise.⁹¹ To better understand Fourier image transform, a brief explanation about Fourier transforms in general is required. All complex waves are composed of a sum of simple waves and the basic concept of Fourier transform is decomposing complex waves into its basic unit sine and cosine waves. The same concept applies for images. Fourier transform of images breaks down the images into frequencies. The frequencies are then broken down to their basic sinusoidal elements. In images, this is referred to as discrete Fourier transform and computed using the **Fast Fourier Transform (FFT)** algorithm. The strongest waves have the highest coefficients and play the most significant role in determining the characteristics of the signal. Coefficients below a certain threshold are then discarded. The resulting frequencies can then be transformed back in order to reveal an image with less noise.⁹²

1.3.7 – Section summary: In this section, the primary elements and components of post capture image processing were highlighted. These include aberrations, data sampling frequencies, the concept of a pixel and the related concepts of signal, background, and noise. The more quantitative image analysis techniques of thresholding, filtering and Fourier analysis were also touched upon. Of course the field of image analysis is vast and a thorough overview of the field is beyond the scope of this thesis, however the components mentioned in the preceding pages provide a strong foundation for more complex analyses.

Chapter 2 – System Design

The previous chapter explored the physiology of the cardiac system, action potentials, and rhythm. The importance of various ions and ion channels, genetics, as well as external factors, such as the nervous system and the effect of physical load on the heart and its rhythm were emphasized. I then highlighted various imaging techniques, from very advanced two photon microscopy, to the more common brightfield microscopy and newer alternatives such as smartphone imaging and lens free imaging. The chapter ended with a broad overview of pertinent concepts in post image analysis.

Given that background, in this section, I will highlight the details of the design of RAP, its various components as well as the reasoning behind each design choice.

2. System Design

One key element from the above pages is that each system presents a specific set of trade-offs with regards to speed, resolution, image quality, and price. A perfect system does not yet exist and is not, to our understanding, possible. However, using a new perspective and a novel design we present a system that not only requires less trade-offs but more importantly enables new scientific discoveries by allowing the recording of multiple samples either simultaneously or with very fast switch times (whichever is best suited to the experiment), and doing so inside an incubator to image cells in their natural environment. This is primarily achieved by employing the use of a parabolic reflector, custom 3D printed parts, optomechanical components, a camera, lens arrays, and a microcontroller-controlled LED, and a novel cooling and stabilization mechanism, assembled in a unique optical setup. As we go through the components, an important point is that the many of the components can be exchanged based on the needs of the experiment and the budget, while keeping the novelty of the design intact. In all cases the design reduces the burden of trade-offs, offers increased speed without the equivalent increase in cost, and increase in resolution without the equivalent decrease in speed.

2.1 - System Design: Camera

Our system uses one camera unit. A few considerations lead to the selection of this specific camera, mainly: framerate; the size of the sensor; pixel size; design and shape; and price. In our case, as we were interested in analyzing cardiac monolayer beat patterns in multiwell plates, we needed a camera that has a big enough sensor to capture a field of view of approximately 2mm in diameter, and be able to record at a minimum of 25 frames per second per well for at least 8 wells. The resolution needed to be better than 1 megapixels in order to capture the wave patterns of the cardiac monolayers. The camera we chose fulfills these requirements, but if another experiment requires another set of criteria, another camera could easily be substituted. Our chosen camera is from Basler (Basler acA1300-200um) (Figure 4) and is capable of imaging in grayscale at up to 752 frames a second (fps). The PYTHON 1300, CMOS Sensor has a Max. Image Circle of 1/2" with a sensor Size of 6.1 mm x



Figure 4 The camera currently used in our system is the Basler acA1300-200um.

2.1 - System Design: Camera

4.9 mm, a resolution (H*V) of 1280 px * 1024 px and Pixel Size (H*V) of 4.8 μm * 4.8 μm . The dimensions of the camera itself are 29mm by 29mm by 29mm (L*W*H). The camera costs approximately \$443 USD and was purchased from Edmond Optics. The camera connects to the computer using a USB 3.0 port and runs on the custom PylonViewer software provided by Basler. It also connects to the Arduino via a **Transistor–Transistor Logic (TTL)** cable (round plug on the back of the camera in figure 4).

The camera is set to only take a picture with a pre-set exposure time when triggered by the Arduino using the TTL cable. This ensures that the frame rate of the camera and the LED ON time exactly match so that the camera starts the light collection process for each frame when and only when the corresponding LED is ON, and continues for the pre-set exposure time.

In our setup, the camera is removed from the casing and flushly inserted into the system in a custom designed and 3D printed casing (Figure 5 B&C). This casing significantly reduces the height of the blockage around the lens as compared to the original ring seen in the right image in Figure 4. This is necessary because the raised ring around the sensor in the original casing that the camera ships in blocks light that is reaching the camera on an angle, and in our system most of the light is hitting the camera on an angle. The angular incident rays hitting the the camera from the surface of the mirror can be seen in Figure 5A.

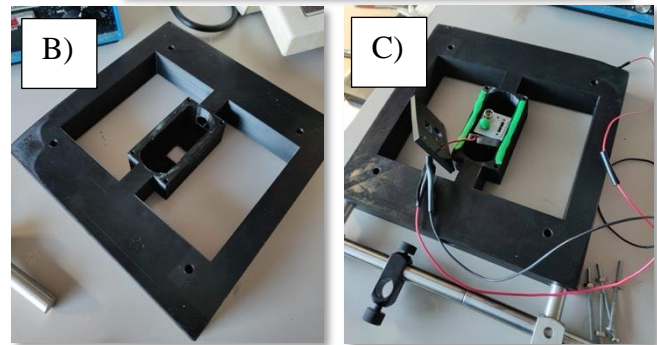
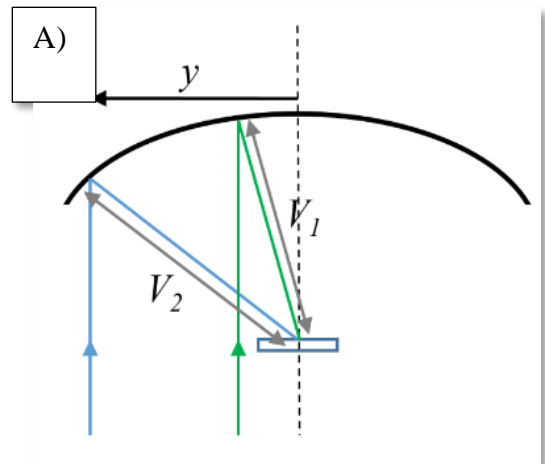


Figure 5 A) Path of light from the LEDs to the surface of the mirror and thence to the camera.² It can be seen that as y – the horizontal distance between the surface of the mirror and the optical axis – increases, so does the angle of incidence B) 3D printed camera assembly, top view C) 3D printed camera assembly with the camera and fan inserted. The plastic cover is then fastened to secure the housing.

2.2 - System Design: Lenses

2.2.1 - Our setup: RAP uses two types of lenses. The first is an array of **planoconvex** lenses and the second is a **parabolic reflector**. This parabolic reflector acts as the equivalent of a second (focusing) lens for all the samples. Currently an array of 25mm plano-convex lenses and an array of 6mm plano-convex lenses with focal points of 100mm and 72mm respectively from Edmond Optics are used (Figure 6). The details of the parabolic reflector are explained further in section 2.3.

These lenses are housed in customized 3D printed lens holders (Figure 7A). The dimensions of the holders are designed to match a standard 12 well and 96 well plate (125.7 mm by 85.25 mm) and the lenses are positioned directly above where the wells would be. That is, the center of each lens is 26mm apart for the 12 well plate and 9mm apart for the 96 well plate. Each lens opening is comprised of a larger opening where light passes through and a brim that provides enough edge for the lens to sit firmly inside (Figure 7 B, blue arrow). However, as explained further in section 2.4.2, the camera



Figure 6 General structure of Achromatic, planoconvex lenses. Such lenses are flat on one side, convex on the other, and are not corrected for chromatic aberrations. Picture obtained from: <https://www.edmundoptics.com/f/uncoated-plano-convex-pcx-lenses/12002/>

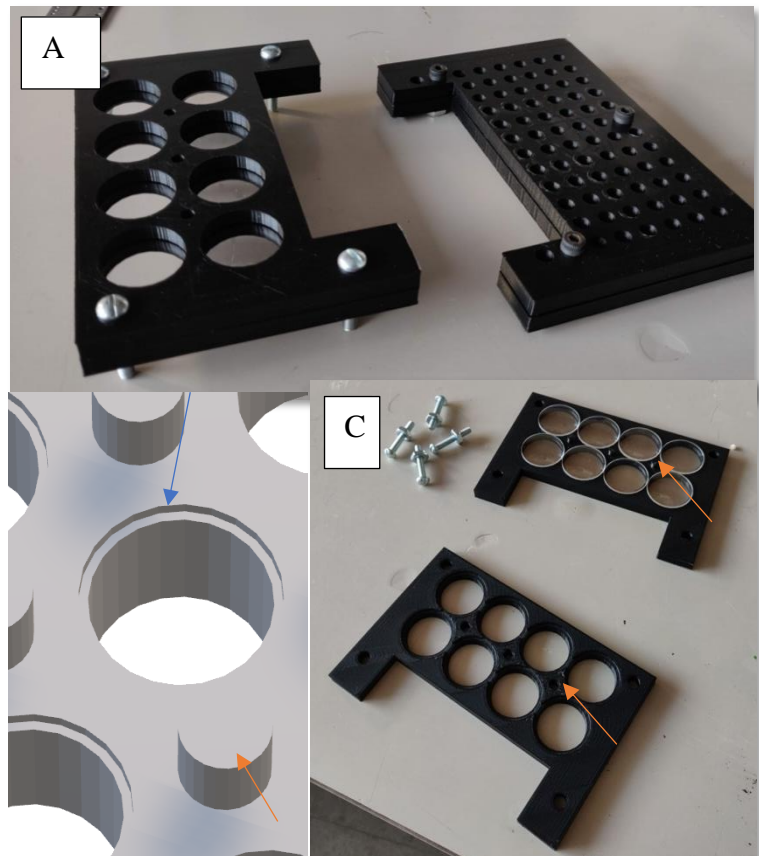


Figure 7 A) Custom designed and 3D printed Lens holder arrays B) zoomed image of an individual lens barrel well showing the opening where light travels. The arrows point to the brim where the edges of the lens sits, (blue arrow) and support columns (orange arrow), C) Lens holder array parts showing the 3D printed components as well as nuts and bolts, before they are assembled. The lens holders are comprised of two parts, one side features support columns and the other features holes to where the support columns are inserted. The lenses are placed on the brim of each hole and the two sides are placed on top of one another, with the support columns providing stability. The two sides are then screwed fast to each other. One such assembly is designed to hold 8, 25mm lenses atop a 12 well plate, and the other is designed to fit 80, 6mm lenses atop a 96 well plate.

2.2 - System Design: Lenses

and fan assembly inevitably take up some space above the samples. This in turn blocks the light coming from the first 2 rows of wells of the 96 well plate and the 1st row of wells for the 12 well plate. The lens arrays are thus designed to omit the corresponding lenses and instead accommodate the camera and fan assembly. As a result, the lens arrays corresponding to the 12 well plate only have 8 lenses and the lens assembly corresponding to the 96 well plate omits the first 2 rows, as seen in Figure 7. The top and bottom half are then fastened together using screws and nuts. Raised columns and corresponding holes (Figure 7 B&C, orange arrows) keep the stability and uniformity of the holder so that all lenses are in the same plane.

It is of note that in our setup lenses can be added and interchanged in the optical path to increase zoom, reduce aberrations, take up less space, cost less or more or address any specific needs of the experiment. In reality, there are many possibilities. A great example is our own two holder plates where one is designed to hold 25 mm lenses to fit above a 12 well plate and the other to hold smaller 9mm lenses and fit above a 96 well plate (Figure 7A).

Lens optics can be complicated and diverse, and a thorough review of all the possible designs, and elements is beyond the scope of this thesis, and interested readers can refer to the myriad sources available on the fundamentals of optics and lens design. A brief explanation of optics however is needed for a better appreciation of the optical setup of RAP. Here I will only attempt to explain what is needed to layout the functioning of our RAP system specifically.

Our system is a multi-lens system, with infinity corrected objectives with a **focal length** of 100mm and **Numerical Aperture (NA)** of 0.124 for the 25mm lenses and focal length of 72mm and NA of 0.043 for the 6mm lenses; and a parabolic mirror with a focal length of 100mm is used to converge the rays (where traditionally a **tube lens** would be) onto the camera sensor. The magnification of the overall system is 1X for the 25mm lenses and 1.4X for the 6mm lenses, and **chromatic aberrations** are not a large concern as the images are recorded in monochrome and the illumination is likewise in monochrome. **Spherical aberrations** and **astigmatism** is present, yet small enough, relative to the overall size and magnitude of the cardiac waves imaged, to not interfere with results of the biological experiments. The **depth of focus** of the system is 0.458mm, and the **resolution** is accurate up to 8.14 μm . The **field of view** is a maximum of

2.2 - System Design: Lenses

4.28 mm. To understand what these specifications mean, as well as the overall lens setup of RAP, a quick review of the basics of optical lenses is necessary.

2.2.2 - Fundamental basics: The simplest lens is a thin lens. Such a lens is theoretical, follows the

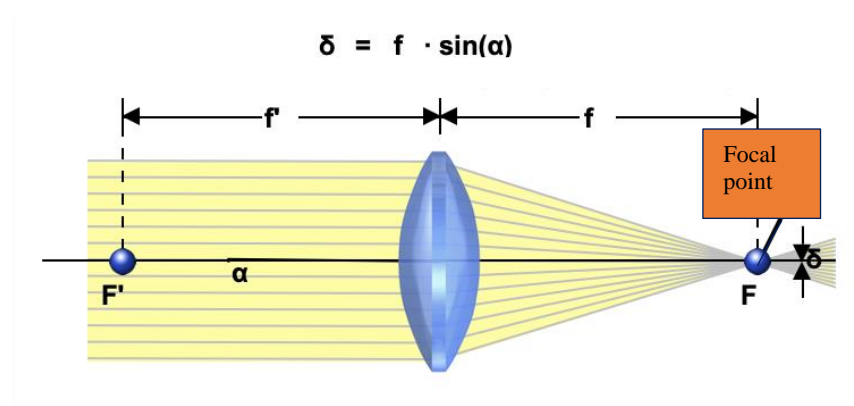


Figure 8 The ideal thin lens, focuses all collimated light that is parallel to its optical axis on its focal point, here depicted by F. Image obtained from an applet from: <https://www.olympus-lifescience.com/en/microscope-resource/primer/java/components/perfectlens/>

and that there are no aberrations. Such a lens focuses all parallel rays coming through it on a single point, aptly named **focal point**, as shown in figure 8.

The reverse is also true, a **point source** of light (light that emanates in all directions from a point) placed at the focal point of the lens, results in collimated light exiting the other side of the

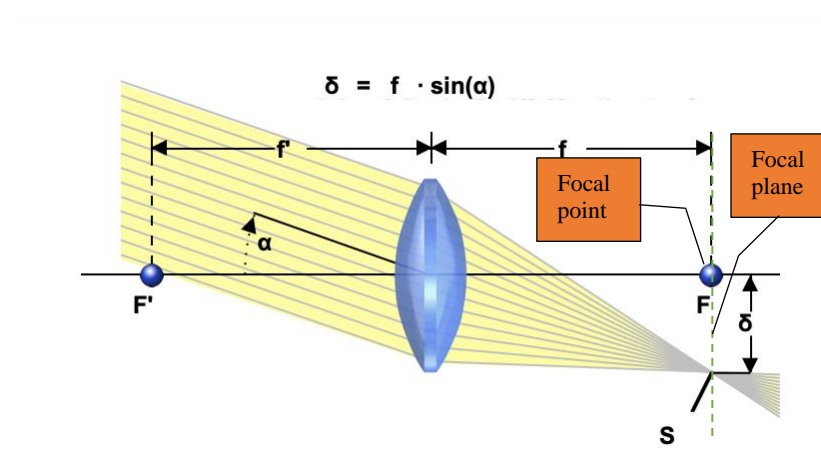


Figure 9 An ideal thin lens focuses parallel light, not parallel to the optical axis on a point on its focal plane, here depicted as S/ The distance of S from the optical axis depends on the angle, α , between the collimated light and the optical axis. Image obtained from an applet from the following link: <https://www.olympus-lifescience.com/en/microscope-resource/primer/java/components/perfectlens/>

basic principles and equations of a lens, and is free of the inevitable defects that occur during the manufacturing of any physical lens. Such a theoretical lens is thin, meaning that light traveling through any part of the lens is subject to the same laws,

lens. Rays that are parallel to each other but not parallel to the optical axis and not perpendicular to the plane of the lens are focused on the **focal plane** of the lens (dashed line in figure 9), but off the optical axis. And the reverse is also true; a point source placed on the focal plane of a lens but off of its optical axis (point “s” in

2.2 - System Design: Lenses

figure 9) will produce collimated light that is at a set angle (α) to the optical axis of the lens.

Other than the special case of the focal point and collimated light, any point source of light on one side of the lens placed beyond the focal point will correspond to an **anti-point** on the other side of the lens where the diverging rays from the point source converge again. The relationship between any point and its antipoint is given by the **thin lens equation** and is dependent on the location of the object and the focal point of the lens.

Equation 1 Ideal Thin lens equation

$$\frac{1}{o} + \frac{1}{i} = \frac{1}{f}$$

,where o is the distance of the object from the lens, i is the distance of the image from the lens and f is the focal point.

Rearranging for the distance of the image, $i = \frac{o*f}{o-f}$. We can see then that far from the focal point, large changes in object position result in only small changes in image position.

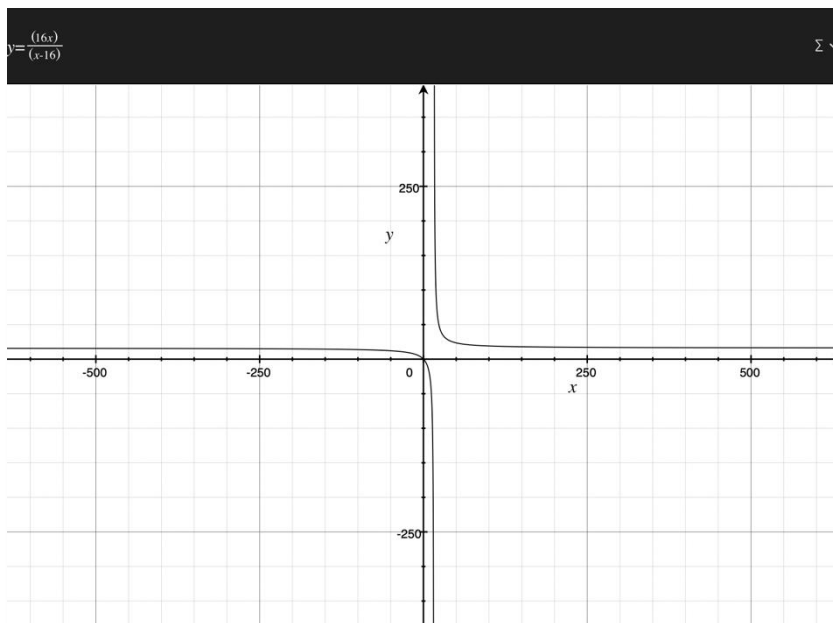


Figure 10 Graph of image vs object distance for a simple lens. x represents the change in object position and y represents the corresponding shift in the distance of the anti-point from the lens. The rearranged ideal thin lens equation is used to draw this graph. An arbitrary focal point of 16 is chosen. Units are not specified as the same principle holds for various units. The graph shows that far from the focal point (in this case values $\gg 16$) large displacement of objects, translate to only small changes in the position of the image.

Cameras focus using this principle. By moving the lens forwards or backwards, they position the camera sensor to where the image is formed. As the anti-point only moves minimally as a result of large variations in object position, given the lens equation above, the camera lens assembly can accommodate large variations in object placement, even though the lens itself is only centimetres

2.2 - System Design: Lenses

long. The asymptotic relationship can be seen in the graph shown in figure 10, for a lens with a focal length of 16mm, the x axis represents the change in object position and the y represents the corresponding shift in the distance of the anti-point from the lens.

In microscopy, objects are generally significantly closer to the lens relative to the focal point of the lens compared to a usual photography set up. In such circumstances, lens properties for objects within one and two focal points from the lens become more relevant. I discuss these properties next.

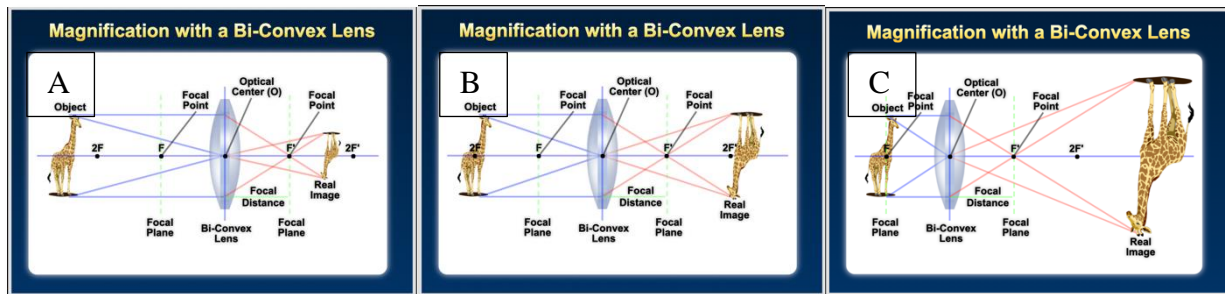


Figure 11 The other three most common cases of object position in front of a lens, in addition to the case described above. A) if the object is placed beyond $2F$, the image is real, inverted, and is smaller than the object B) at exactly $2F$ the image is real, inverted and the same size as the object, C) at just longer than F but less than $2F$, the image is real, inverted, and magnified. The images are obtained from an applet from: <https://www.olympus-lifescience.com/en/microscope-resource/primer/java/lenses/magnify/>

Rays from point sources closer to the lens than the lens's focal distance diverge instead of converge and as a result form a virtual image instead of a real one. A **virtual image** is an image that cannot be projected to a screen. Objects more than $2F$ away from the lens converge to form a minimized image (figure 11 A), objects exactly at $2F$ converge to produce an image of the same size as the original object (Figure 11 B), and objects closer than $2F$ but further than F converge to form a magnified image (Figure 11 C). Objects in this range produce a magnified real image and that is where most older microscopes function. The degree of magnification depends on the curvature of the lens, which in turn determines the focal point. In a multi lens system, each image can be treated as the object of the next lens and magnification multiplied accordingly.

Additionally, the special case that occurs when the object is exactly at the focal point of the lens, i.e. collimation of light, can be utilized to add more versatility to the set up. The simplest case is that of a 2-lens set up.

2.2 - System Design: Lenses

2.2.3 – Multi-lens setup: An optical setup where the object is placed at exactly the focal distance

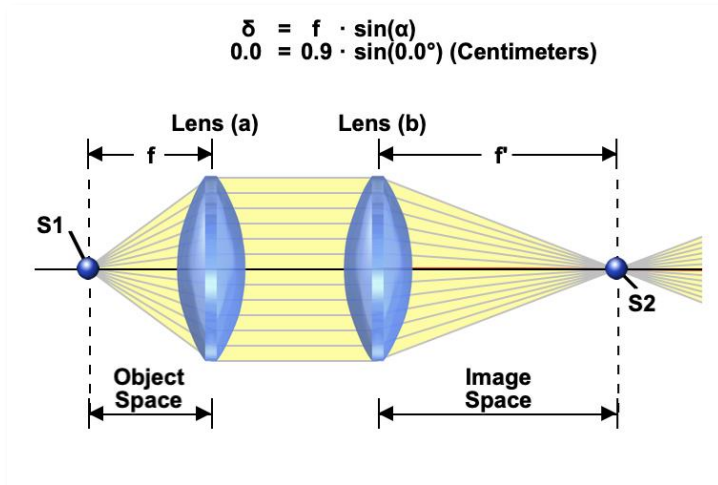


Figure 12 In an infinity corrected system, an object is placed exactly at the focal point of one lens, here S_1 , thus collimating the light, the second lens, which is located along the same optical axis, focuses the collimated light on its own focal point, here S_2 . The resulting magnification is given by the ratio of the two focal points and can be written mathematically as follows:

$m = \frac{f_2}{f_1}$. Image obtained from an applet from: <https://www.olympus-lifescience.com/en/microscope-resource/primer/java/components/twolenssystem/>

of the lens and results in collimated light, is known as an **infinity focused** setup. This collimated light is then focused by a second lens onto its focal point (Figure 12) and the resulting image is magnified by a ratio of the focal length of the second lens to the first lens according to the following formula: $m = \frac{f_2}{f_1}$. This design has two major benefits, first the position of the sample and imaging screen (or sensor) are fixed to exactly the focal point of the corresponding lens, which can make manufacturing easier and more standardized; second, the distance between the two lenses, where the light rays are travelling in a parallel beam, can be very accommodating to the introduction of auxiliary accessories without the need for significant modifications of the optics. Since the light rays are parallel, bring the lenses closer to each other or separating them further away will not have a significant effect on the optical properties of the setup. The accessories that can be included in this light path consist of prisms, filters, mirrors and more. This is important because whereas in simple theoretical diagrams such components may not take any space, in practice they do, and this design is significantly helpful in their accommodation. Objectives that collimate light in such fashion are called **infinity corrected** objectives and it is of this set up that our RAP device is based on.

Those are the basics of lens function. These basic principles can then be combined in tandem and in a myriad way to produce the desired effects and many additional lenses can be combined in an array to correct for various forms of aberrations but nevertheless the basic principles stay the same. The next three sections will explore aberrations, illumination, and some other measurements.

2.2 - System Design: Lenses

2.2.4 - Aberrations: Of course, real lenses, objectives and imaging systems are generally much more complicated than the simple cases described above. In the vast majority of cases,

complications and imperfections occur due to practical and physical constraints. To correct for these **aberrations** and bring the outputs of a lens assembly, like an objective lens of a microscope, as close to an ideal thin lens as possible, additional lenses are generally introduced.

Two primary limitations in most setups that must be

corrected are chromatic and spherical aberrations (Figure 13). **Chromatic aberration** refers to the fact that light rays of different wavelength (i.e. different colors) are bent with slightly different angles as they pass through a simple lens and thus do not all focus at exactly the same point. **Spherical aberrations** are primarily due to the fact that light passing through the edges of a lens does not focus on exactly the same point as light travelling through the center of a lens. Modern objective lenses have many lens components, each complementing each other, that are meant to correct for such aberrations as a whole. Our system however does not suffer from color aberrations extensively because it is a monochrome system. Spherical aberrations are present, yet due to the low magnification of the system, these aberrations are not severe.

2.2.5 - Other measurements: Other more complicated calculations relevant to our system are magnification, numerical aperture, resolution, depth of field and field of view. **Magnification** is of two types, optical and digital. **Digital magnification** is computational and is dependent on display sizes and software. **Optical magnification** is magnification using physical optical components. Digital magnification does not increase resolution, but optical magnification can. The optical magnification of our system, as it is an infinity corrected two lens system, depends

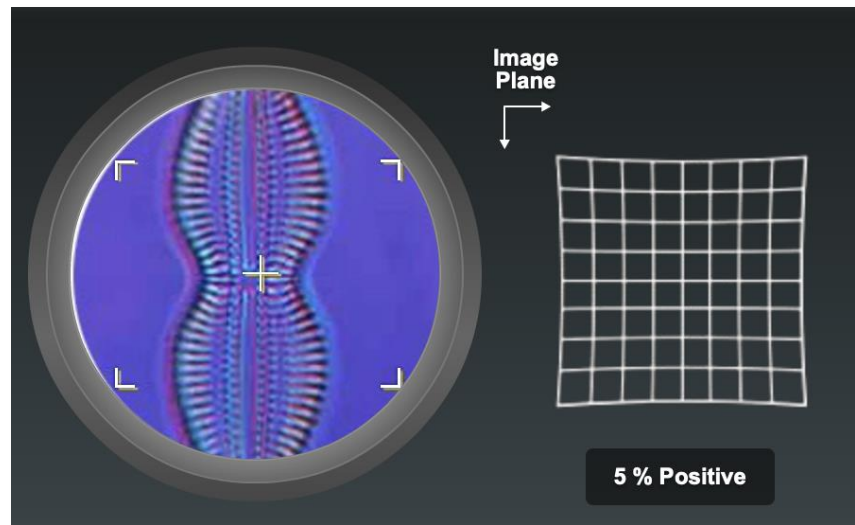


Figure 13 An example of a spherical aberration. We can see that lines closer to the edges are more warped than the lines closer to the center. This is caused by the slight variations in the angle of curvature of light, as it passes through the edges of the lens versus its center. Modified from an image obtained from: <https://www.olympus-lifescience.com/en/microscope-resource/primer/java/aberrations/distortion/>

2.2 - System Design: Lenses

on the ratio of the focal length of the second lens to the focal length of objective lens. In our system, the parabolic mirror acts as the second lens and its focal length is used in the calculations. The formula is then, with f_p denoting the focal point of the parabolic mirror and f_o denoting the focal point of the objective lens:

$$m = \frac{f_p}{f_o} = 100\text{mm} / 100\text{mm} = 1X \quad \text{for the 25mm lens , and}$$

$$m = \frac{f_p}{f_o} = 100\text{mm} / 72\text{mm} = 1.4X \quad \text{for the 6mm lens}$$

The next concept is **Numerical Aperture (NA)**. NA is a measure of how wide of a field of view the lenses can collect light from, which depends on the focal length of the lens and the diameter of the lens, the wider the lens and the shorter the focal length, the wider the angle, as shown in Figure 14. RAP uses 25 mm diameter lenses with a focal length of 100 mm above the wells in a 12 well plate and 6 mm diameter lenses with a focal length of 72 mm above a 96 well plate. Given the Numerical Aperture formula: $NA = n \cdot \sin(\mu)$ or $NA = n \cdot \sin(\theta)$, the NA of the device is calculated as follows:

$$\text{Numerical Aperture (NA)} = n \cdot \sin \theta = 1 \cdot \sin \theta$$

For 6mm lenses:

$$\theta = \tan^{-1}\left(\frac{3.1}{72}\right)$$

$$NA = \sin\left(\tan^{-1}\left(\frac{3.1}{72}\right)\right) = 0.043$$

For 25mm lenses:

$$\theta = \tan^{-1}\left(\frac{12.5}{100}\right)$$

$$NA = \sin\left(\tan^{-1}\left(\frac{12.5}{100}\right)\right) = 0.124$$

The next concept is resolution. The **resolution** of a device, as previously explained is the smallest distance between two points where such two points can still be distinguished as two separate points in the image. The relationship between this distance, r , and wavelength of light, λ , and numerical aperture (which itself is a function of focal length and lens diameter) is: $Resolution(r) = \frac{\lambda}{2 \cdot NA}$. It is interesting to note that resolution is not a function of magnification. As a result, using the wavelength of blue light 700nm and a NA of 0.124 the resolution can be calculated as such:

$$r = \frac{700nm}{2 \cdot 0.043} = 8.14\mu m$$

In a digital set up, if r is smaller than the sensor pixel size the limiting factor of resolution becomes the sensor's pixel size of the camera. In RAP this is not the case as the optical resolution is lower than the sensor's pixel size, thus the limiting factor is the optics.

The next concept is **depth of field**. Theoretically, given any optical single sensor set up, only 1 plane of light is ever in focus with a lens. Yet once subjectivity is factored in, that is, the ability of human observers to categorize ever so slightly out of focus images as in focus, there is a range over which images still appear in focus. This can be quantified with different formulas, but a common formula is the one developed by Rudolf Oldenbourg and Michael Shribak:⁹³

$$DOF = d_{wave} + d_{geom} \\ = \frac{\lambda * n}{NA^2} + \frac{p_{sens} * n}{NA * M}$$

Equation 2 Depth of Field formula, Oldenbourg and Michael Shribak

According to this formula the depth of field of our system is :

$$DOF = \frac{\lambda * n}{NA^2} + \frac{p_{sens} * n}{NA * M} = \frac{700nm * 1}{0.043^2} + \frac{4.8\mu m * 1}{0.043 * 1.4} \cong 0.458 mm$$

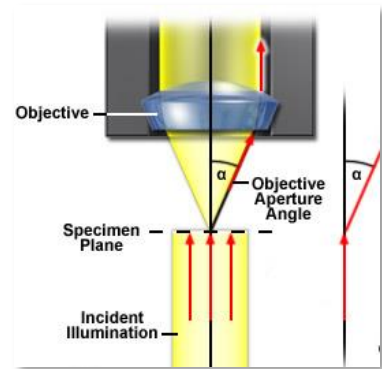


Figure 14 Numerical Aperture is a measure of how wide of a field of view the lenses can collect light from. This depends on the focal length and the diameter of the lens. A wider lens and a shorter focal length results in a wider angle α . Different applications may benefit from smaller or larger numerical aperture. Imaged modified from: <https://www.zeiss.com/microscopy/us/solutions/reference/basic-microscopy/numerical-aperture-and-resolution.html>

2.2 - System Design: Lenses

The last concept is Field of View. The **field of view** is the diameter of the observable area under a microscopy system. Field of view is given by the formula:

$$FOV = \frac{\text{Field Number}}{\text{Magnification}} = \frac{F}{M}$$

In our system the field of view is:

$$FOV = \frac{\text{Field Number}}{\text{Magnification}} = \frac{6\text{mm}}{1.4} = 4.28 \text{ mm}$$

This field of view is somewhat smaller than the diameter of our 96 well plates, measured to be approximately 6.94mm. The FOV then represents approximately 60 % of the each well.

Again, it is important to note that the numbers concerning magnification, numerical aperture, resolution, depth of field, and field of view, heavily depend on the lenses and mirror used, and as such can be easily modified by interchanging the lenses and the parabolic mirror with other ones that better suit the experiment's needs. The optical values achieved by our current setup have been optimized to best suit experiments concerning cardiac monolayer beat patterns.

2.3 - System Design: Dome

The main property of a parabolic mirror is that it converges any **parallel rays** coming perpendicular to the mirror on its focal point, with the curvature of the dome determining the position of the focal length (Figure 16). It is this property that is being primarily utilized in this design. In our double lens optical setup, the dome, also referred to as a parabolic or concave mirror (Figure 15) acts as the second lens. There exists a large degree of flexibility in the choice of dimensions for the dome. The specific dome used in our setup, can, in principle, be changed. Given the requirement of the experiment and the resources available, the dome size can be chosen to satisfy the required needs. The current mirror is a “220mm Dia x 100mm FL Alum. Coated, Parabolic Reflector” from Edmond Optics with a 220 mm diameter, and a focal length of 100 mm. The reflective range is 400 to 700 nano meters.



Figure 15 View of the Dome (Parabolic reflector) from the side (A) and top view (B & C)

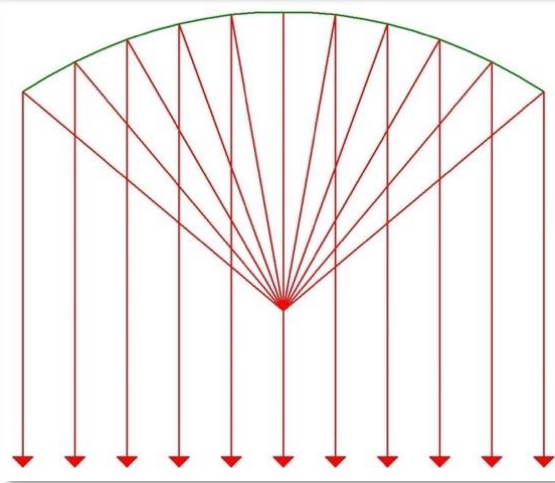
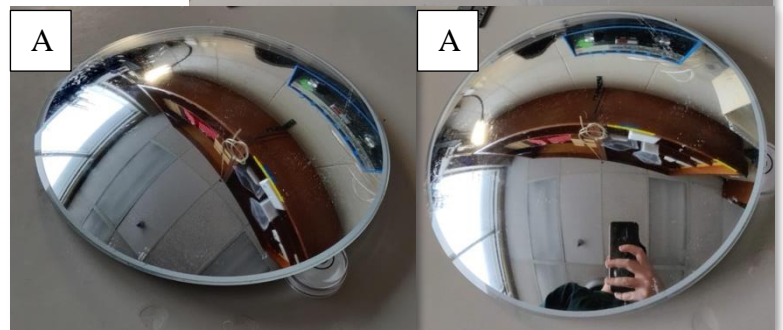


Figure 16 A concave mirror, here referred to as the Dome, focuses all parallel light on its focal plane.² Parallel light that is also parallel to the optical axis of the mirror is focused on the focal point of the mirror. Collimated light that is not parallel to the optical axis is focused on the focal plane but a certain distance from the focal point.

2.4 - System Design: Illumination

can fit inside a greater variety of incubators, with the trade-off of additional components and cost.

The increased distance of LEDs allowing light to act as a source of plane waves comes at the expense of lack of light intensity and decreased brightness. There exists an optimal point then at which the light rays from the LEDs are plane enough while still providing enough photons. Finding this distance was a key component in designing the frame. Through experimentation it was found that the optimal distance between the light sources and the sample is about 3.5 cm. The experiment that was designed was simple, a calibration grid was used, and several images were taken at different heights (Figure 19), graphed (Figure 20) and the distance that produced the image with the highest sharpness was selected as the optimal distance. This distance was $152/32$ inches = 4.75 inches = 12cm. The choice of what constitutes the sharpest image was made using custom written software that detected the edges in an image and the image of the calibration grid with the most detected edges was chosen as the sharpest image. I should emphasise that this only works because images of the same grid were being compared, this method cannot be utilized to compare the sharpness of images of different subjects.

2.4 - System Design: Illumination

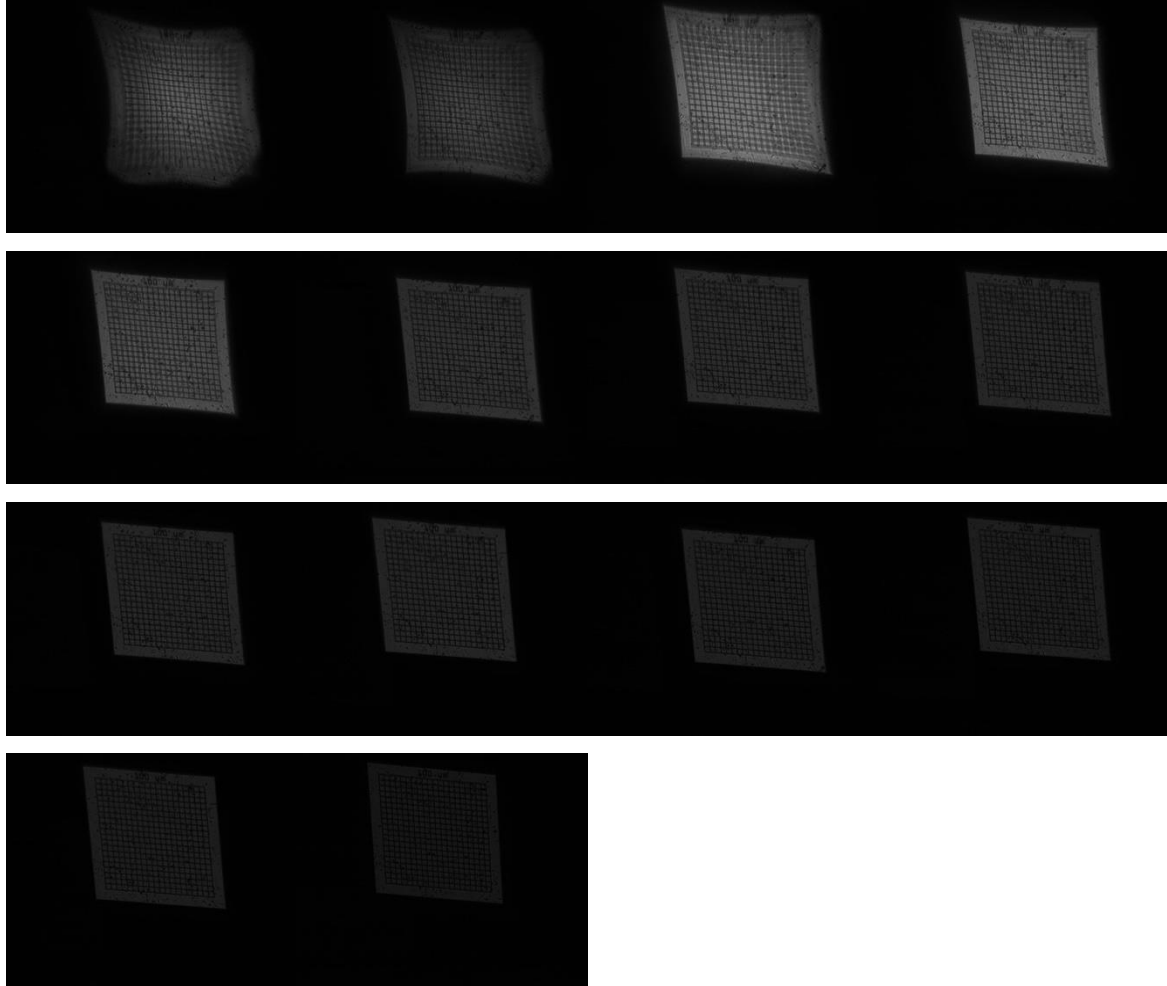


Figure 19 Images of the same calibration slide at increasing distance from the LED light were captured. A trade-off between image brightness and spherical aberrations can be clearly seen. As the distance from the LED to the sample increases, the aberrations decrease but the image also gets dimmer. The images from closest to furthest are in normal English reading order. The grid measures 2mm by 2mm with 100 μm divisions. The grid is called “Multi-Grid standard stage Micrometer” and was purchased from Edmond optics.

2.4 - System Design: Illumination

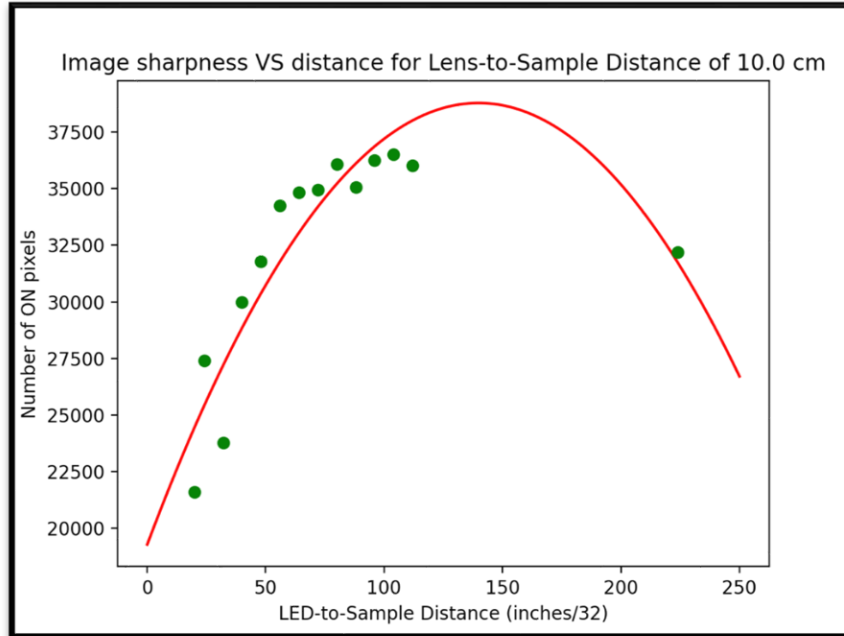


Figure 20 Focus optimization graph. A custom software was used to detect edges in the pictures, and the pixels representing the edges were counted and reported as ON pixels. There is a trade-off between image quality and image brightness. As the distance of the sample and LED increases the number of ON pixels increase, that is more edges are detected, until less edges become detectable as the sample moves too far from the LED and the images become extremely dim. The solid line shows the interpolated curve. The optimal distance then appears to be at approximately 150/32 inches. As the measuring device measuring the LED-to-Sample distance operated using inches, those distance are reported in the same units to preserve greater accuracy.

The next factor in achieving the desired illumination are the components needed to avoid light bleedings, that is, the stacked blocks that prevented light from bleeding out into other samples when the LED under one sample is turned ON. These two pieces can be seen below in figure 21 and their arrangement can be seen in figure 22. The effective result is that only a uniform light beam that is under the sample will be allowed to reach the sample and subsequently reach the

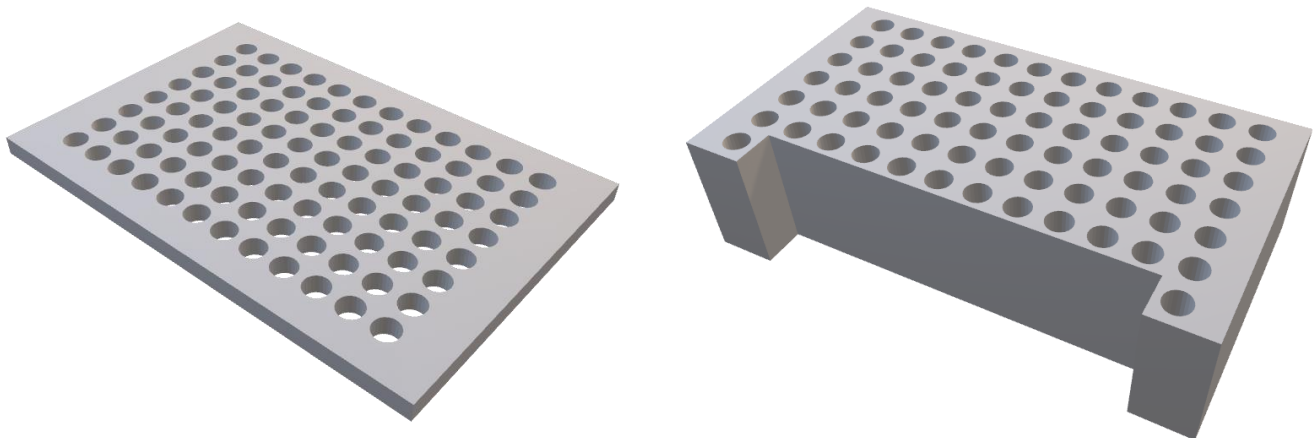


Figure 21 3D printed blocks prevent light from one LED to bleed and illuminate an adjacent sample. The height of the smaller piece to the left is 10mm and the height of the piece to the right is 30mm.

2.4 - System Design: Illumination

lens and any divergent light will be blocked by the plastic piece so that it does not reach the camera. This reduces halo effects. This even illumination can be seen in figure 23.

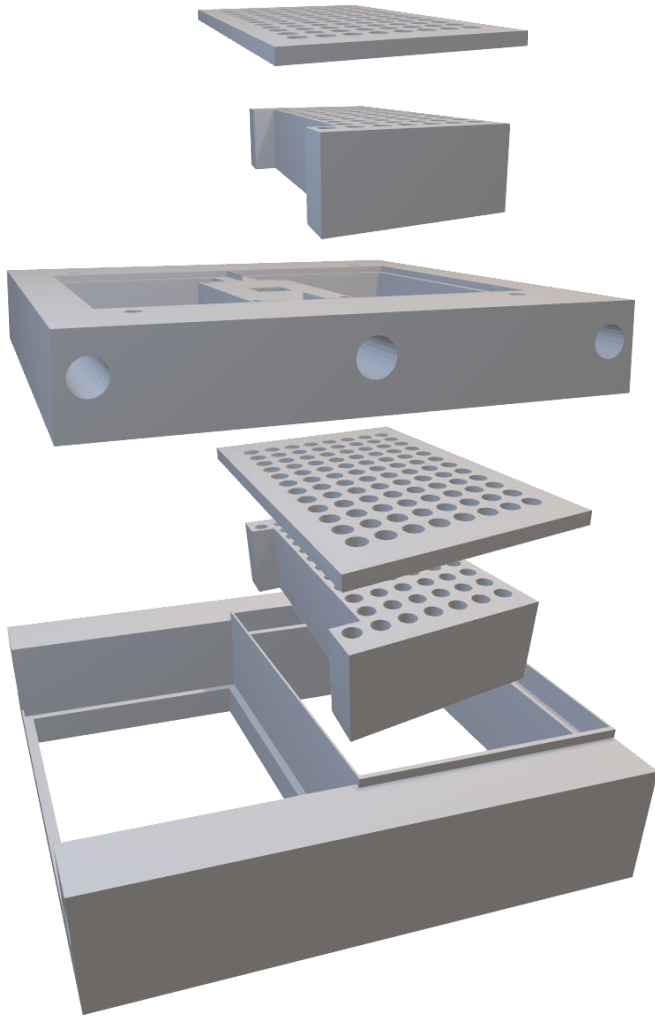


Figure 22 Stacking arrangement of components along the light path. 2 sets of light blocking stacks help improve illumination uniformity, accuracy and precision.

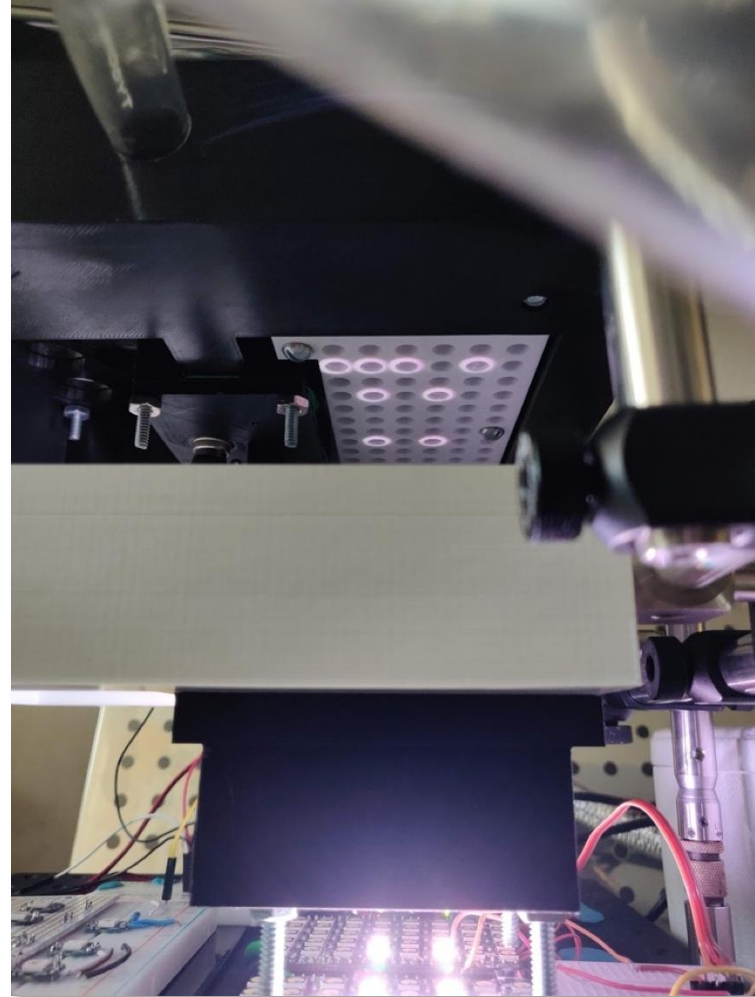


Figure 23 A coherent and even illumination can be seen beneath each sample. Each illuminated ring is from one individual LED. The arrangement of light blocks ensures that while the LEDs are flashing sequentially, there is no halo image from an adjacent sample, due to bleeding of light.

2.5 - System Design: Skeleton/frame

2.5.1 - Design choice: The main frame of the device is a combination of optomechanical elements by Thorlabs and Edmond optics and custom parts designed on google SketchUp and 3D printed using Prusa3Ki, with PLA as the main filament. Figure 24 shows the general skeleton of the device. Several factors have gone into the choice of design and materials. The design is a combination of sourced parts as well as 3D printed parts in order to create a good balance between customizability, cost, flexibility and stability. PLA was chosen because it is strong and relatively inexpensive. PLA has a melting point of between 130 °C and 180 °C and at room temperature is quite sturdy but not brittle. It also has the benefit of being affordable and quite readily available.

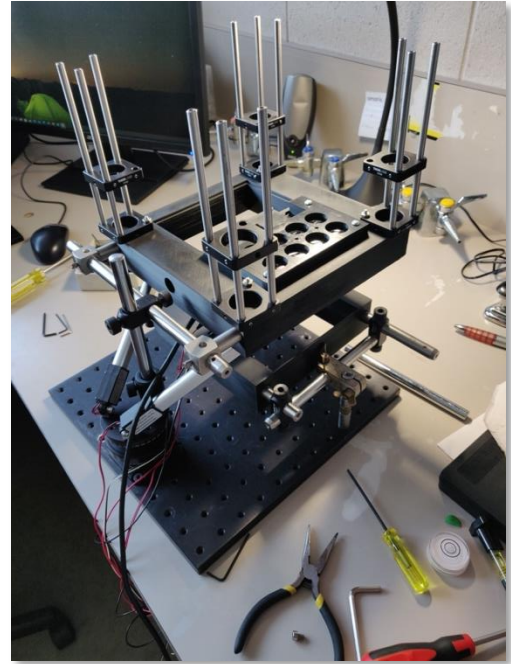


Figure 24 Components of the main frame, consisting of 3D printed parts as well as optomechanical components.

The size of the design was considered in a way that it can fit inside most commercial incubators. The total height is a maximum of 30 cm. This was decided from a survey of the size of most commercial incubators in which the device would be placed. Additionally, the general aesthetic look of the device was also taken into consideration in the design.

2.5.2 - 3D printed parts: Two 3D printed components form the main frame of the system. One is the top piece that encases the camera and its fan, and supports the lens holders and the dome. Figure 25A shows the top view and Figure 25B shows a zoomed in version of the camera holder component. The piece is attached via a rod and two actuators to the lab jack. The lab jack moves the assembly in the vertical direction. The top piece is also connected via more rods from the front side to the sample holder piece (Figure 30) for additional stability. This design is meant to reduce vibration as explained further in section 2.9. This top piece is the more complicated piece of the two 3D printed frame parts. The frame features two holes on the side that hold the metal rods (Figure 30, gold arrows). Two large rectangular openings allow for light to pass through (figure 29, red arrows) and the wedges on the side of the openings support the weight of the lens

2.5 - System Design: Skeleton/frame

holders (figure 29, green arrow). The lens holders are the same size as a 12 well/96 well plate (85mm by 127.1 mm, W*L), however the internal designs can be

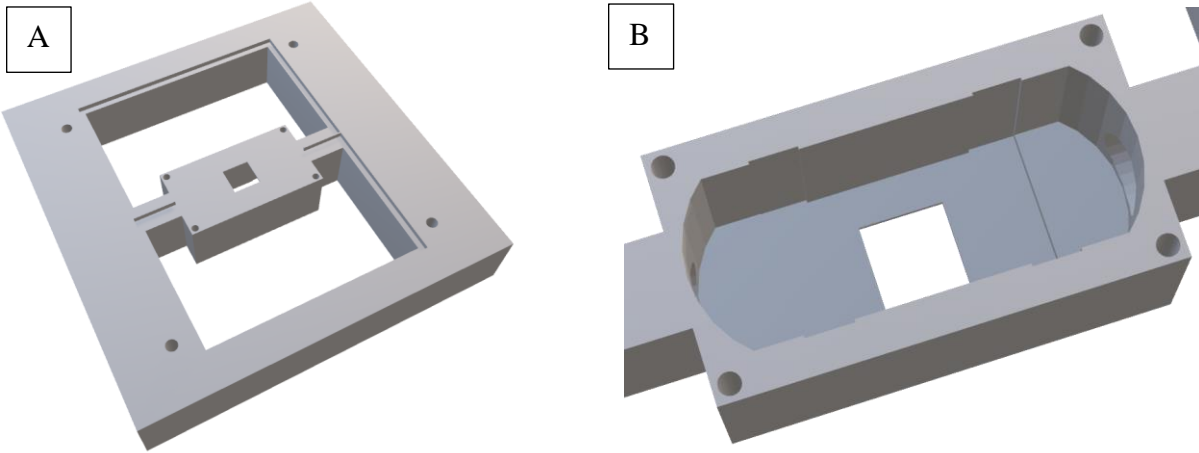


Figure 25 The top 3D printed component supporting the lens arrays as well as the camera and fan housing. (A) The top view of the 3D render is shown as well as (B) the zoomed in image of the inside of the camera housing.

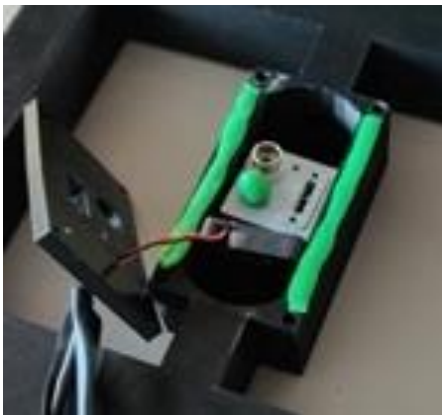


Figure 26 The camera can be seen inside the 3D printed housing. The cooling fan is positioned adjacent to it. The wires pass through the lid, and the lid closes with the green bluetacks sealing the housing.



Figure 27 3D render of the lid for the camera holding assembly.

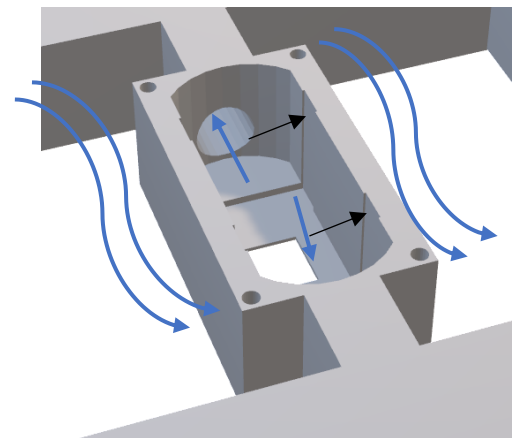


Figure 28 Air flow through the camera holder component. The blue arrows show the openings for air to travel in and out, through the camera. The wedges are where the two fans sit on either side of the camera, circulating the air through the camera.

2.5 - System Design: Skeleton/frame

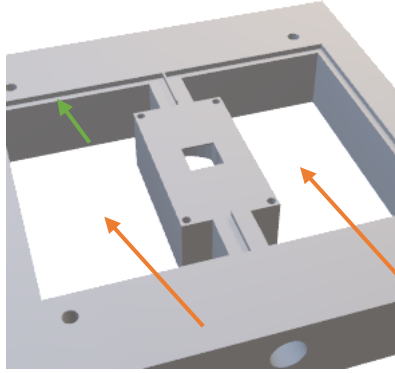


Figure 29 The Lens holder openings consist of two rectangular openings (red arrows) with a brim around the edges (green arrow) to support the weight of the lens arrays.



Figure 30 2 holes on the sides of the frame (gold arrows) allow for optical metal rods to be inserted. The metal rods attach the piece to the rest of the components.

modified to support the appropriate lens array, as explained in section 2.2.1. The large rectangular opening then ensures that light from the samples can reach the lens no matter the specific lens array set up. In between the lens holder openings exists the camera setup. This inevitably blocks some of the light from the samples due to the size of the dome vs the collective size of the camera setup and the 2 lens arrays. But the camera holder is designed to block as little light as possible. The camera holder assembly can be seen in Figure 25B. The camera housing consists of a few key components. First the camera has to fit in snugly in the housing to minimize motion and the sensor needs to be exposed as much as possible. The walls of the housing should be as thin as possible in order to allow as much angular light as possible to reach the camera sensor. Figure 26 shows the camera inside the 3D printed housing. Two slots on either side of the camera allow for the tight placement of two cooling fans, as seen in Figure 28 black arrows. The fans are placed in opposite direction of each other so that a uniform airflow is established. Once the camera and fan are placed securely in place, the enclosing is closed with the lid shown in Figure 27. The Lid is designed to allow for wires from the fans, the USB from the camera and the TTL trigger cable to pass through. The lid is fastened tightly using 4 screws. The green Blue-Tack putty seen in Figure 26 are used to seal the enclosing and the green Blue-Tack ball is designed to mold to the camera's geometry and hold it as straight as possible. This is necessary as even small angular deviations of the sensor can reduce the uniformity of focus throughout an image. This is because the image formed by the parabolic mirror is on a plane that is parallel to the plane of the mirror itself. If the flat surface of camera sensor is not exactly aligned with this flat plane on which the image is formed, but instead deviates by a given angle, the sensor will not be able to capture the entire image with optimal focus. Instead,

2.5 - System Design: Skeleton/frame

different parts of the image will be out of focus by varying amounts, based on the distance of the plane of the sensor to the plane of the image.

Two holes on either side of the camera housing allow for the airflow through the camera (Figure 28, blue arrows). Air can thus pass through the electronic components of the camera. The airflow is directed to an icebox which provides cool air for the camera and accepts warm air from the camera and transfers the energy to melt the ice in the box. This is further explained in section 2.7, as part of the cooling mechanism of the device.

The second 3D printed piece is the sample holder which holds the samples and is attached to the breadboard via metal optical posts (Figure 31). Throughout the design there was a consistent attempt to make the design as small and compact as possible so long as functionality, and stability are not compromised. This bottom piece holds the 12 well and 96 well plates in place. It has two large rectangular openings to allow the passing of light (Figure 31 red arrow), similar to the top piece, and has wedges around the rectangular openings to support the plates and prevent them from falling through (Figure 31 green arrow). This functions similarly to how the top piece supports the lens holder arrays. The walls surrounding the sample are shorter than the height of the plates to facilitate for easy placement and removal of the plates. The height of the holder as a whole is the shortest possible while still allowing for an opening for the metal rods to pass through and providing sufficient structural stability given PLA as the main material and Prusa 3D 3K as the printer.

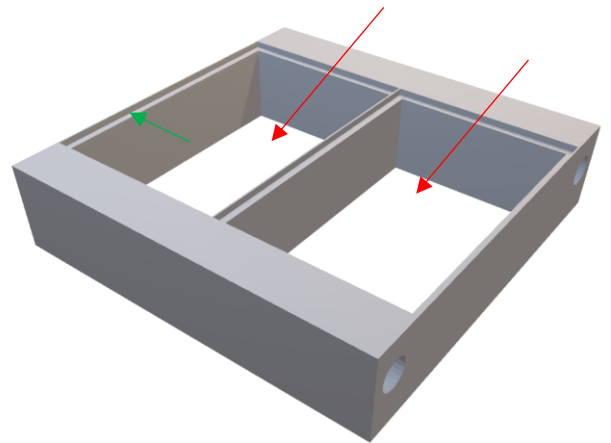


Figure 31 Sample holder assembly. Similar to how the lens holder assembly is constructed, the sample holder assembly also features 2 large rectangular openings (red arrows) with brimmed edges to support the sample plates (green arrow).

2.5 - System Design: Skeleton/frame

2.5.3 - Metal components: The main metal components are the **breadboard**, the optical posts, fasteners, a **compact optical lab jack**,

two **motorized actuator**, and nuts, bolts and screws. The breadboard is an optical breadboard designed to reduce vibrations and hold the components together. The breadboard chosen for our setup is from Edmond optics (Figure 32) and was chosen because it is the thinnest board available that can also provide enough stability. Quarter inch optical posts are used primarily as a skeleton to connect the 3D components to the lab jack and to the base where needed. These are connected to each

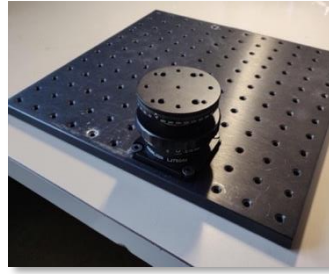


Figure 32 The lab jack is fastened to the breadboard using screws.



Figure 34 The Linear Actuator helps support the top 3D printed piece and is additionally used for adjusting and leveling the top half.

other through optical rod fasteners. A compact lab jack is used to hold the main functional component while being actuable to adjust the focus of the system (Figure 33). This is explained further in the next section, section 2.5. Two motorized actuators (Figure 34) also provide adjustability in leveling the lens and camera plane as there can be slight variations due to the shape and flatness of different tables or incubator shelves supporting the device in various settings. The actuators also serve, in combination with metal rods connected to the front of the lens and sample holders, to hold the camera and lens assembly firmly in place as it can tilt down under its own weight. The role of the actuators is explained further in the next section.



Figure 33 The Lab jack supports the weight of the top half of the system and is used to manually adjust focus.

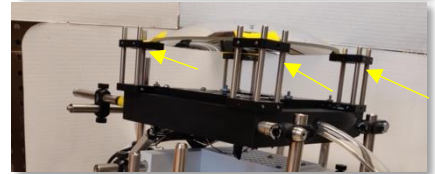
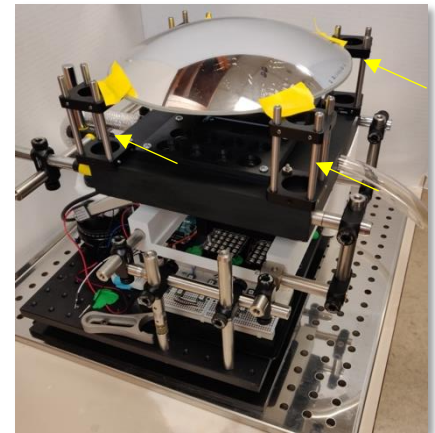


Figure 35 The metal posts (yellow arrows) support the dome. These posts can be finely adjusted with precision.

To hold the dome in place, a group of 4 thin optical posts are attached to the top of the frame so that the dome can be placed on top of them, as seen in Figure 35, yellow arrows. The dome is

2.6 – System Design: Adjustability and focus

placed on top of 3D printed plastic piece because the dome has to move in conjunction with the camera and lens assembly so that the camera is always positioned at the focal point of the mirror. The optical posts are used instead of 3D printed parts because micrometer precision is needed to adjust the positioning of the dome on top of the camera so that the camera sensor is exactly at the focal point of the dome. As the depth of focus of the system is in the micrometer scale and the precision of the 3D printer is only in the 10th of a millimeter scale, the use of 3D printed components in this regard was not feasible.

2.6 – System Design: Adjustability and focus

To focus the samples three complementary methods are employed in our system. First is the use of a manual lab jack (Ø2.64" [Ø67.0 mm] Compact Lab Jack from Thorlabs) as seen in Figure 33. This lab jack is capable of a vertical movement of about an inch, and as previously described, the top assembly is mounted on this lab jack. The lab jack is screwed tightly to the breadboard (Figure 32), and is raised and lowered by turning the ring around the jack. Automated, more precise actuators can be placed instead of the manual jack if the experiment requires it, however such a component would considerably add to the overall cost of the device. The RAP system is unique in that all samples are sitting on a single plain; thus, the optimal focus is one that results in the best AVERAGE focus. This is achieved by moving the sample plate in the z direction and capturing multiple images and then selecting the z-position that results in the sharpest image, as selected by eye or a custom algorithm that defines sharpness based on the number of real edges detected.

For the second method of focus, two actuators (12V Micro Linear Actuator 100mm Stroke 32N, from Elmwood electronics) are additionally used (Figure 34). The purpose of these two actuators is to level the top half assembly to reduce angular aberrations and keep everything in the same plane. This is because if the top half assembly which holds the lens arrays is at an angle as compared to the bottom half holding the samples, the distance of each lens from the sample will vary as a function of the angle of tilt. The setup can be seen in the set up shown in Figure 36.

2.6 – System Design: Adjustability and focus

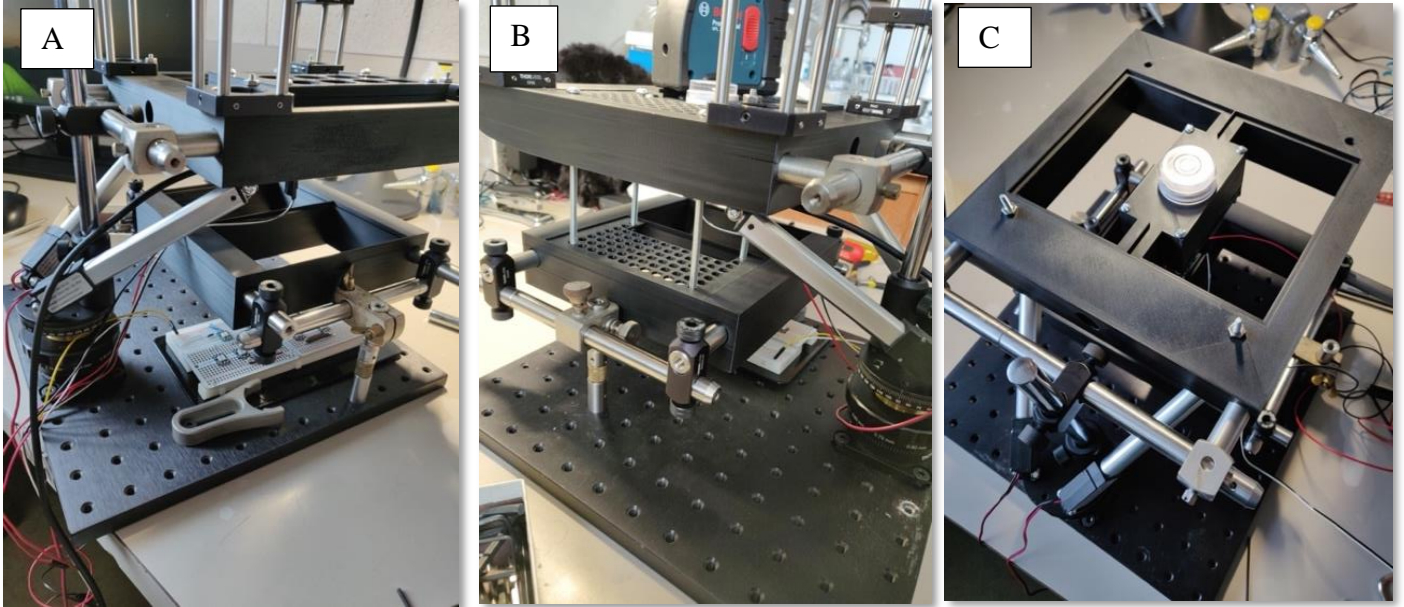


Figure 36 The positioning of the actuators to balance the lens and camera holding assembly A) Right side view B) Left side view C) Top view.

The next concept to note is focus using the inherent optical properties of simple lenses and different wavelengths of light. When using a simple lens, light waves of different frequency (different colors) passing through a simple lens converge at slightly different points. This chromatic aberration in most cases is corrected in optical systems using additional corrective lenses. Our system however uses monochrome light and we instead use this optical property of light to our advantage. Since each wavelength focuses at slightly different distances from the camera sensor, changing the LED color will result in slightly different parts of the sample being in focus. This can be seen from Figure 3C in our eLife paper (Figure 37 below). The picture shows that while one part of the sample is in better focus with blue light, left column, green square, another part of the sample is in better focus using red light, orange square, right column. The details of this concept are also further explained in our paper. ²

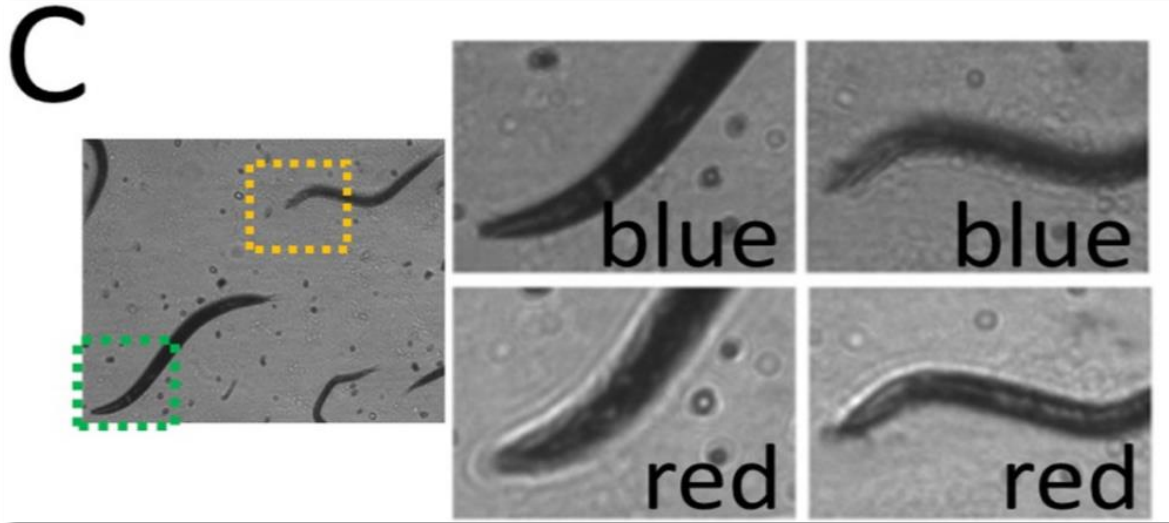


Figure 37 Light of different colors and hence frequencies are focused by a simple lens at slightly different focal points.² We take advantage of this phenomenon to improve focus by changing the wavelength of illumination instead of the position of the sample. In this example the part of the sample in the green square is focused better using blue light, and the part of the sample in the orange square is focused better with a red illumination.

2.7 - System Design: Electronics

2.7.1 - Arduino Uno: In the current version of the device an Arduino board (Figure 38) is used to control the device. An Arduino is a **microcontroller** that can run a preprogrammed algorithm on a loop. In the current RAP setup, the Arduino is used to control the LED array, power the fan cooling the camera, and trigger the camera via a TTL cable for each blink of an LED. As at the moment the device is connected to a computer for image storage and analysis and thus the onboard electronics do not need to process the



Figure 38 An Arduino Uno device is a powerful microcontroller device commonly sourced from commercial retailers. In our device the microcontroller is used to control the LED array, trigger the camera, and power the fans colling the camera

images, an Arduino board with its low cost, is sufficient to control the LED's and trigger the camera with millisecond accuracy and has sufficient power to supply the small cooling fans. As the system gets more self-sustaining, a raspberry Pi device or perhaps an even more powerful computer can be alternatively used so that it may also control the image capture and storage without a need for constant connection to an external computer system. The system may also be setup to support WiFi capabilities for connection to the internet.

2.8 - System Design: Cooling system

2.7.2 - LEDs: The details of illumination were already mentioned in greater details in the illumination section (section 2.4). A brief explanation of the electronics of the LED boards however are explained here. Two sets of LEDs are used to illuminate the samples. A NeoPixel Shield 40 RGB LED from Adafruit Industries LLC, which is a board with LEDs 9mm apart. This matches perfectly with spacing of a standard Eppendorf 96 well plate. To have a perfect spacing for the 12 well plate however, a custom board had to be designed. This custom board is made up of individual NeoPixel LEDs that are soldered together on two partially overlapping breadboards (Figure 18). Each pixel is made up of 3 compound LEDs with red, green and blue channels and the brightness of each is controllable. The NeoPixels are connected in a series and are individually addressable via a single data cable using the Arduino. These lights produce a relatively even, partially coherent, point source of illumination.

2.8 - System Design: Cooling system

The electronics of RAP generate heat. The heat generated by the LEDs are negligible, however the heat generated by the camera was observed to disturb the homeostasis of the incubator when left running inside the incubator for more than approximately 15 minutes. As most incubators are not designed to handle heat generating devices being placed inside them and since the aim was to be able to image cells under physiological conditions inside an incubator, we needed to find a way to place the device inside an incubator. A main design challenge of the device then became finding a way to place the device inside an incubator without overheating the camera components and more importantly without heating up the incubator and disturbing the homeostasis of the cells.

To cool the device then, we use a novel design with an ice box (Figure 40), connected with flexible pipes to the camera holding unit (Figure 39). As the fan operates, cool air is drawn from one side of the camera through designated openings and hot air is blown out from the other opening into the icebox, thus increasing the thermal energy of the ice. The energy that is generated by the camera then primarily melts the ice as opposed to warming up the incubator. The insulated icebox functions so that neither the ice cools the incubator, nor the incubator melts the ice. The complete design produces a closed loop air circulation system and can be seen in Figure 41.

2.8 - System Design: Cooling system

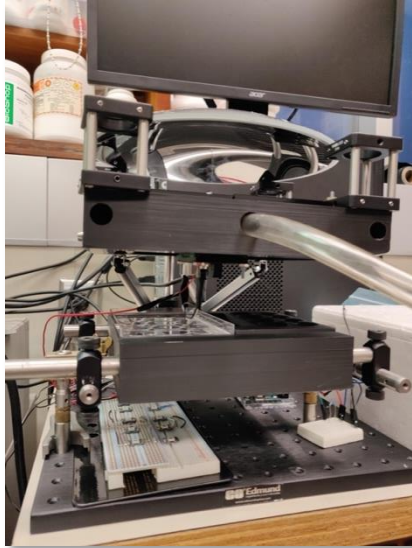


Figure 39 The cooling tubes are inserted into the middle hole of the lens holder assembly.



Figure 40 The ends of the tubes are inserted in the ice box. Cool air is drawn from the box and warm air flows into the box increasing the temperature of the ice.

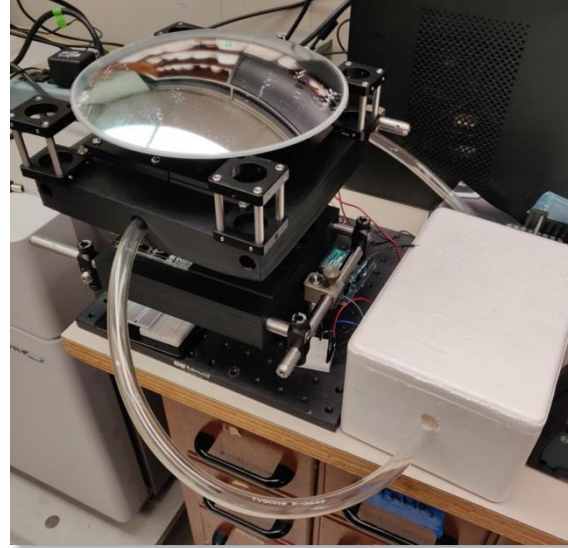


Figure 41 The overall cooling setup sitting outside an incubator for demonstration purposes. The design is then inserted inside an incubator for use.

The icebox design was tested to ensure that the camera can run inside an incubator without disturbing the incubator condition. As the table below (Figure 42) shows, after the initial adjustment period of about 30 minutes, the temperature reading of the incubator, the temperature reading of the camera and the CO₂ readings of the incubator remain relatively stable, with values of 37.2 °C and 5.00% CO₂ level for the incubator and 63 °C for the camera.

The longevity of the ice inside the icebox depends to a considerable degree on the material used to construct the box. The icebox used in RAP is made up of Styrofoam which has a thermal conductivity value of 0.033 (W/m K). The material can also be changed with a PLA box filled with aerogel or fiber glass which have thermal conductivity of 0.13 and 0.003 respectively, if the needs of the experiment dictate. The ice inside the icebox needs to be replaced once the ice has melted and reached the temperature of the incubator. To calculate how much ice is needed for a given period of time, the formula for thermal conductivity, as seen in Equation 3, can be used.

2.8 - System Design: Cooling system

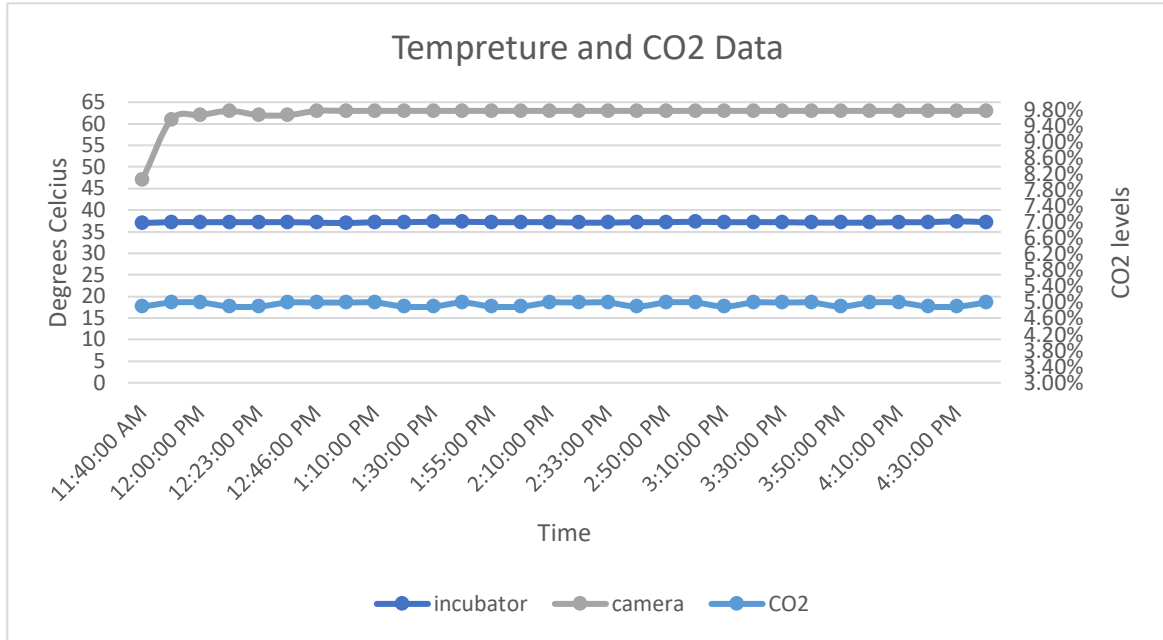


Figure 42 Temperature and CO₂ data from the camera and incubator readings. While using the icebox the temperature of the incubator is constant at 37.2 degrees C, fluctuating only +/- 0.1 °C. The CO₂ level is constant at 5.00%, fluctuating by only 0.1%. The temperature of the camera initially increases to approximately 62 °C, but once it has reached that temperature it stays constant around that temperature, fluctuating by only 0.1 °C.

Equation 3 Thermal conductivity equation

$$K = \frac{QL}{A\Delta T}$$

Where:

- K** is the thermal conductivity in W/m. K
- Q** is the amount of heat transferred through the material in Joules/second or Watts
- L** is the distance between the two isothermal planes
- A** is the area of the surface in square meters
- ΔT** is the difference in temperature in Kelvin

2.8 - System Design: Cooling system

Rearranging the formula for Q (Equation 4) tells us that a material like aerogel with a lower thermal conductivity allows us to create much smaller and thinner walls to give the same thermal insulation, since for a constant Q and decreasing K, L should also decrease.

Equation 4 Heat transfer rate formula

$$Q = KA \frac{\Delta T}{L}$$

Under a theoretical perfectly isolated environment, we expect about 1Kg of ice to melt per 25.8 hours using the current 3W camera and two 0.3 W fans. This translates to 1000g/25.8 hours or 38.7g per hour. For water, this translates to approximately 40ml of ice melted per hour.

In practice 260ml melted in 5 hours, which is

approximately 30% higher than expected, but is

explained by the imperfect insulation of the icebox as well as imperfect seals between different components in the air circulation path. Three main areas are where the tubes are inserted in the top 3D printed housing, the location where the body of the camera seals the camera sensor opening (Figure 25 B), and the seal (Figure 26) around the bottom lid. The calculations can be seen below in Equation 5:

Equation 5 Energy transfer formula

$$1 \text{ Watt} = 1 \frac{\text{Joule}}{\text{second}}$$

$$1 \text{ hour} = 3600 \text{ seconds}$$

Joules in 1 hours running the camera at 3 W

Watts and 2 fans at 0.3 W each = $3600 * 3.6 = 12,960 \text{ Joules}$

melt 1 kg of ice = 334000 Joules

$$\frac{334000 \text{ joule}}{12960 \text{ joule/hour}} = 25.8 \text{ hours}$$

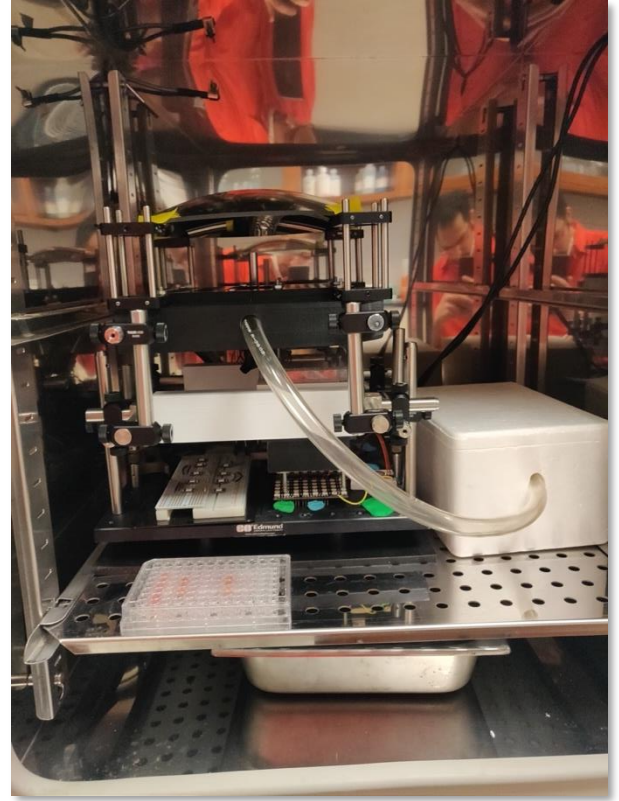


Figure 43 The complete setup fits well inside an incubator.

2.9 - System Design: Fluorescence

Whether fluorescence microscopy is possible is still under question. We predict that fluorescence imaging should be possible given the optical setup, however this would require significantly more expensive optics. Fluorescence microscopy then will be one of the initial goals for the next versions of the system and is considered as part of our future directions.

2.10 – System Design: Vibration isolation

In many expensive microscopy setups, large and heavy **air tables** are used to dampen the noise that is inevitably generated by the environment, such as the building, the movement of machinery in the surrounding lab, the movement of components inside the microscope, but as we intended to place and operate the device inside a commonly available biological incubator, we

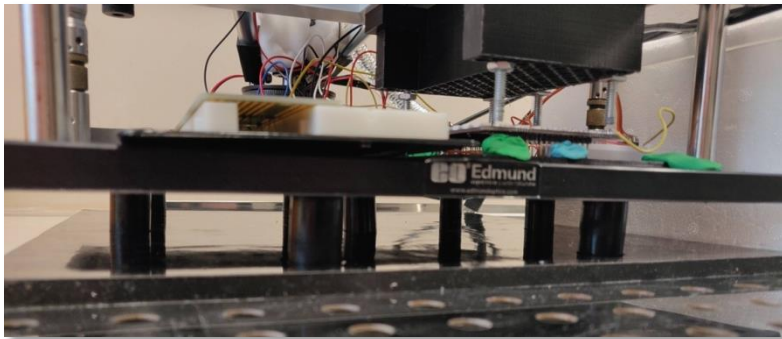


Figure 45 The vibration legs and pad dampen high frequency vibrations.

could not rely on such tables and had to come up with a unique design to counteract noise. To overcome this challenge, two primary methods were employed. The first was the use of vibration isolation pads as can be seen in the image below. These pads are made of Sorbothane (Thorlabs AV3) rubber and are effective at dampening higher frequency vibrations. However lower frequency vibration still presented a challenge.

To solve this problem, we employed the concept of relative motion. The primary idea is that if two objects move in synchrony, relative to a third object, they behave as though they were stationary *relative to each other*. This can be demonstrated with an example. Suppose a camera and a rose are positioned on a table (Figure 45). If either the camera or the rose vibrates



Figure 44 The concept of a rose and a camera can be used to illustrate relative motion. If either the rose or the camera vibrates while the camera is taking an image of the rose, the resulting image will have a significant amount of noise. If, however, both the camera and the rose be anchored to the table and the table vibrates and consequently vibrates both with the same frequency and in sync, the resulting image will be of lower noise, since the camera and the rose were not vibrating relative to each other.

2.10 – System Design: Vibration isolation

independently and an image is taken by the camera of the rose, the image will be blurry and noisy. If however both the rose and the camera are anchored to the table and the table vibrated, the rose and the camera will vibrate in sync. If another image is taken by the camera of the rose under this new setting, the image will contain significantly less vibration noise compared to the first image. This occurs because the camera and the rose are stationary relative to each other.

In our case the solution to the low frequency vibration was to firmly anchor the sample holding platform to the platform containing the camera and lens setup so that they would vibrate in sync. This was done with the use of metal rods and optical fasteners. This can be seen below in Figure 46. If the system needs further focusing adjustments, the fasteners are first loosened, the lab jack is then used to adjust the focus, and then the fasteners are fastened again. All results shown throughout this thesis were recorded with the aid of these vibration reduction designs. Noisy recordings without the use of vibration reduction are available upon request.

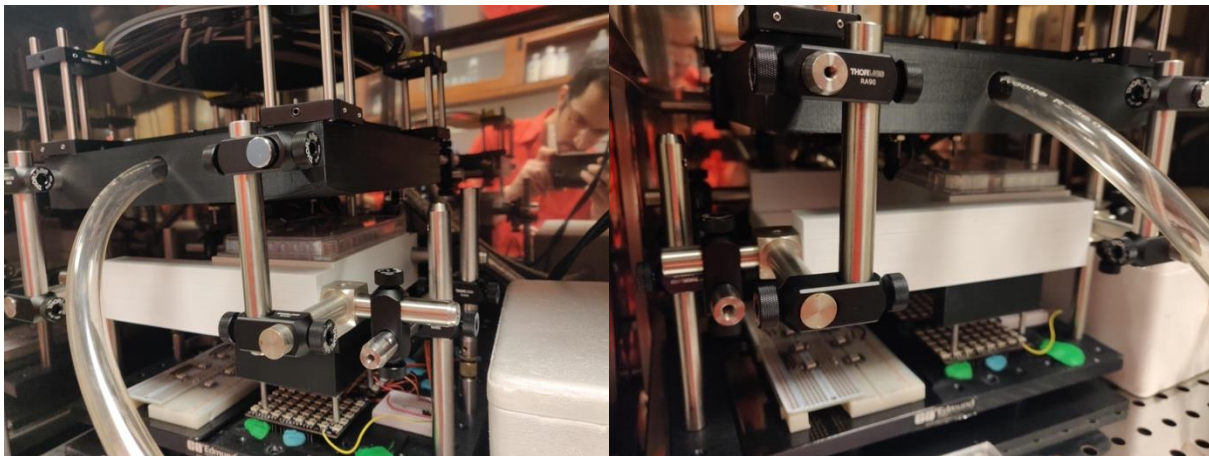
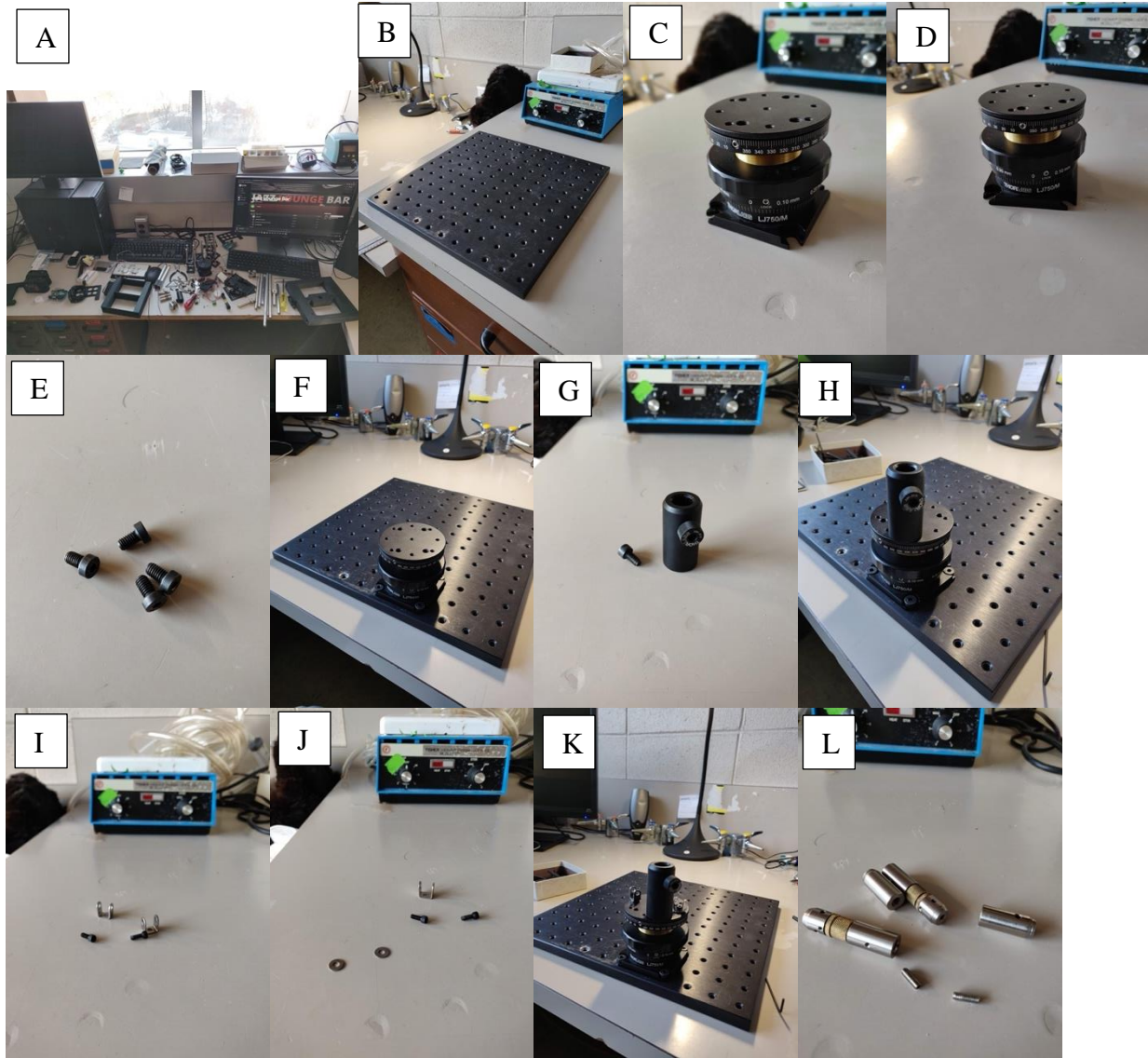


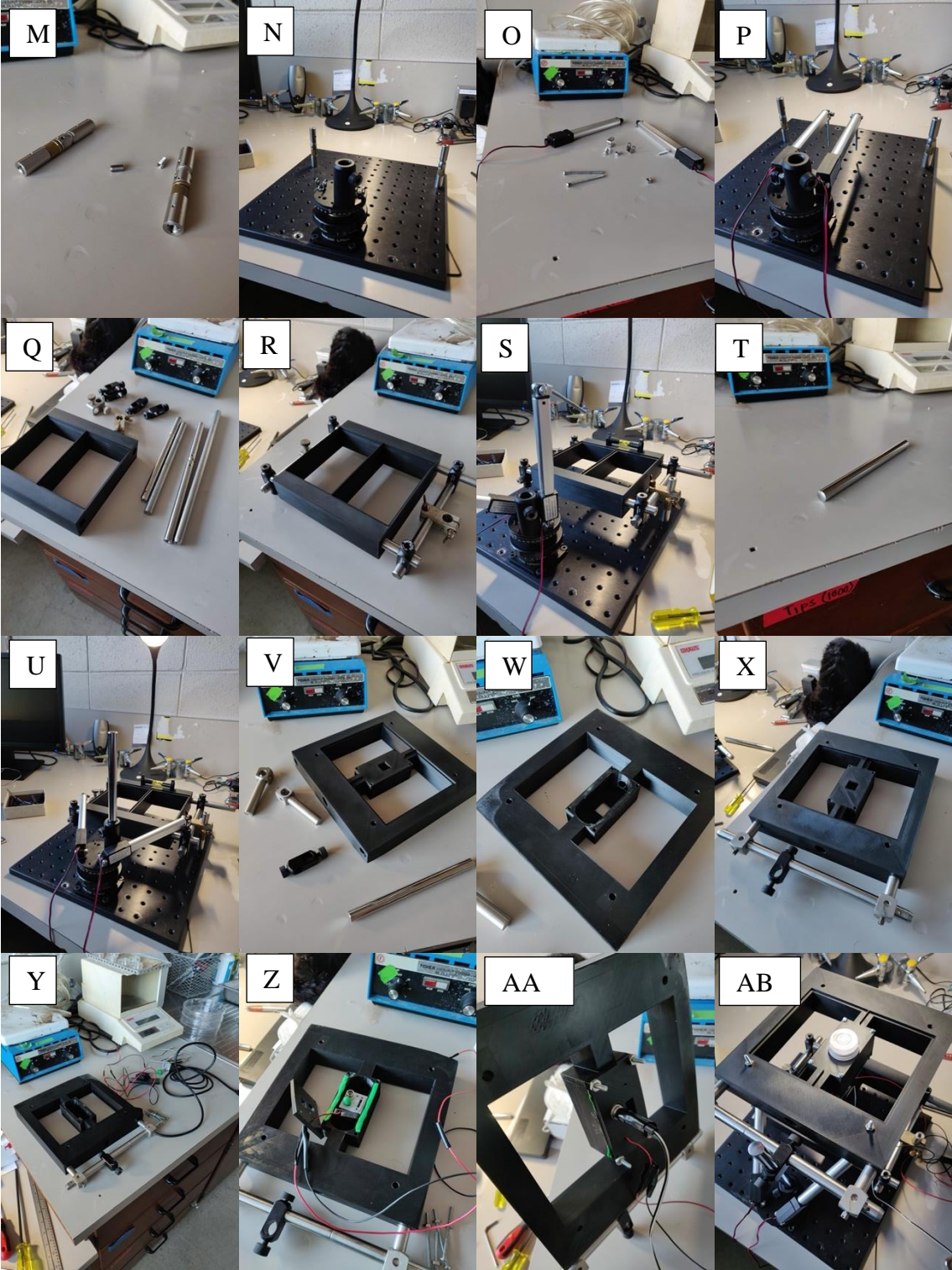
Figure 46 The optical posts and fastener anchor the imaging and sample platforms together so that any vibration caused by the environment is synced between the two platforms. In effect they fasten the two components together so that there is little to no relative motion.

2.11 – System Design: Assembly steps

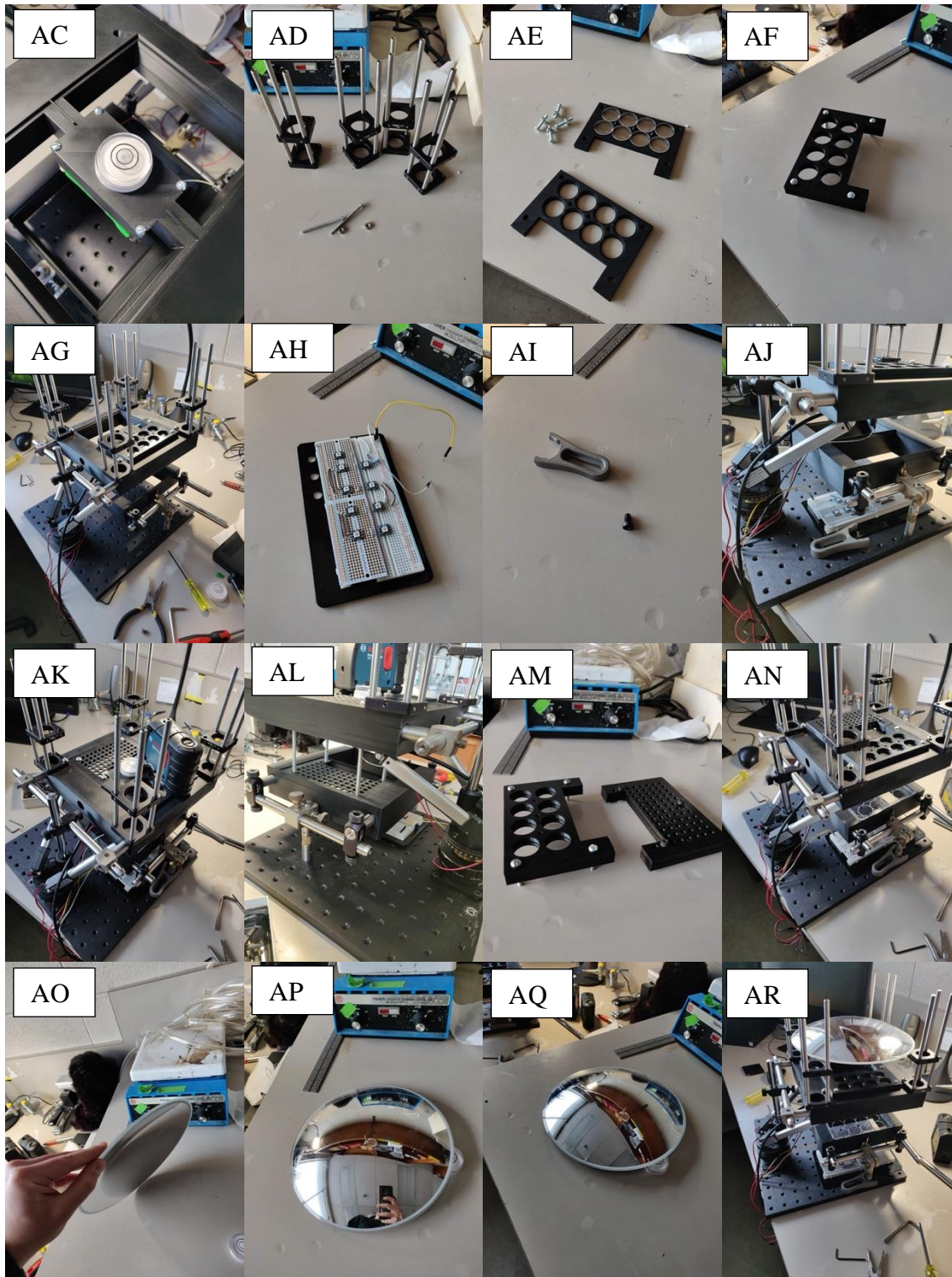
The below pictures show the assembly of the device, the individual parts as well as how they fit together. They are in normal English reading order.



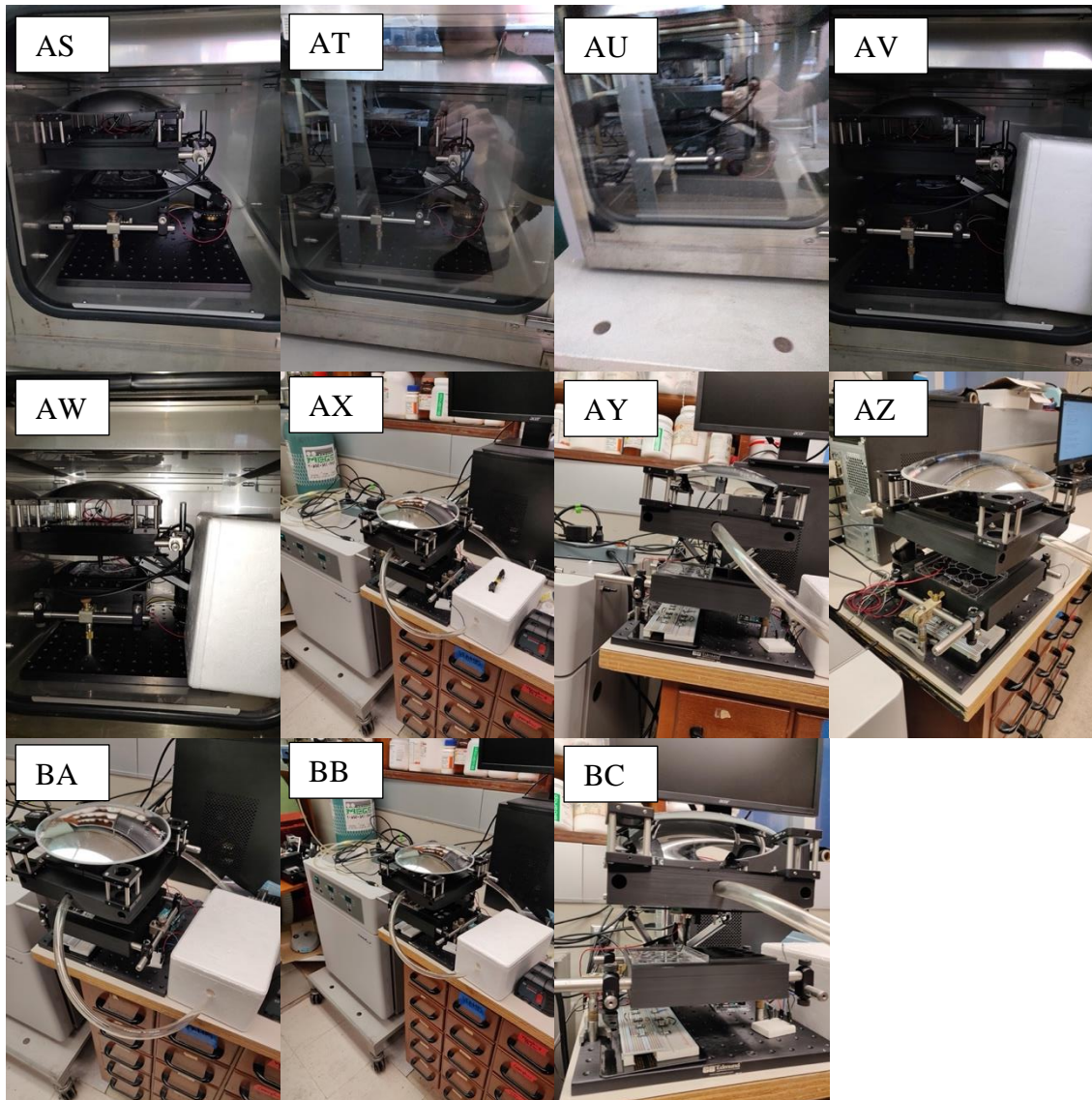
2.11 – System Design: Assembly steps



2.11 – System Design: Assembly steps



2.11 – System Design: Assembly steps



The following are some of the major outsourced parts used in the project:

- 300mm x 300mm, Breadboard, from Edmond optics (part # 54-638) – **B**
- Ø2.64" Compact Lab Jack, from Thorlabs (part # LJ750) – **C**
- Ø1/2" Pedestal Post Holder, from Thorlabs (various length) – **G**
- Ø1/2" Translating Optical Posts, from Thorlabs (part # TRT2) – **L, M**
- Ø1/2" Stainless Steel Optical Posts from Thorlabs (Various length) – **Q, T**
- 12V Micro Linear Actuator 100mm, from elmwood electronics (part # C1375)– **O**
- Basler acA1300-200um, from Edmond optics– **Z**
- Mini-Series Ø6 mm Posts, from Thorlabs (part # various length) – **AD**
- Standard 30 mm Cage Plates, from Thorlabs– **AD**
- Array of 25mm plano-convex lenses and an array of 6mm plano convex lenses with focal points of 100mm and 72mm respectively from Edmond Optics– **AM**
- NeoPixel RGB LEDs from Adafruit industries (part # 1430) – **AH**
- 220mm Dia x 100mm FL Alum. Coated, Parabolic Reflector (part # 68-793) – **AO-AQ**

Chapter 3 – Proof-of-Concept experiment

The previous section highlighted the details of the design of RAP, its various components, including the electrical components, 3D printed parts, as well as optomechanical components. Furthermore, the reasoning behind each design choice was explained.

In this section, this design is validated using a proof-of-concept experiment using cardiac monolayers. The overall aim is to show the capabilities of RAP in detecting small differences between control and test conditions in the context of a physiological experiment.

3. Proof-of-concept experimental design:

3. Proof-of-concept experimental design: Effect of confluency and time on cardiac monolayers

3.1 - Overall Design: To support the main claim of the thesis, cardiac monolayers plated at different plating densities to give a range of confluencies were imaged for five consecutive days, from *inside an incubator*. There were a total of three test conditions; two test conditions with 3 replications each, and one test condition with 4 replications. They were in two plates as seen in Figure 47. The results were processed for beat rate, as well as beat rate irregularities. The hypothesis was that the device will be able to distinguish small differences between the different groups in a statistically significant way. Each confluency at each day represents a separate group, and the different wells with the same confluency on the same day represent the repetitions. There are thus 2 factors affecting the independent variables: **time** and **confluency**. A two-way ANOVA with repeated measures was thus conducted, followed by multiple one-way ANOVAs to test the results. An alpha value of 0.05 was judged as statistically significant.

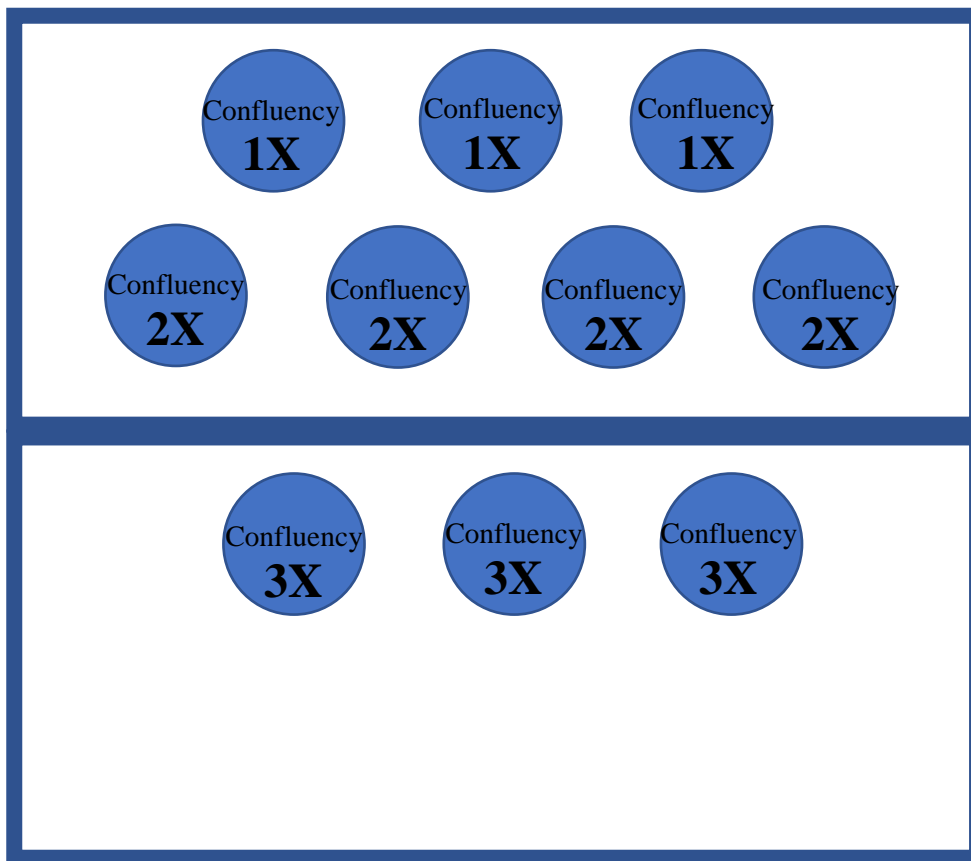


Figure 47 Experimental set up. Two plates were used in our experiment. One plate had 3 wells of 1X confluency and 4 wells of 2X confluency. The other plate had 3 wells of 3X confluency. Confluency refers to the concentration of cells per square millimeter.

3. Proof-of-concept experimental design:

3.2 - Cell preparations: The samples consisted of cardiac monolayers cultured from rat ventricular cells. Mice were bred and sacrificed at 3 days old. Their heart ventricular cells were harvested and cultured according to standard protocols. The details for a cell culture protocol can be found in JOVE titled Isolation and Culture of Neonatal Mouse Cardiomyocytes.⁹⁴ The cultures were incubated inside a standard lab incubator for approximately a week to allow for the biological processes to stabilize. The cell culture media was changed every 48 hours.

3.3 - Imaging Conditions: After the culture was ready, the cells were placed inside the incubator which contained the RAP device. The incubator was set to 37°C and 5% CO₂ level. The cells were kept in this incubator for 4 days, only to be taken out for a media change once a day. The plates were switched from one side of the device to the other during each imaging session so that all the samples could be imaged.

3.4 - Electronics setup: The details of the electronics setup can be found in section 2.6. Once set up however, the newest version of PylonViewer was used to operate the camera, and the Arduino IDE was used to send the codes to the Arduino. The delay period between each LED was set as a trade-off between framerate and exposure time; that is, the higher the exposure time, the brighter the picture and the lower the effective frame rate. The arduino code itself takes ~3 milliseconds to be executed, and this time needs to be taken into account when setting the software delay between each LED as a delay line in the code. That is the actual ON time for each LED is a function of both the digital delay introduced in the software, as well as the time required to run the code. Furthermore, the LEDs and the camera frame rate should match, this means that the LEDs should not blink, and thus trigger the camera, faster than the camera is able to image, otherwise this results in dropped and ignored triggers and out of sync imaging, which can lead to inconsistent picture quality as well as a lower frame rate. A few different exposure times were recorded, but the best results presented in the next chapter used an exposure time of 5.25ms.

3.5 - Data processing: As each LED turns on, the camera is triggered by the Arduino through the TTL cable and an image is captured. The images are thus obtained in sequence and on a loop and thus need to be further separated into different groups, each group corresponding to a separate well, using python programming. Described more thoroughly, the camera captures one image at a time when triggered by the TTL cable. The software is setup so that each LED flash

3. Proof-of-concept experimental design:

corresponds to one trigger for the camera. As previously described, the camera only sees, and thus images, the sample whose LED beneath it is ON. And as the LED's are flashing in sequence, the camera is effectively capturing a sequence of images in a loop. The image sequence for the top plate containing 7 samples (three samples of 1X confluency and 4 samples of 2X confluency) is shown in Figure 48. The *first* frame of the first sample is captured, then the *first* frame of the second sample, then the *first* frame of the third sample and so on until the *first* frame of the seventh sample is captured. The loop then repeats, and the *second* frame of the first sample is captured, then the *second* frame of the second sample, then the *second* frame of the third sample and so on until the *second* frame of the seventh sample is captured. This loop continues until the desired number of frames are captured, as a good reference point, 750 frames were captured per sample in our experiment.

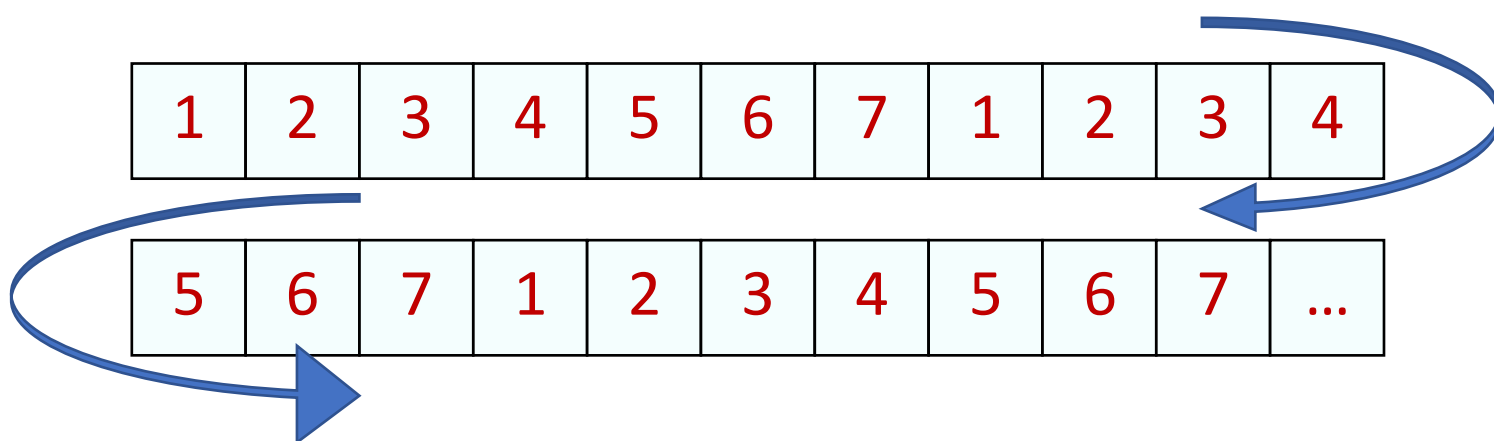


Figure 48 The camera records the images in sequence. The LEDs flash sequentially and in a loop. The resulting image sequence can be seen in this picture and follows the order of 1,2,3,4,5,6,7 and then repeat.

The images are then sorted into their respective groups, so that all images in one group refer to consecutive frames of one sample, as seen below in Figure 49. Seven groups were thus generated, each containing a sequence of images over time of a separate well each. Each group contains 750 frames. The sequence of images can then be played back as a movie. This effectively means that 7 samples are recorded near-simultaneously. Each group is then individually processed using custom written software (GView). It is important to note that the order by which the wells are imaged can be assigned by the experimenter and that the wells do not necessarily need to be physically adjacent, hence the term *Random Access Parallel Microscopy* in RAP, referring to the ability of the device to access any well in any random order.

3. Proof-of-concept experimental design:

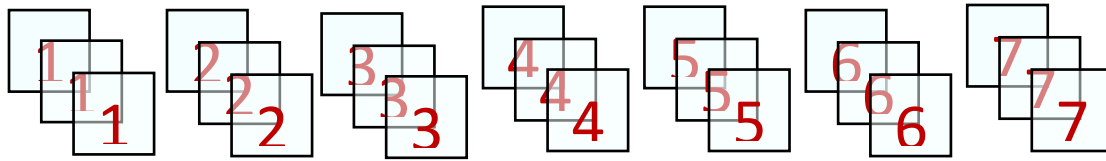


Figure 49 The sequential images recorded by the camera are grouped in specific compartments, each compartment belonging to an individual well. As an example, every 7th image from the first image refers to the first well and the images are grouped together in one compartment. The same principle applies for the 7th image from the second image, and so on. The sequence of images in each compartment can then be played back as a movie.

Once imported in GView, **Regions Of Interest (ROIs)** are selected and analyzed from the image sequence. The software (GView) looks for motion as a function of a change in pixel intensity and provides a data value corresponding to the average change in pixel intensity. These data can then be analyzed with a data analysis tool such as excel or python. In our experiment, once each ROI was analyzed using GView and the corresponding data generated, Python was used to generate a separate graph for each ROI using the generated data. Again, the data represent the absolute value of the average pixel intensity for each frame as compared to 6 frames period. This is explained in more details in section 4.2. The generated graphs were then manually reviewed, and the more representative graphs were selected for presentation in the results sections below. Python was further used to analyze the beat rate and regularity. The beat rate and beat variability were analyzed by measuring the time between each larger peak. This was done by first identifying the larger peaks. Two conditions were applied to identify the peaks. First a threshold was manually selected for each graph. This was based on what value the majority of larger peaks and only larger peaks exceeded. Furthermore, the absolute peak intensity values ($[I(t)]$) satisfied the following condition:

$$[I(t-2)] < [I(t-1)] < [I(t)] > [I(t+1)] > [I(t+2)] \quad \text{where } t \text{ is the frame number.}$$

The equation states that a peak is considered a peak if the average intensity value at a given time point is larger than the two preceding and the two following time points. Once the peaks were selected. The time between them were measured. The average time was taken to be the average beat period and the standard deviation of the distribution of beat period was calculated as a measure of beat-to-beat irregularities. These values are shown in the results section in the next chapter. Visually, GView represents movement as a filter that is applied to the videos, which will be shown in the results section.

Chapter 4 – Results

The previous chapter outlined the details of the proof-of-concept experiment. In this section the results are analyzed and show that statistically significant differences can be measured. The section starts with a few static results showing the resolving capabilities of RAP, and continues with the biological results.

4. Results

Our results consist of two parts: optical calibrations results to demonstrate the optical properties of the device, and results from a proof-of-concept biological experiment that shows the usefulness of the RAP system in a biological context. The results show that RAP can take good quality images, but the images reveal some limitations, particularly spatial aberrations, as shown in section 4.1. These aberrations however are small enough as to not preclude the collection of useful information in a biological setting. As a result, RAP can simultaneously record multiple cardiac monolayers inside an incubator and provide useful information regarding cardiac beat rate and beat regularity and wave propagations, as shown in section 4.2.

4.1 - Results: Focusing and image acquisition

The first set of results shown below are example images of calibration slides overfitted with transparency films. Random letters of size 3 font are printed on the transparency films. Four examples can be seen below with different calibration slides beneath the transparency films. Figure 50 shows a circular target, figure 52 shows a calibration with a millimeter scale target. Both targets are from Zeiss. Figures 51 and 53 shows a calibration grid from Edmond optics, which they call *Multi-Grid Standard Stage Micrometer* on their website. Figure 51 is a grid where lines are 100 μm and Figure 53 shows a grid where lines are 50 μm apart. The purpose of these images is to calibrate as well as demonstrate the optical properties of the device. The calibration slides also aid in determining resolution and aberrations. An example of where these calibration slides are used to calibrate the device can be seen in section 2.4, where numerous images of the same grid were taken and compared to find the optimal light placement.

While the calibration slides are used for finer calibrations, the letters printed on the transparency sheet are primarily used to locate the samples during calibration, for initial coarser calibrations, and for detection of light bleeding. This is to ensure that when light under a specific desired sample is turned off it is no longer visible and when light under another specific sample is turned on, it is visible and only that sample is visible. If light bleeds from an LED placed under the desired sample and illuminates an adjacent sample, a faint picture of that sample will overlap the image of the desired sample. The relatively larger letters printed on the transparency sheet make this bleeding easier to see.

4.1 - Results: Focusing and image acquisition



Figure 50 Printed 3pt font letters with a circular scale slide. The slide with the circular target is placed above the translucent film with the letters printed on it. The letters help in locating the slide and for focusing as they provide a course target for initial focus. The slide serves to aid for finer focus and precision measurements.

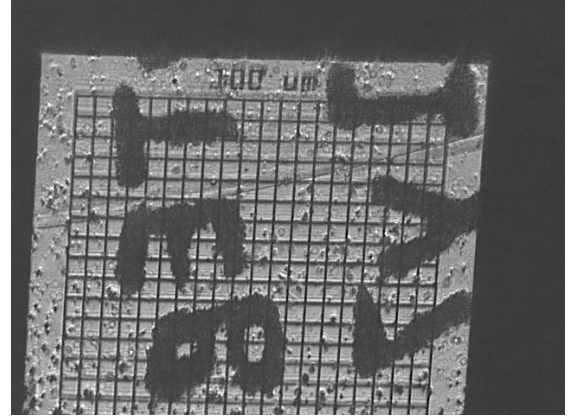


Figure 51 Printed 3pt font letters with a 100 micrometer per division grid slide overlay. The slide with the grid target is placed above the translucent film with the letters printed on it. The letters help in locating the slide and for focusing as they provide a course target for initial focus. The slide serves to aid for finer focus and precision measurements.

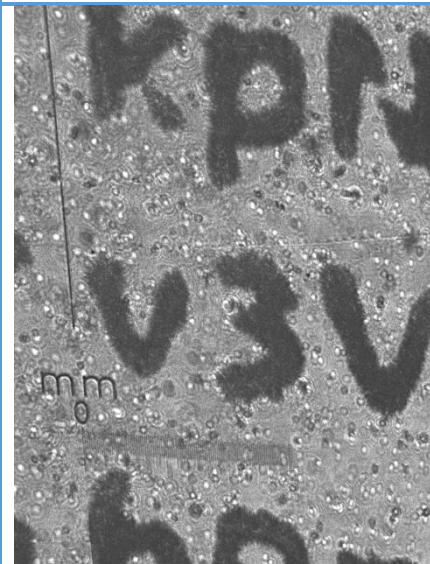


Figure 52 Printed 3pt font letters with a millimeter scale slide. Like the above images, the slide with the mm scale is placed above the translucent film with the letters printed on it.

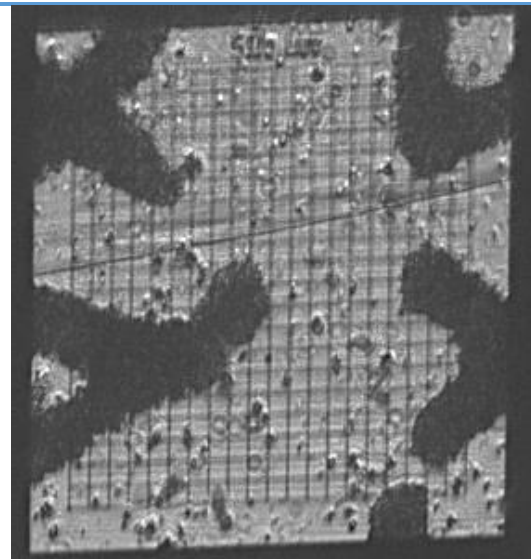


Figure 53 printed 3pt font letters with a 50 micrometer per division grid slide. Like the above images, the grid slide is placed above the translucent film with the letters printed on it. The 50 and 100 micrometer grids are both engrained on the same slide from Edmond Optics.

Two characteristics are pertinent and of note in the above images: resolution and spatial aberrations. The first point to consider is resolution. As the results above show, the current setup can easily distinguish between lines that are $100\ \mu\text{m}$ apart, and less clearly lines that are $50\ \mu\text{m}$ apart. But the magnification and resolution of the system can be adjusted easily by changing the

4.1 - Results: Focusing and image acquisition

objective lenses, and thus it is straightforward to change the resolution of the device, based on the needs of the experiment and the available budget. This interchangeability of lenses was explained more thoroughly in section 2.2. What is of greater note however are the aberrations, particularly spatial aberrations. The aberrations are inherent to the optics of a parabolic reflector and are not easy to correct by changing the hardware. They can however be overcome to a large degree by software processing. I emphasize that these aberrations, although present, did not adversely impact our ability to capture functional data from the monolayers as demonstrated in the next section (section 4.2). The results in the next section were not corrected for spatial aberrations, yet provide clear and useful biological information.

The aberrations are described in detail in our paper published in eLife.² In brief, the images are subject to two transformations. First is caused by the spatial separation of the optical axis of the lens from the optical axis of the parabolic reflector. This separation results in a bilateral

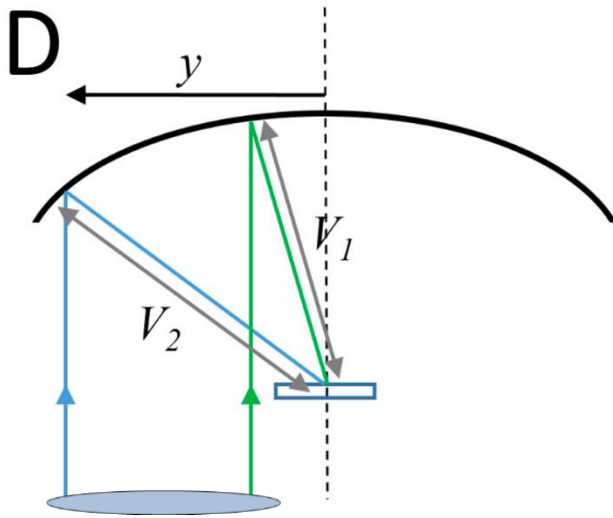


Figure 54 In the context of a parabolic reflector, the distance between the mirror surface and focal point increases as we move away from the optical axis.² That is, $V_2 < V_1$.

magnification and is due to the changing distance between the surface of the parabolic mirror and the focal point. This distance is depicted in Figure 54 by V . This distance increases as we move further from the optical axis of the parabolic reflector ($V_1 < V_2$). This can be seen in a modified version of figure 1 D from our paper (Figure 54).² This shift is the same in both the X and Y direction. Taken together this means that collimated light from the lens is not focused at exactly the same location on the camera sensor and

thus introduces aberrations, in this case uneven magnification. The magnification this produces then is the ratio of V at any given y to the focal point of the mirror, and since V itself is given by the equation:²

$$V = \left\{ y^2 + \left(f_m - \frac{y^2}{4f_m} \right)^2 \right\}^{\frac{1}{2}}, \text{ the magnification can be given by } M = \frac{1}{f_L} \left\{ y^2 + \left(f_m - \frac{y^2}{4f_m} \right)^2 \right\}^{\frac{1}{2}}$$

4.1 - Results: Focusing and image acquisition

where y is the lateral displacement, f_L and f_m is the focal length of the lens and parabolic mirror, respectively.

The second factor causing aberrations is the stretch due to the fact that light hits the sensor at an oblique angle. The magnitude of the stretch is described by the following equation:

$$S = \frac{1}{\cos \left[2 \tan^{-1} \left(\frac{y}{2f_m} \right) \right]}$$

where S is the magnitude of the stretch in one axis, y is the lateral displacement, and f_m is the focal length of the parabolic mirror.

The total magnification is then a combination of the stretch due to the oblique angle of the light and the magnification due to the increasing distance of mirror surface to the focal point and is given by the following equation:

$$M_C = M \times S.$$

This is represented graphically in Figure 1E of our paper (Figure 55).²

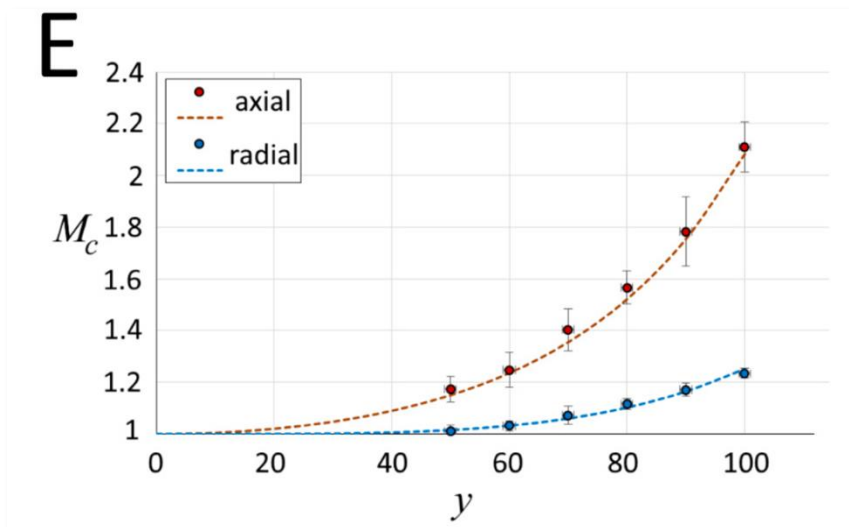


Figure 55 The magnification increases as we move away from the optical axis both axially and radially, albeit axial magnification increases at a greater rate than radial magnification.² The focal point of the mirror f_m , and focal point of the lenses f_l , resulting in the magnifications presented here were 100mm and 72mm respectively.

4.2 – Results: Effect of confluency and time on cardiac monolayers

Presented below are the biological data from the proof-of-concept biological experiments set forth in section 3. The raw data is collected from the camera as a sequence of images looping in series, as explained above in section 3. Once the videos have been processed, numerical data are generated for each **Region Of Interest (ROI)**. For each video, corresponding to an individual well recorded on a specific day, multiple ROIs were selected in GView. As there were over 40 ROIs, it is not feasible to include all the graphs and filtered movies in this report, hence only select representative graphs and an image sequence are shown below. The image sequence for *Day 4- Confluency 2X-Well 3*, consisting of screenshots of the movie generated by GView after the filter has been applied is shown below in Figure 56. (The complete movie can be seen on my YouTube page: <https://www.youtube.com/watch?v=MVTUrJKDEbE> and the raw footage can be viewed at: <https://youtu.be/G0p-O3Y-p9c>) The below sequence shows a frame every 0.2 seconds. A cardiac wave propagating from top left to the bottom right is visible and shown by the arrows.

The filter illustrated below compares each image in the image sequence to an image 6 frames prior and maps the change in pixel intensity. The intensity of the pixel represents the intensity of motion. The intensity is calculated from the absolute value of the change in pixel intensity between any frame (P_t) and the frame 6 frames prior to it (P_{t-6}). The basic idea is given by the following equation:

$$\Delta P_t(i, j) = |P_t(i, j) - P_{t-n}(i, j)|$$

This equation in brief shows that the pixel intensity (at pixel i, j) of a frame is subtracted from the intensity of a pixel at the same position at a previous time point (in our case $n=6$ frames) and the absolute value of that difference is calculated. This is explained further in our eLife paper.² This is a relatively novel way of looking at cardiac wave propagation. In more conventional studies electrical probes are used.⁹⁵ Using optical recordings however provides us with significantly greater spatial information.

4.2 – Results: Effect of confluency and time on cardiac monolayers

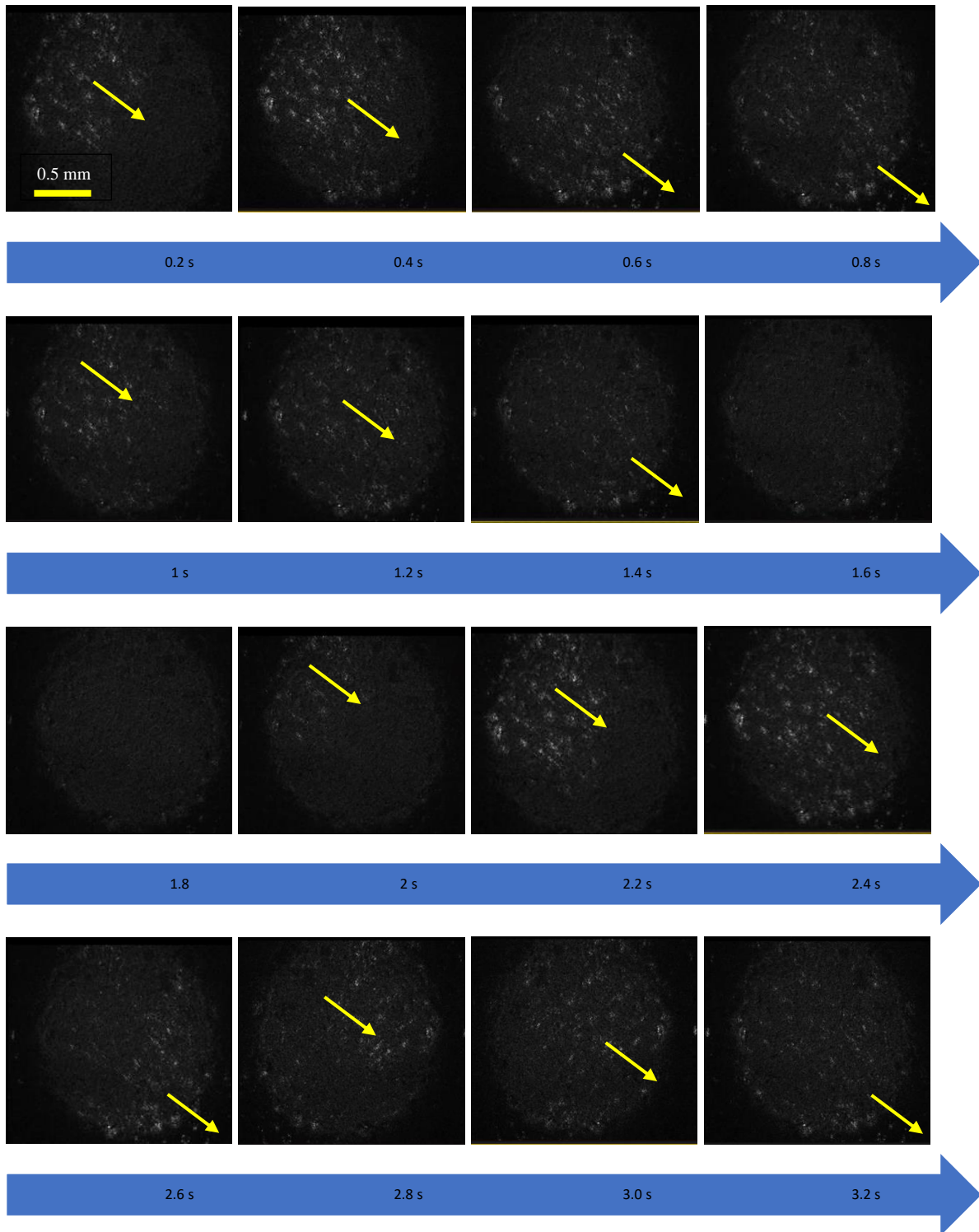


Figure 56 The sequence of images corresponding to each well is imported in GView and a filter applied. The filter compares absolute pixel intensity of a frame to 6 frames prior. The resulting movie shows the direction of cardiac waves. Here the movie corresponding to the sample Day 4- Confluency 2X-Well 3, is shown as a series of still images spaced 0.2 seconds apart. A clear wave can be seen travelling from the top left to the bottom right. The beat then rests for 0.4 seconds before it starts again. The yellow arrows show the direction of the wave. The complete movie can be seen on my YouTube page: <https://www.youtube.com/watch?v=MVTUrJKDEbE> and the raw footage can be viewed at: <https://youtu.be/G0p-O3Y-p9c>

4.2 – Results: Effect of confluency and time on cardiac monolayers

For each frame, like any of the frames seen above in Figure 56, all white pixels can be averaged and displayed on a graph as a single value. This is what is seen in the 10 representative graphs. Figure 57 shows 5 representative wells imaged on day 2 and Figure 58 shows 5 representative wells imaged on day 4. In these graphs each y value corresponds to the average change in pixel intensity, when compared to 6 frames prior, for a given time point (x value). It is important to note that the graphs do not represent action potentials but rather contraction and relaxation of the cardiac monolayers, essentially, they are motion transients. The first spike shows cardiac contraction, and the second spike corresponds to cardiac relaxation. These contraction and relaxation are initiated by action potentials, but they are also influenced by other factors, such as calcium concentrations, which is the reason the graphs below are not equivalent to the shape of a cardiac action potential. This is explained further in a paper by my supervisor, Dr. Gil Bub, in Nature Photonics.⁹⁵

4.2 – Results: Effect of confluency and time on cardiac monolayers

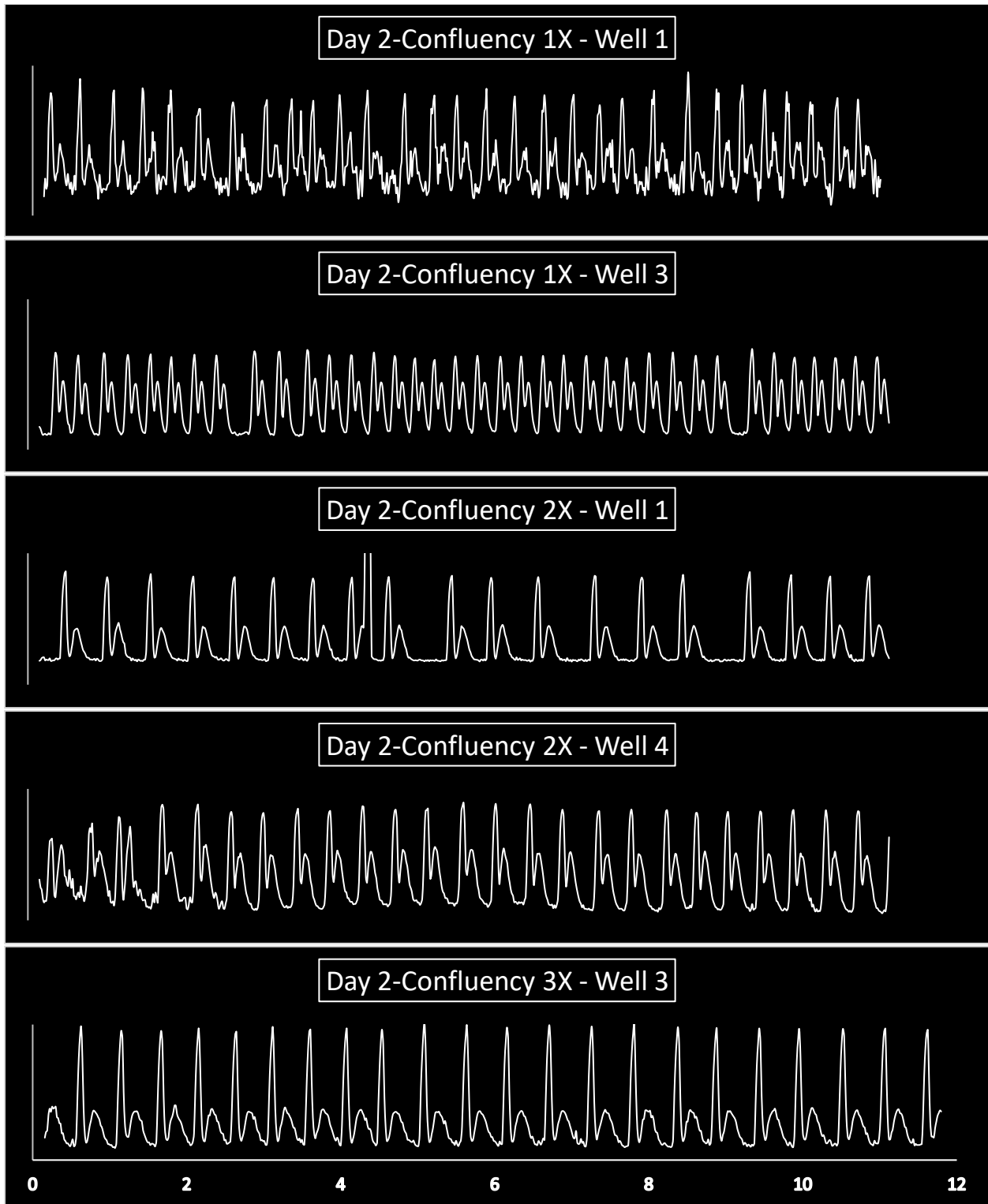


Figure 57 Five representative graphs from samples imaged on the second day are shown. Different beat patterns can be seen for each well. What is equally important are the pauses that can be seen sporadically in some traces. Two examples can be seen in the graphs titled Day 2-Confluency 1X - Well 3, and two can be seen in the graph titled Day 2-Confluency 2X - Well 1. The graph titled Day 2-Confluency 1X - Well 1 can be seen to have more irregular activity compared to the graph titled Day 2-Confluency 3X - Well 3. What is of particular note is that these irregularities are randomly and sporadically spread out through the different samples and time. No two arrhythmias are the same. This means that it is extremely important that many samples are imaged over a long period of time so that rare sporadically spread events can be observed.

4.2 – Results: Effect of confluency and time on cardiac monolayers

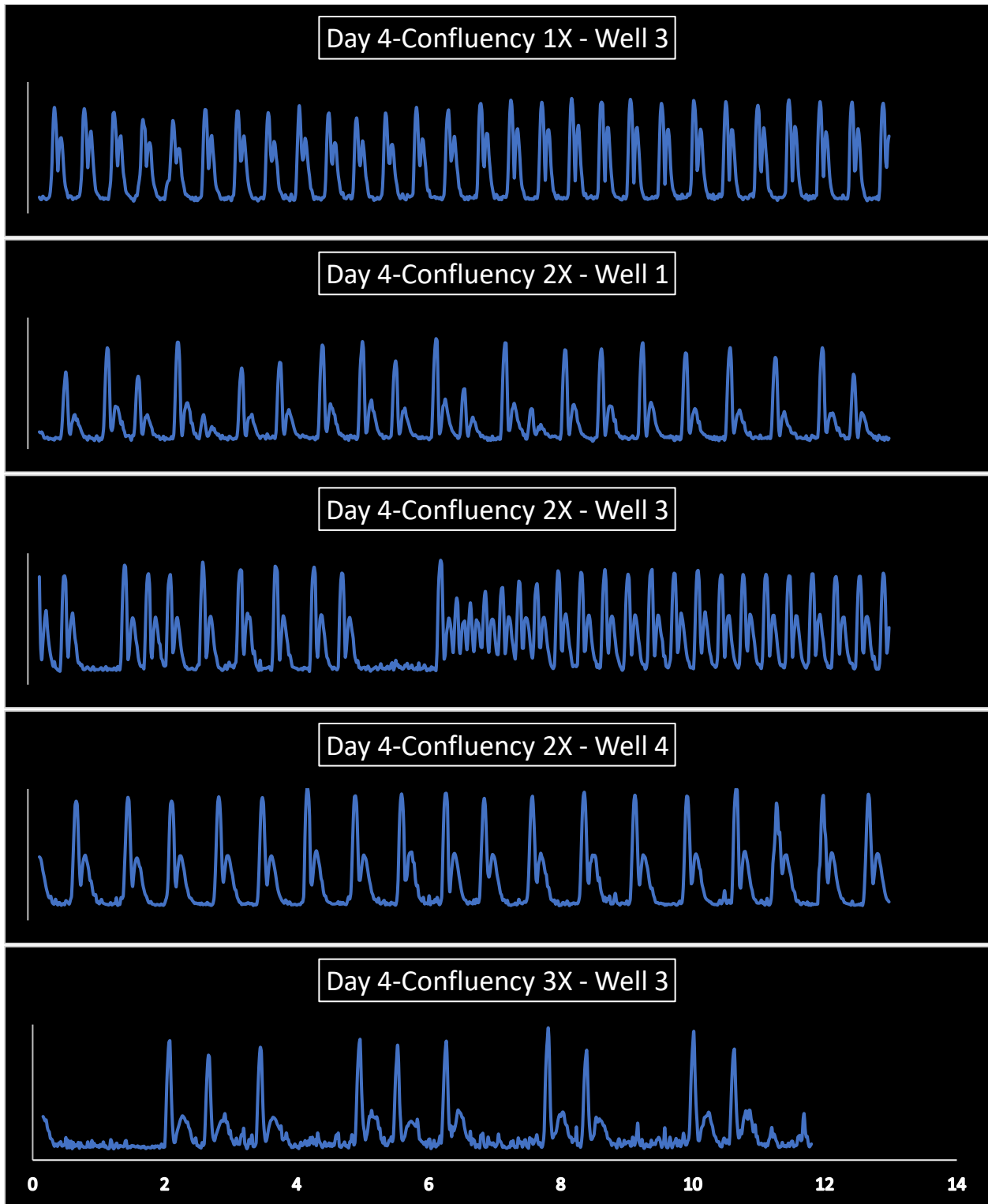


Figure 58 Five representative graphs from samples imaged on the fourth day are shown. Different beat patterns can be seen for each well. Here we can see the initiation of a tachycardia in one of the wells (Day 4 -Confluency 2X – Well3). The monolayer can be seen beating regularly except for the periods of 2-4 seconds and 6-14 seconds. The rapid rhythm at $t=6$ seconds is characteristic of a re-entrant pattern of activation. During the same time period we can see a regular beat in the graph titled Day 4-Confluency 2X - Well 4. Because the device was simultaneously imaging the wells, diverse rhythms, including the initiation of a re-entrant wave, can be captured. If the samples were imaged sequentially, it would be much more likely that such short-duration, sporadically spread out irregularities would be missed.

4.2 – Results: Effect of confluency and time on cardiac monolayers

It can be seen from the above graphs that the beat rate and beat regularity change based on confluency as well as time. Some samples, like *Day 4 - Confluency 2X – well 4* show more regular beat patterns, whereas a sample like *Day 4 – Confluency 3X – well 3*, shows a more irregular rhythm. What is even more interesting is a sample like *Day 4- Confluency 2X – well 3*, where a regular beat pattern is observed until suddenly there is a pause followed by a very rapid rhythm at $t=6s$. (filtered footage: <https://www.youtube.com/watch?v=MVTUrJKDEbE> ; raw footage: <https://youtu.be/G0p-O3Y-p9c>) This pattern is characteristic of a re-entrant wave: re-entrant waves are potentially fatal if they occur in the intact heart and capturing spontaneous initiation events may lead to a deeper understanding of their dynamics. What is equally of note is that such re-entrant waves are sporadic and are sparsely spread out over different wells over different days, and in many cases they only last for a few seconds. Thus, the only way to study them is to simultaneously record many samples over a long period of time, otherwise there is a high likelihood that the event would be missed while the imaging device is busy imaging another well.

To further clarify this point, it is most pertinent to note the time interval of the anomalies and their frequency. The graphs show that a re-entry can sometimes occur only once or twice in a 30 second time interval and sometimes not at all. When it does occur, it lasts for only 2 or 3 seconds. This means that for an arrhythmic event, such as a re-entry, to be detected the sample should be imaged for significantly longer than the duration of the event, yet at a fast enough frame rate to be able to capture all the dynamics of the process over the 2-3 second time period. Consequently, if multiple samples are of interest and each are observed for 30 seconds, the time dedicated to imaging each sample is a significantly lower fraction of the total imaging time of the microscope, as compared to the case of RAP where all are being recorded simultaneously. Put another way, if 7 samples are recorded from a plate for a period of 30 seconds each, the total imaging time would be $7*30=210$ seconds. Each well then would be imaged for $30/210*100%=14.2\%$ of the time that the microscope is recording. This necessarily means then that any irregular activity occurring in a well in the other 85.8% of the time would be missed, because the microscope would be recording other samples. Another characteristic of note can be seen at *Day 4 confluency 2X- well 1* where different peaks have different amplitudes indicating varying beat strength. Overall, the ability of RAP to capture these data and the possibility of

4.2 – Results: Effect of confluency and time on cardiac monolayers

post-capture mathematical computational analysis that these data allow is the main result of the experiment. An example of such post-capture computations is Fourier analysis.

While many of the recorded ROI data produce clean graphs, some ROIs in certain wells produce noisy data, as can be seen in *Day 1 confluency 1X, well 1*, and *Day 4 confluency 3X well3* in the graphs above or *Day 1 confluency 1X, well 2* in the graph series below. In such cases, noise can be reduced by the use of Fourier analysis. As explained in the introduction, Fourier analysis can be used to separate data into their component frequencies, and the list of frequencies can then be used in various ways. One way they can be used is to reduce noise as seen in the two graphs below. The top graph shows the original unfiltered data. The bottom graph shows the relative influence of varying frequencies that contribute to the data. Frequencies with peaks below a certain contribution strength (in this case as judged by eye) are then zero-ed out and the remaining frequencies converted back to the middle graph. The logic behind this approach is that frequencies that only minimally contribute to the overall signal can be removed without major detriments to the overall signal. These signals typically either provide little to no scientific value but complicate the analysis nonetheless or are only representative of the noise in the system. We can see that the middle graph looks smoother when compared to the top, unfiltered graph.

4.2 – Results: Effect of confluency and time on cardiac monolayers

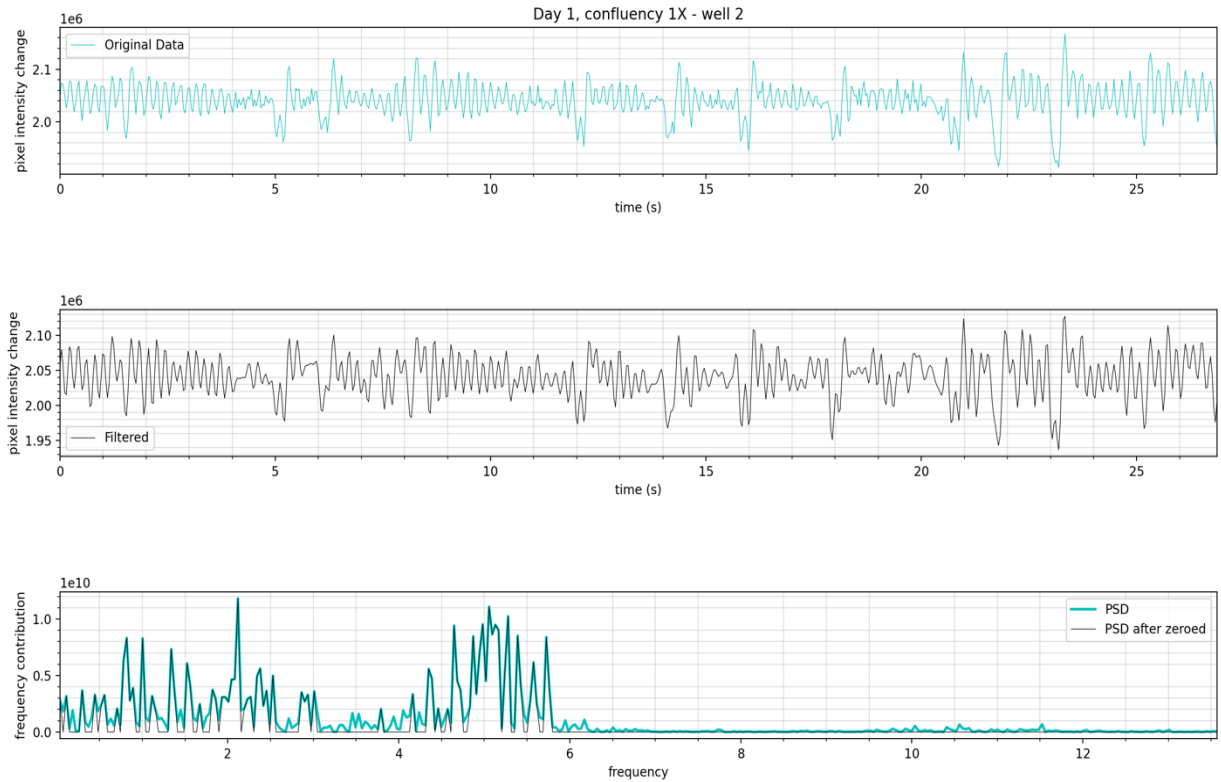


Figure 59 An example of how Fourier Analysis can be used to further process the data. In these three graphs, data from Day 1, confluency 1X – well 2 was used. The top graph shows the original data. Once the Fast Fourier Transform is applied, the darker line on the bottom graph is produced. The peaks show the contributing strength of each frequency to the original data. The shorter lines and specific ranges are then zeroed out, producing the thinner line. This frequency series is then converted back using a reverse Fourier transform and the middle graph is produced. As can be seen the middle graph is a cleaner version of the top graph with less noise.

Certain patterns can then be more easily identified. An example is **Torsades de pointes** pattern. Torsades de pointes is a condition where a cardiac ECG trace can be seen shifting around an imaginary baseline.⁹⁶ An example is seen in Figure 60 below. The similarities in the previous graph can be seen more clearly in the denoised middle graph in the graph series above (Figure 59) for the second well of confluency *Day 1-confluency 1X - well 2*.

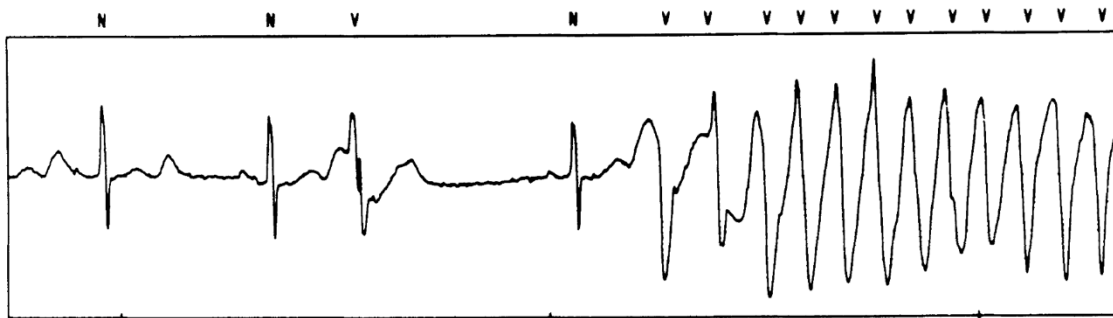


Figure 60 Torsades de pointes is a condition where the ETC can be seen shifting around an imaginary baseline.⁹⁶

4.2 – Results: Effect of confluency and time on cardiac monolayers

In another example that shows a relatively normal beat pattern, such as the graph series below showing *Day 4 - confluency 3X - well 3*, Fourier analysis can help us to obtain a more easily interpreted graph as compared to the raw data, with less high frequency noise. This can be seen from the visibly smoother lines in the middle graph in Figure 61.

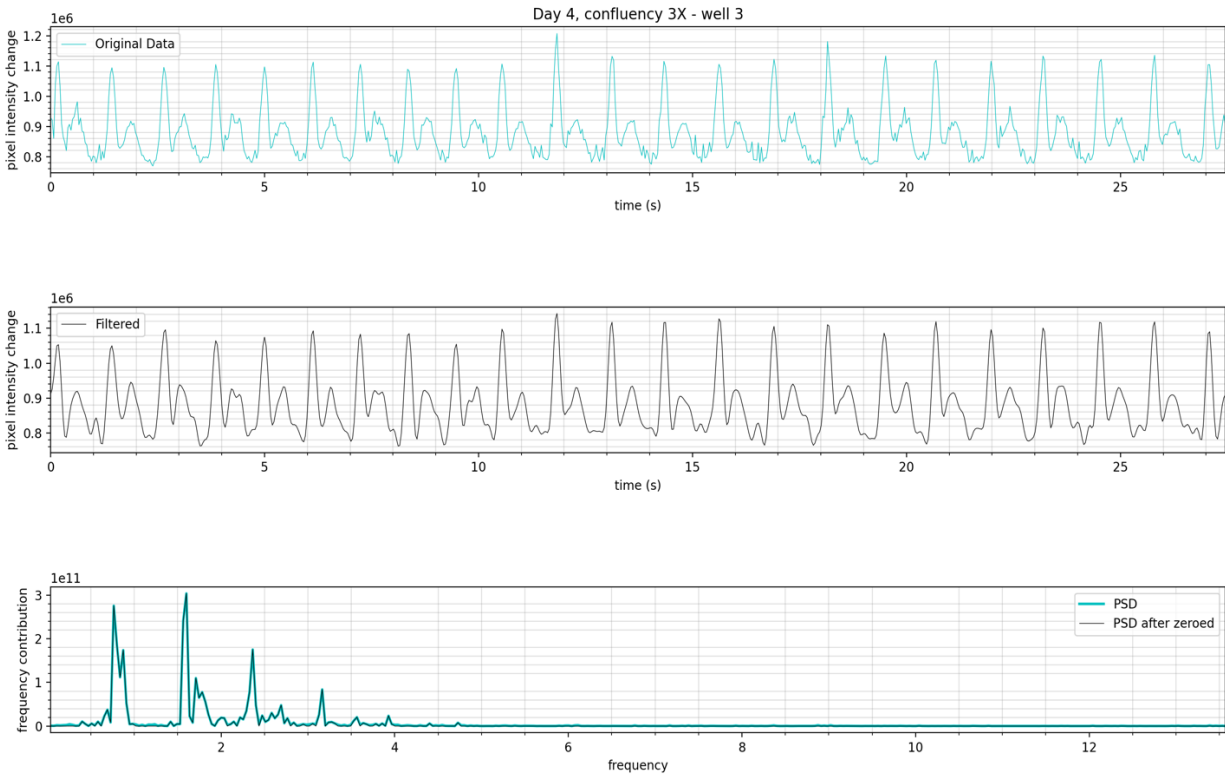


Figure 61. Similar to the previous graph, another example of how Fourier Analysis can be used to further process the data can be seen in Day 4 – confluency 3X – well 3. Again, the top graph shows the original data. Once the Fast Fourier Transform is applied, the darker line on the bottom graph is produced. The peaks show the contributing strength of each frequency to the original data. The shorter lines and specific ranges are then zeroed out, producing the thinner line. This frequency series is then converted back using a reverse Fourier transform and the middle graph is produced. As can be seen the middle graph is a cleaner version of the top graph with less noise.

The charts presented so far are only representative graphs of the collected ROIs. The beat rate and irregularity data from *all* ROIs were organized in the two tables below. The first table (Table 1) shows beat rate data and the second table (Table 2) shows beat irregularity data. To quantify beat irregularity, the standard deviation of the distances between peaks were calculated and judged to represent the irregularity of the beat. The rationale for using standard deviation as a measure for irregularity is that this measure quantifies how much a value in a data series deviates from the average value. Please also note that confluency 2X had 4 wells associated with it in our experiment, however for consistency and compatibility with statistical tests, the most representative 3 were selected. Data from the 4th well is available upon request.

4.2 – Results: Effect of confluency and time on cardiac monolayers

	Day 1	Day 2	Day 3	Day 4
BPS - 1X-rep1 (b/sec)	1.30	1.11	1.58	0.82
~~~~~ - rep2 (b/sec)	1.70	1.34	1.79	1.14
~~~~~ - rep3 (b/sec)	2.40	1.36	1.70	1.02
BPS - 2X-rep1 (b/sec)	1.56	0.69	0.64	0.74
~~~~~ - rep2 (b/sec)	1.50	0.71	0.79	0.30
~~~~~ - rep3 (b/sec)	1.21	0.94	0.78	0.71
BPS - 3X-rep1 (b/sec)	1.10	1.73	0.82	0.81
~~~~~ - rep2 (b/sec)	1.53	1.67	0.81	0.70
~~~~~ - rep3 (b/sec)	1.42	1.92	1.45	1.05

Table 1 Each cell in the table represents the beats-per-second for each condition calculated by averaging the distance from one peak to the next in a representative ROI from each condition. A peak is judged to be a peak if its value passes a selected threshold (varies by each ROI), and furthermore satisfies the following condition: $[I(t-2)] < [I(t-1)] < [I(t)] > [I(t+1)] > [I(t+2)]$, where a peak point refers to the absolute value of the intensity change at a specific frame t . The biological repetitions are indicated by the rep number. The units are in beats/sec.

	Day 1	Day 2	Day 3	Day 4
SD - 1X-rep1 (sec)	0.29	0.10	0.15	0.58
~~~~~ - rep2 (sec)	0.11	0.10	0.02	0.15
~~~~~ - rep3 (sec)	0.02	0.09	0.02	0.04
SD - 2X-rep1 (sec)	0.18	0.22	0.19	0.28
~~~~~ - rep2 (sec)	0.14	0.11	0.14	1.04
~~~~~ - rep3 (sec)	0.11	0.06	0.10	0.30
SD - 3X-rep1 (sec)	0.10	0.02	0.27	0.34
~~~~~ - rep2 (sec)	0.04	0.04	0.50	0.30
~~~~~ - rep3 (sec)	0.05	0.03	0.33	0.47

Table 2 Each cell in the table represents the standard deviation for each condition computed by calculating the standard deviation of the peak-to-peak distances in a representative ROI from each condition. The biological repetitions are indicated by the rep number. The standard deviation is taken to represent beat irregularity in the monolayer cardiac beat patterns. The more regular the beat, the lower the standard deviation. The units are in beats/sec.

The next step is to determine the statistical significance of these data. In order to know whether the data observed are significantly different from each other or not, 2 two-factor **ANalysis Of VAriance (ANOVA)** tests were conducted, with one factor being confluency and the other being time. The first two-factor ANOVA was run to identify whether the different data points representing *beat rate* are statistically significant, and the second ANOVA was run to identify whether the different data points representing *beat irregularity* are statistically significant, corresponding to tables 1 and 2 respectively. The results are summarized in tables 3 and 4.

4.2 – Results: Effect of confluency and time on cardiac monolayers

Source of Variation	SS	df	MS	F	P-value	F crit
Days	2.38597063	3	0.795	13.061	0.000	3.009
Confluency	1.91723234	2	0.959	15.743	0.000	3.403
Interaction	1.59395388	6	0.266	4.363	0.004	2.508

Table 3 A Two factor ANOVA was conducted with one factor being time and the other confluency using the data in Table 1. p-values below 0.05 are colored in red. A p value <0.05 corresponding with the “Interaction” row can be interpreted to mean that the null hypothesis “the two co-factors do not depend on each other” is rejected. As the p-value for both days and confluency are less than 0.05, the null hypothesis “there is no difference among the days” is rejected, and the null hypothesis “there is no difference among the confluencies” is rejected.

Source of Variation	SS	df	MS	F	P-value	F crit
Days	0.50531609	3	0.168	6.221	0.003	3.009
Confluency	0.06341357	2	0.032	1.171	0.327	3.403
Interaction	0.23481235	6	0.039	1.445	0.239	2.508

Table 4 Using the data in table 2, a two factor ANOVA was conducted with one factor being time and the other confluency. P-values below 0.05 are colored in red. A p-value > 0.05 corresponding with the interaction row can be interpreted to mean that the null hypothesis “the two co-factors do not depend on each other” is rejected. The null hypothesis “there is no difference among the days” is rejected, but the null hypothesis “there is no difference among the confluencies” is not-rejected.

Once it was determined from the two-factor ANOVA tests that the populations do indeed differ in a statistically significant way overall, the next step was to run multiple single factor ANOVAs for each population. That is, for each day, the confluencies were compared and the different wells treated as repeat measures. This was done once for beat frequency and then once again for beat irregularity. The question that these tests answer is: what is the probability that the results would have been obtained, if the samples were from the same population. The results of the tests are summarized in table 5 below. P values less than 0.05 were judged as statistically significant and lead to a rejection of the null hypothesis that the data are obtained from the same sample. P values less than 0.05 are colored in red in the table below.

	between confluencies				between days		
	Day 1	Day 2	Day 3	Day 4	1X	2X	3X
beat frequency	0.338	0.000	0.006	0.117	0.039	0.002	0.008
SD	0.474	0.126	0.012	0.547	0.524	0.138	0.001

Table 5 Single Factor ANOVA summary. The table tests the null hypothesis “the results obtained were drawn from the same population”. In cases of a p value <0.05, colored in red in the above table, this null hypothesis is rejected. For example, a p value of 0.000 for Day 2 between confluencies should be interpreted as follows: the null hypothesis “all data gathered from the different confluency levels on day 2 and analyzed for beat frequency are from the same population” is rejected.

4.2 – Results: Effect of confluency and time on cardiac monolayers

The data for each ROI was then averaged with the other ROIs from the same sample and time point and organized in the table below, table 6. In this table, for confluency 2, all 4 wells were included in the calculation of the average. As each value now represents an average of averages (i.e. the beat rates are an average of the peak distances for each graph, and those values are then averaged to provide the values below for each table cell) a **Standard Error of the Mean (SEM)** could be calculated for each. The first table shows beat rate data and the second shows beat irregularity data, along with corresponding SEMs.

	Day 1	Day 2	Day 3	Day 4
Confluency 1X (sec)	1.80	1.27	1.69	0.99
Confluency 2X (sec)	1.45	0.88	0.96	0.72
Confluency 3X (sec)	1.35	1.77	1.03	0.85
SEM-CoN1X (sec)	0.32	0.08	0.06	0.09
SEM-CoN2X (sec)	0.08	0.12	0.23	0.16
SEM-CoN3X (sec)	0.13	0.07	0.21	0.11

Table 6 Using the data in table 1, for each confluency with 3 repetitions, the average of the repetitions and the standard deviation of the repetitions were calculated to compute an average beats/second value for each confluency and day. As the values in each cell are averages themselves, their standard deviation is referred to as Standard Error of the Mean (SEM) and reported in the bottom rows.

	Day 1	Day 2	Day 3	Day 4
Confluency 1X (sec)	0.14	0.10	0.06	0.26
Confluency 2X (sec)	0.11	0.12	0.11	0.53
Confluency 3X (sec)	0.06	0.03	0.37	0.37
SEM-CoN1X (sec)	0.08	0.00	0.05	0.16
SEM-CoN2X (sec)	0.03	0.04	0.03	0.18
SEM-CoN3X (sec)	0.02	0.01	0.07	0.05

Table 7 Using the data in table 2, for each confluency with 3 repetitions, the average of the repetitions and the standard deviation of the repetitions were calculated to compute an average standard deviation (beat irregularity) value for each confluency and day. As the values in each cell for the top 3 rows are averages themselves, their standard deviation is referred to as Standard Error of the Mean (SEM) and reported in the bottom rows.

Overall, it was shown that the averages were different for all conditions, however they were statistically significant in only some of the cases. These results show then that our RAP device can catch statistically significant data *when* such differences exist, and not indicate a difference when one does not exist. Using statistical terminology, our device lowers the probability of committing a type I and type II error which is explained further in the discussion section (section 5.1). The above tables can be summarized graphically as seen below.

4.2 – Results: Effect of confluency and time on cardiac monolayers

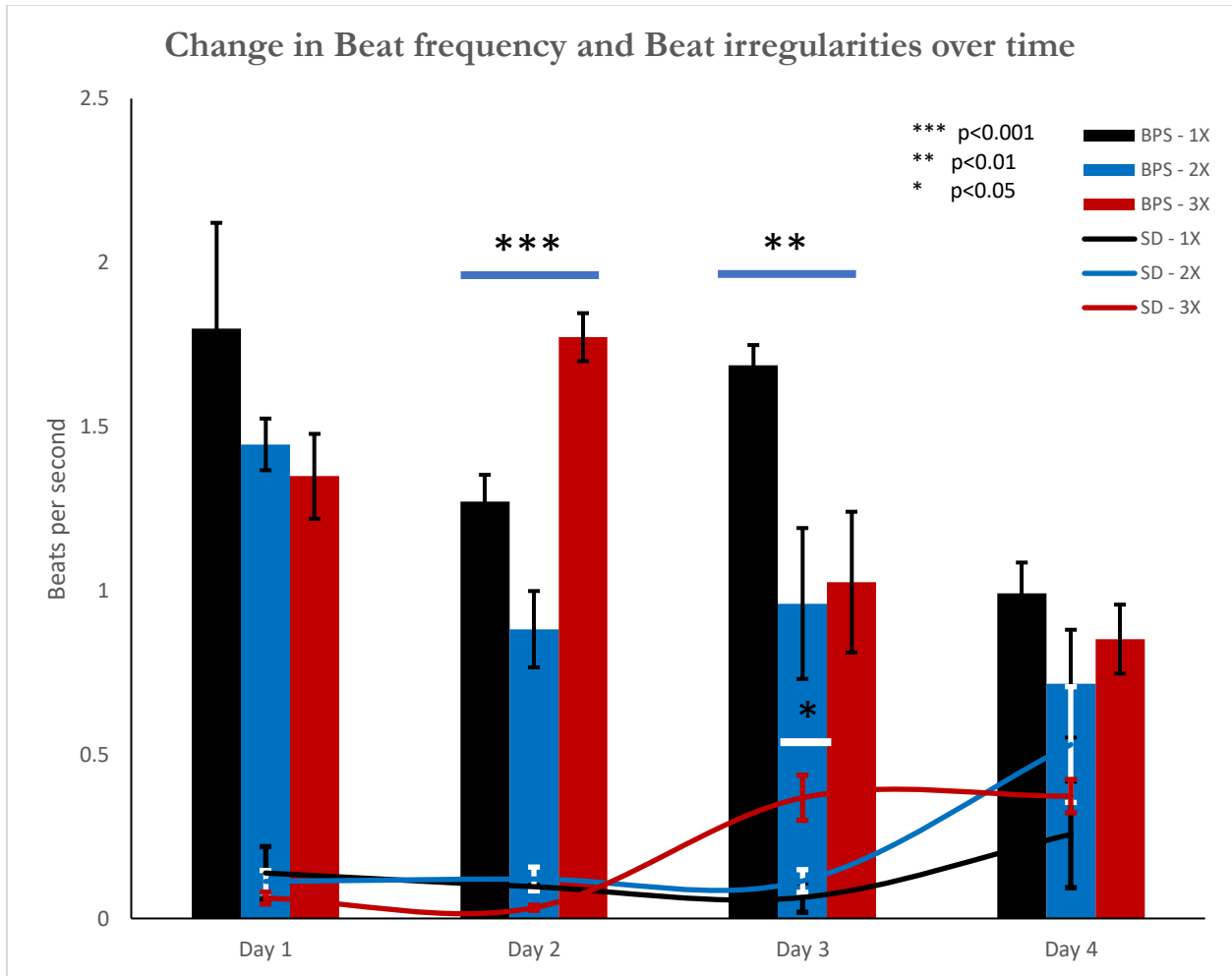


Figure 62 Collectively the above data can be summarized in a table like the one presented here. The data show that beat frequency (bars) and beat regularity (lines) change as a function of time, and change at different rates based on their confluency (black representing 1X, blue representing 2X, and red representing 3X). The asterisks show the level of statistical significance. Overall, this graph shows that RAP can provide a coherent data set to identify small differences over confluency and time when they exist, and only when they exist.

The above graph (Figure 62) shows the average beat frequency for different confluencies over 4 days as columns and the standard deviation of the distribution pertaining to the distance between each peak of the ROI graphs as lines. The standard deviation is a measure of how much, on average, a data point differs from the mean and is therefore taken to be a measure of beat irregularity. Each confluency is represented by a different color that is constant between lines and columns. Statistical significance is shown with asterisk above the lines and columns. It can be seen from the graph that there is a statistically significant difference between different confluency conditions on day 2 and day 3 but not day 1 and day 4. We can also see that there is a statistically significant difference between irregularities on day 3 but not any other day. This demonstrates the importance of being able to measure multiple confluences simultaneous and

4.2 – Results: Effect of confluency and time on cardiac monolayers

doing so over several days, so that small differences can be detected when they exist and only when they exist.

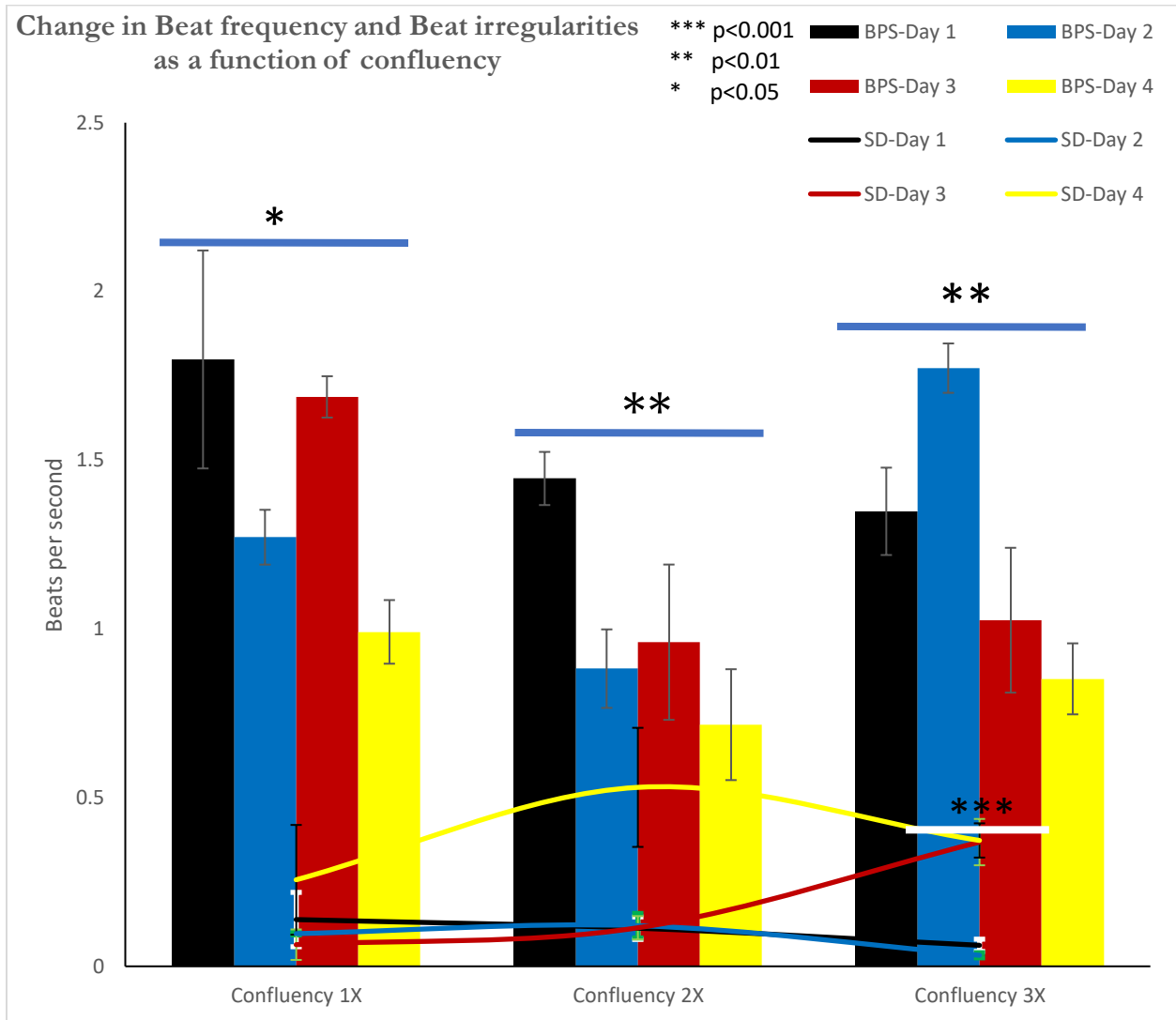


Figure 63 Similar to Figure 62, the data show that beat frequency (bars) and beat regularity (lines) change as a function of time, and confluency. This graph groups the data in a different way as compared to Figure 62 where different time points are grouped and represented by different colors. Black represents day 1, blue represents day 2, red represents day 3, and yellow represents day 4. The asterisks show the level of statistical significance. Overall, this graph shows that RAP can provide a coherent data set to identify small differences over confluency and time when they exist, and only when they exist.

The above graph (Figure 63) presents the same data as seen in Figure 62, but groups the days together instead of confluencies. In this graph, for each confluency, the data from each day is compared. We can see that for a given confluency, different beat rates are observed for different days and that these differences are statistically significant. However only confluency 3X shows a difference in beat irregularity across the 4 days. This again demonstrates the importance of being able to measure multiple confluences simultaneous and doing so over several days.

Chapter 5 – Discussion

The previous chapter showcased the results that RAP is capable of obtaining, both in terms of the resolving power using the static calibration slides, as well as its efficacy in a biological setting. This chapter will further elaborate on and discuss the obtained results, and further explain the significance of RAP with regards to the workflow of a good experimental design, statistical analysis, as well as pertinent physiological realities that are present in a typical experiment. The chapter will conclude with an exploration of current limitations and possible future directions.

5. Discussion

Collectively, the results show that with the presented novel design of RAP, it is possible to make statistically significant high-throughput dependent discoveries under physiological conditions without incurring exuberant costs. The results show that these statistically significant results can be measured even if the effect under study is small and rare. This was demonstrated by simultaneously imaging multiple cardiac monolayer samples, which present rare and randomly spread ectopic properties, over time inside an incubator and analyzing their beat frequency and beat irregularity. Statistically significant differences were observed both within various groups as well as between various groups. These results show the impact that the technique could have and the study of important biological questions that it can enable. In order to further elaborate on these capabilities, a brief overview of experimental and statistical concepts follow.

5.1 – Discussion: Experimental design, statistical analysis and reducing variabilities

5.1.1 - Introduction: The main goal of an experiment is to determine whether a certain manipulation has a specific effect. To achieve this goal, a population with a manipulation, called an **experimental group**, is compared to a population without the manipulation, called **control group**. In most of science, and particularly in biology, it is impractical to measure the entire population of interest. Instead, we use **samples** to estimate the **statistical parameters** of a population. Furthermore, as most biological processes are a consequence of many other processes, measurements almost always show **variability** no matter how tightly the experiment is controlled. In brief then, biological experiments aim to determine the effect of a specific manipulation on a population's **mean** and **variance** and use samples to estimate these parameters. Statistics and probabilities are used to calculate and analyze these means and variabilities. To understand these concepts deeper and how they relate to RAP, a more detailed explanation of experimental design, mean, variance, type I & II errors, statistical power, and sample size is required.

5.1.2 - Experimental design: A good experiment will be able to, with the most accuracy, determine the smallest effect of a manipulation. This is generally achieved by reducing variance

5.1 – Discussion: Experimental design, statistical analysis and reducing variabilities

and increasing **sample size**. To explain this further we should first have a clear definition of variance with regards to a biological experiment. **Variance** is a measure of the inherent variability between measured data and arises due to the random interaction of many processes that influence the certain measurement under study. Of the countless influential processes and factors that affect the process being measured, from genetic to environmental to circumstantial, some factors play a significantly more important role in controlling a specific outcome than others.¹

Another concept is the idea of a **lurking** or **confounding** variable. Lurking variables are variables that affect both the dependent and independent variables, that were not directly measured in the experiment.² Good studies identify the most pertinent of these lurking variables based on previous literature and control or randomize them based on the intentions of the study. The study then manipulates the levels of the **explanatory variable**, sometimes called the **independent variable** and measures the **response or dependent variable**. To control for all the other smaller and unidentified factors that might affect the response variable, a good experiment has a control group, where everything is similar to the treatment group as much as possible except for the factor under study. This does not reduce the variability, however, but rather allows us to use statistics to make stronger inferences from our results. The assumption is that, on average, the unaccounted variables will affect the control and treatment group to the same degree, and the differences between the treatment and control group can be more accurately attributed to the independent variable. A well-designed experiment then in summary controls for the greatest number of influential factors and has sufficient sample size to make an accurate conclusion.

5.1.3 - Type I and type II error: The usefulness of a statistical test is in reducing the probability of committing a type I and type II error. A **type I error** is the rejection of a true null hypothesis, and a **type II error** is the non-rejection of a false null hypothesis. The probability of a type I error

¹ This abstraction might become a little clearer with an example. Imagine a scientist is interested in measuring the effect of fat consumption on body weight. In determining the effect of eating 100 grams of fat on body weight, it is possible that the mood of the consumer a day after consumption will influence the weight gain. However the species, that is whether the consumer is a chimpanzee, a rat, an elephant or a human, will have a much larger impact. That is to say, some factors, like *species*, will be more influential than others, such as *mood a day after consumption*.

² Consider a study analyzing the effect of computer use time on blood pressure. Suppose also that the study finds that blood pressure and computer use time are positively correlated. It is possible however that anxiety can increase both computer use time and blood pressure. In this case, anxiety would be a lurking variable.

5.1 – Discussion: Experimental design, statistical analysis and reducing variabilities

is determined by **alpha** (α). Alpha is the highest probability of committing a type I error that the experimenter is willing to accept. Statistical tests that provide a p value provide the probability of the observed results being observed if the null hypothesis were true. The p value is then compared against alpha and accepted or rejected based on whether it is greater or less than alpha.

The probability of committing a type 2 error is β and is more difficult to calculate as each mean of the population and each sample size can have a different β . To calculate β , the distribution of the null hypothesis is compared against a sample population with a specific mean. Briefly, the strategy is to define a desired power and then calculate the sample size required for that specific power.

5.1.4 - Post experimental analysis: It is important to note, that a well-designed study will both make a test more powerful as well as provide a smaller p value with the post-hoc statistical tests. This will then enable scientists to identify smaller differences between the experimental and control groups with more certainty and identify small effects of a manipulation. These post-hoc analysis tests include tests such as the student's t-test that is used for comparing the difference between two populations or ANalysis OF VAriance (ANOVA) for more than two groups and the many more tests designed to provide the most accurate results for various experimental designs. Ideally any statistical test used appropriately on a good experimental design will lead to the same general conclusion. No statistical measurements can be sufficient however, in compensating for a poor experimental set up.

5.1.5 - Our device: How do these concepts apply to RAP? Let's consider our proof-of-concept experiment. Our proof-of-concept study investigates the relative effect of monolayer confluency and time on arrhythmias in cardiac monolayers. We studied three different concentrations 1X, 2X, and 3X. What is particularly important is that arrhythmias can take a long time to develop, taking hours or even days. Once developed however the process only takes a fraction of a second and its occurrence can be randomly distributed over time. The process should be studied under high speeds at prolonged periods of time so that these arrhythmias may be recorded.

Without the RAP system, in order for us to carry out such study, the best approach would have been by **passaging** the cell lines and when enough cells are available, putting the cell lines in

5.1 – Discussion: Experimental design, statistical analysis and reducing variabilities

multiple wells of a plate with the corresponding confluencies. The plate would then be placed under a high-throughput device capable of maintaining physiological conditions and imaged in sequence. This process would then be repeated automatically using the same automated high-throughput microscope where the robotics would be able to switch the samples in a few seconds.

This process would have worked well if the time scale of change were slower than the delay caused by the imaging process in regards to switching from one well to another, and with regards to the length of the time it takes to record one sample. That is to say, if the processes were indeed slow and evolved over weeks, differences of a few seconds would be negligible. In our case however, the change occurs at the scale of fractions of a second to a few seconds, where relatively fast cameras that can record at the millisecond exposure time can be used to study the dynamics of the change, that is, *how* does tissue confluency affect beat rate over time. In such a case a typical high-throughput microscope will be much more likely to miss pertinent biological activity. First because of the time it takes to move from one sample to the next and second because as each well is only imaged for a small fraction of the total time. For example, in a plate with 7 samples, each sample is being imaged less than 1/7th of the time, and the rest of the time is dedicated to either switching between samples or imaging other sample. An event such as the one seen in *Day 4- Confluency 2X – well 3* then, where a regular beat pattern is observed until suddenly there is a transition to a rapid rhythm at $t=6$ s, could have easily been missed if the microscopy system was busy imaging any of the other 6 samples. RAP solves this by imaging all the wells simultaneously.

If neither RAP nor a conventional high-throughput system were to be used, there would be three other primary options. The first is to employ the use of several high speed synchronized microscopes to study the effect of different concentrations on the same cell line and passage. This would introduce equipment and personnel variability, be very resource and cost intensive and thus very impractical. Alternatively, then, we would use different passages for each concentration and study them sequentially using the same optical setup. This would introduce variabilities as the passages, although similar, are not identical, as monolayer plating processes result in spatial heterogeneities that are difficult to control. As the third option the same passage but at a later time can be studied, which would introduce even greater variability since it has

5.1 – Discussion: Experimental design, statistical analysis and reducing variabilities

undergone significant physiological change such as changes in fibroblasts and gap junction expression.

And here is where the concepts described above with regards to experimental design and statistics become relevant. We assume that the distribution of cardiac beat patterns is normally distributed.⁹⁷ Cardiac monolayers that are displaying abnormal rhythms (e.g. re-entry) also produce normally distributed patterns, but with means and standard deviations that are shifted. The goal is to be able to distinguish these distributions from each other without committing a type I or type II error. In order to decrease the likelihood of committing these errors, the goal becomes to decrease the variance of the measurements, and effectively make the distributions with different means easier to distinguish. The main point is that the variance can only be decreased by increasing sample size and reducing biological and experimental variability. This is what the RAP system provides.

With all of the previously described non-RAP setups, the variabilities introduced would decrease the statistical power of the results. Accounting for these variabilities can only be addressed by increasing the number of samples. However in many standard setups, this can be a herculean task. As most animal cultures cannot be passaged enough times to satisfy the increase in sample number requirements, new cultures need to be started which further increase variability.

It should be noted that in labs with large budgets, commercial immortal cell lines can be used, which can support a larger number of passages, helping the situation but still the fundamental challenges remain. Our RAP system, by allowing multiple samples from the same culture and passage to be imaged simultaneously under the same conditions, significantly abates the variation in data and increases the sample number so that statistically significant and scientifically relevant information can be found even when the magnitude of the effect is small or the event is rare or short lived, such as re-entrant waves in cardiac monolayers. And because all the samples are recorded simultaneously, the probability of missing a short duration event is eliminated. Numerically, this reduction in variance and higher probability of recording these rare events is translated to a lower p level and is calculated by using statistical tests.

5.1 – Discussion: Experimental design, statistical analysis and reducing variabilities

In our case, once the data were collected at physiological conditions, they were analyzed using a two-way ANOVA with repeated measures, considering concentration as one factor and time as the other. For each day, different concentrations were treated as different groups, and 3 samples with the same concentration were considered the repeated measures. One factor ANOVAs followed to gain a finer understanding of the underlying data. The null hypothesis, as required by the statistical analysis, was that there is no difference in arrhythmia frequency between samples.

Taken together, the main benefit is that the device enables and increases our ability to control for more factors, cofactors and lurking variables, therefore decreasing variability, as well as allowing for more samples to be analyzed and consequently reducing the standard error and increasing the power of the test. The ability to image multiple samples simultaneously for extended periods of time inside an incubator and therefore decrease the variability that would inevitably be introduced by imaging different passages or the same passage at different time points sequentially. Thus the ability to make measurements in parallel is one of the greatest benefits of the device. This is particularly pertinent in cases where fast processes that develop over long periods of time, such as arrhythmias in cardiac monolayers, need to be studied and compared.

However there is one more benefit. The above scenarios describe the best possible case where money and resources are not an obstacle. The benefits of the RAP system become even more pronounced when compared to similarly priced devices, around \$25000 USD. A typical system that costs under \$25000 USD, would generally be a low throughput, manual setup device where a researcher would need to move and refocus the sample one by one and manually repeat the process for hours or even days, which essentially becomes impractical, and the between sample delay can increase up to minutes. It is not uncommon for even the most basic, low throughput commercial microscopes to cost as much or twice the cost of our presented setup. Furthermore, if a research team wanted to endeavor to build their own devices by following the instructions presented in this thesis, the complete set of components required can be purchased for under \$5000-\$6000 USD at the time of the writing of this thesis. If one had a limited budget then, and the need for high throughput microscopy, our setup is a serious choice that should be considered. This point is not emphasised to a large degree in this thesis however because this is a primarily scientific thesis and not a business or economical one.

5.2 – Discussion: The effect of concentration and time

Arrhythmic events in monolayer cultures are rare events in two ways: first, factors that lead to arrhythmia only lead to a change in the *probability* of arrhythmias and are not deterministic in nature. Second, in a sample that demonstrates arrhythmias, the duration of ectopic events can vary, and they can appear and disappear spontaneously and randomly and do so only infrequently. What this translates to, in addition to a need for greater sample numbers and reduced variability as discussed above, is a need for extended recoding periods. Without longer durations, rare abnormalities can easily be missed. This long duration recording is only possible as RAP can function inside an incubator so that the cells are imaged under physiological conditions. Overall, then, the results showed that the device was able to distinguish between different arrhythmia rates and regularity, between different confluency levels as well as between different time periods.

It is clear then that although the present study does not provide biological information that are truly novel, they do indeed demonstrate the capabilities of the RAP system to be applied to future experiments whose design pivots round a novel biological question. At this stage, the results of our experiment were designed to confirm the capabilities and relevance of the system for biological studies. One main example of where these capabilities can prove essential is cardiac drug discovery research. Using RAP, the effect of various compounds can be studied so that even a compound that slightly increases the probability of arrhythmias or a re-entrant wave, which can potentially be lethal, can be identified.

5.3 - Discussion: Other Designs and potentials

5.3.1 - Design and alternative versions: I have thus laid out the main concept for RAP, a new, cost efficient, high throughput microscopy system. It is natural though to ask, as I myself grappled with the concept myself: why this specific design? Why these specific components? Some design decisions have been made either based on accepted scientific facts; for example, that the parabolic dome will focus all parallel light at its focal point, thus placing the camera at the focal point to detect the light rays; or made through experimentations such as in deciding the distance of the LEDs from the sample; or in some cases based on the realities of the situations that it will be serving; such as the general common dimensions of a scientific incubator dictating the aspired overall size. For many of the less influential decisions however, in most cases, an alternate can work just as well, as long as the fundamental concept is not altered.

Furthermore, the main concept can be used as a template to apply this setup to other microscopy systems, according to the research requirements. As previously mentioned, some of the main components can be swapped out for other components that fit the needs of the experiment better. One example is the main camera that can be replaced with cameras that have higher frame rates or other desirable characteristics based on the needs of the experiment that it is serving.

5.3.2 - Future versions: We currently have several plans for the future versions of this device. The first goal is to connect the device to the internet so that experiments can be viewed live from anywhere in the world. The second goal is to make the device fully autonomous. Optically we aim to incorporate fluorescence microscopy into the system. Constant improvements such as making the device more robust, user friendly and making it easier to insert accessories in the light path are also noteworthy goals for future iterations of RAP.

5.3.3 - Other potentials: Cardiac rhythms are not the only benefactor of such a system. Many other applications such as studies in c-elegans worms, as shown in our paper ², and many drug screening methods, that benefit from continuous fast imaging of multiple samples can also benefit. In brief, scientifically, any scenario where the process under study can benefit from long duration and simultaneous recording of multiple samples, and where elimination of as many cofactors as possible and thus a reduction in data variance and a more tightly regulated

5.3 - Discussion: Other Designs and potentials

experiment is important, can benefit from the RAP system. Temporally, any situation that could benefit from processing more samples more quickly can benefit from the RAP system, and economically the device can be the most cost efficient choice in many situations.

5.4 Limitations

5.4.1 - General limitations for high-throughput microscopy: Generally, there are three main areas of challenge with regards to high-throughput microscopy: sample preparation, image acquisition, and storage and processing. Additionally, there is an economical aspect that is associated with the significant increase in the cost for a certain image quality. That is, any device that can image 100 samples at a specific resolution sequentially will be significantly more expensive than a device that can image only one sample at the same resolution and quality.⁹⁸

Imaging technologies have come a far way and become relatively good at taking amazingly detailed pictures. However the main challenge remains repeating the process rapidly and accurately. Several new problems then arise. The first is switching between samples, and once the next sample is in place, the challenge is reference matching. That is, if a system is cycling through a number of samples, once the loop is completed and the system is imaging the initial sample, now at a later time point, the optical axis needs to be exactly at that same place and image that exact region as it was when the previous image was captured, otherwise it would be difficult to compare the frames.¹⁰ This can be even more challenging with live cell imaging as the cells themselves move in addition to not being able to survive for long outside optimal conditions.¹⁰ Reference matching is a difficult problem to tackle, but even when addressed, the next challenge is repeating the process over and over again. The device should be reliable enough to run overnight without supervision, as well as making sure that the systems will operate evenly and reliably. An ideal system will be adaptable, produce consistent, reproduceable and reliable results, and have scalable throughput.⁹⁸

Once the image has been captured, the next major limitation is the storage and processing of the data that has been collected. High throughput systems generate a lot of data, and do so at high speeds. The data obtained then needs to be analyzed. In addition to the enormous speed and amount of data due to the imaging of many samples, there is also some added information that needs to be processed, primarily due to the unfiltered nature of the data compared to those with a human operator. In traditional microscopy of one sample, it is relatively easy to link the data obtained to the sample that it represents, as there is only one sample and that information is recorded by the scientist. In addition, a lot of lower quality images and data are omitted and not

5.4 Limitations

even initially recorded, mainly because a scientist is continuously judging the quality and usefulness of the sample and would only capture and save the most useful and in-focus image. This task becomes more challenging in an automated high-throughput system because the device should now be able to judge quality and focus and usefulness of the images, and in most cases, a human operator and scientist should eventually supervise the process.

5.4.2 - RAP specific limitations: RAP solves some of the problems burdening the average high throughput system, but continues to suffer from some of the other ones. Problems such as reference matching and reliability are significantly reduced as there are no moving parts to breakdown or introduce errors and the samples themselves do not move so they do not need to be referenced. However even without the need for reference matching or identifying and removing out of focus images, there is a significant amount of data to be processed and the challenges associated with producing large number of samples and processing large quantities of data are left to a large degree unabated.

Chapter 6 – The Business Side

The previous chapter expanded on the capabilities of RAP and why its existence is beneficial for science given the fundamental concepts of statistics, physiology, and scientific experimental design. Convinced of its advantages then, this section briefly explores the possibility of bringing this technology to more laboratories, by venturing into the business side and bringing RAP to market.

6. The business side

In addition to the novel characteristics of our system, the reduced cost of RAP will enable many brilliant scientists and researchers working in smaller labs to have access to such a technology. This is because although in addition to the novel characteristics discussed above, RAP also shares some important capabilities with other high throughput devices but at a fraction of the price. This includes being able to record multiple samples one at a time, or simply image cells with slower transition times. In those case it would be able to act similar to a conventional high-throughput device, but at a price that is orders of magnitude more affordable. Being a scientific lab, our goal was to ensure that as many people can have access to this technology as possible and the transfer of this device from our lab into the labs and companies that can benefit from it, was the primary goal for our venture into the business world.

6.1 - Gap in the market: In addition a large gap existing in both the scientific and industrial community for the novel capabilities of RAP thoroughly explained in this thesis, currently there are also either no high-throughput devices in the market at this price point or are significantly inferior in either image quality or throughput or both. Most high throughput devices run in the hundreds of thousands of dollars and are complex machines to own, maintain and operate. We thus see a gap in the market, particularly with smaller labs with lower budgets who need access to high throughput microscopy capabilities.

6.2 - Marketing: At the present we do not have any aims for a marketing campaign. Instead, we plan to approach companies that can benefit from this device and companies that might be able to help us bring the device to market. Examples of such companies are incubator companies who might be interested in offering incubators that can also image the cells inside, as well as microscopy companies such as Zeiss, and Edmond optics. We also plan to approach educational institutions who may benefit from RAP to familiarizing their students with high-throughput technologies, as the price can be within school budgets.

6.3 - Manufacturing and production: The prototype is a combination of sourced parts and custom designed and 3D printed parts. The steps and parts needed to build the device are outlines in this thesis and the files for the 3D printed parts are also available. PLA of any color with a printer

6. The business side

capable of at least 0.4mm fineness can be used to reproduce the parts. As such, although complex, building several RAP systems within our lab is currently possible. We will only approach mass manufacturers once we have a complete business plan ready.

6.4 - Patent: The device holds a US and Canada initial patent.

6.5 - Recommended price: The recommended price was set based on the cost of material with a reasonable profit margin given the benefits that it offers. The reasonable profit margin is judged to be 80%. As the cost of the material is approximately \$5000 USD, the price of the device commercially will be approximately $\frac{\$5000 \text{ USD}}{0.2} = \25000 USD .

7. Conclusion

In conclusion, in this thesis I outlined the need for a high throughput imaging technique that is not burdened by the inherent limitations of robotic moving parts and outlined the current imaging setups available in the microscopy world. I then introduced our novel Random Access Parallel (RAP) microscopy system, laid out its detailed design, followed by a proof-of-concept experiment demonstrating the capabilities of the device in a real biological setting. The data were then analyzed, and the importance of throughput, speed and a reduction in data variability explained both within a biological as well as a statistical context. A brief overview was mentioned regarding future prospects, including a potential venture into making the device commercially available. **Overall, then, my project contributed to science a new imaging tool that has the potential to enable numerous new discoveries, while being very accessible to many scientific labs.**

8. References

1. Antzelevitch C, Burashnikov AMMRLBSUNYUSA. Overview of Basic Mechanisms of Cardiac Arrhythmia. *Cardiac Electrophysiology Clinics*. 2011;3(1):23-45. doi:10.1016/j.ccep.2010.10.012
2. Ashraf M, Mohanan S, Sim BR, et al. Random access parallel microscopy. *Elife*. Jan 12 2021;10doi:10.7554/eLife.56426
3. Klimas A, Ambrosi CM, Yu J, Williams JC, Bien H, Entcheva E. OptoDyCE as an automated system for high-throughput all-optical dynamic cardiac electrophysiology. *Nature communications*. 2016;7:11542. doi:10.1038/ncomms11542
4. Yemini E, Jucikas T, Grundy LJ, Brown AE, Schafer WR. A database of *Caenorhabditis elegans* behavioral phenotypes. *Nat Methods*. Sep 2013;10(9):877-9. doi:10.1038/nmeth.2560
5. Likitlersuang J, Stephens G, Palanski K, Ryu WS. *C. elegans* tracking and behavioral measurement. *Journal of visualized experiments : JoVE*. 2012;(69):e4094-e4094. doi:10.3791/4094
6. Hansen A, Eder A, Bönstrup M, et al. Development of a Drug Screening Platform Based on Engineered Heart Tissue. *Circulation Research*. 2010;107(1):35-44. doi:10.1161/CIRCRESAHA.109.211458
7. Larsch J, Ventimiglia D, Bargmann CI, Albrecht DR. High-throughput imaging of neuronal activity in *Caenorhabditis elegans*. *Proceedings of the National Academy of Sciences*. 2013;110(45):E4266. doi:10.1073/pnas.1318325110
8. Taute KM, Gude S, Tans SJ, Shimizu TS. High-throughput 3D tracking of bacteria on a standard phase contrast microscope. *Nature Communications*. 2015/11/02 2015;6(1):8776. doi:10.1038/ncomms9776
9. Starkuviene V, Pepperkok R. The potential of high-content high-throughput microscopy in drug discovery. *British Journal of Pharmacology*. 2007;152(1):62-71. doi:10.1038/sj.bjp.0707346
10. Oheim M. Advances and challenges in high-throughput microscopy for live-cell subcellular imaging. *Expert Opin Drug Discov*. Dec 2011;6(12):1299-315. doi:10.1517/17460441.2011.637105
11. Bub G, Daniels MJ. Feasibility of Using Adjunctive Optogenetic Technologies in Cardiomyocyte Phenotyping – from the Single Cell to the Whole Heart. *Current Pharmaceutical Biotechnology: CPB*. 2020;21(9):752-764. doi:10.2174/1389201020666190405182251
12. Oheim M. High-throughput microscopy must re-invent the microscope rather than speed up its functions. *British Journal of Pharmacology*. 2007;152(1):1-4.

8. References

13. Atmanli A, Domian IJ. Recreating the Cardiac Microenvironment in Pluripotent Stem Cell Models of Human Physiology and Disease. *Trends in Cell Biology*. 2017;27(5):352-364. doi:10.1016/j.tcb.2016.11.010
14. Stoppel WL, Kaplan DL, Black LD, 3rd. Electrical and mechanical stimulation of cardiac cells and tissue constructs. *Advanced drug delivery reviews*. 2016;96:135-55. doi:10.1016/j.addr.2015.07.009
15. Katz AM. *Physiology of the heart*. 4th ed. ed. Lippincott Williams & Wilkins; 2006.
16. Garg P, Garg V, Shrestha R, Sanguinetti MC, Kamp TJ, Wu JC. Human Induced Pluripotent Stem Cell-Derived Cardiomyocytes as Models for Cardiac Channelopathies: A Primer for Non-Electrophysiologists. *Circulation research*. 2018;123(2):224-243. doi:10.1161/CIRCRESAHA.118.311209
17. Roden DM, Balser JR, George Jr AL, Anderson ME. Cardiac Ion Channels. *Annual Review of Physiology*. 2002;64(1):431-475. doi:10.1146/annurev.physiol.64.083101.145105
18. Cui J, Kaandorp JA, Sloot PMA, Lloyd CM, Filatov MV. Calcium homeostasis and signaling in yeast cells and cardiac myocytes. *FEMS Yeast Research*. 2009;9(8):1137-1147. doi:10.1111/j.1567-1364.2009.00552.x
19. Shiferaw Y. Nonlinear onset of calcium wave propagation in cardiac cells. *Physical review E*. 2016;94(3-1):032405.
20. Musunuru K, Domian IJ, Chien KR. Stem Cell Models of Cardiac Development and Disease. *Annual Review of Cell and Developmental Biology*. 2010;26(1):667-687. doi:10.1146/annurev-cellbio-100109-103948
21. Rohr S. Role of gap junctions in the propagation of the cardiac action potential. *Cardiovascular research*. 2004;62(2):309-22.
22. Hou Y, Zhou Q, Po SSHRI, Section of Cardiovascular Diseases UoOHSCOCO. Neuromodulation for cardiac arrhythmia. *Heart Rhythm*. 2016;13(2):584-592. doi:10.1016/j.hrthm.2015.10.001
23. Wu P, Vaseghi M. The autonomic nervous system and ventricular arrhythmias in myocardial infarction and heart failure. *Pacing and Clinical Electrophysiology*. 2020;43(2):172-180. doi:10.1111/pace.13856
24. Laksman Z, Wauchop M, Lin E, et al. Modeling Atrial Fibrillation using Human Embryonic Stem Cell-Derived Atrial Tissue. *Sci Rep*. Jul 13 2017;7(1):5268. doi:10.1038/s41598-017-05652-y
25. Burton RAB, Tomek J, Ambrosi CM, et al. Optical interrogation of sympathetic neuronal effects on macroscopic cardiac monolayer dynamics. *bioRxiv*. 2019:717991. doi:10.1101/717991

8. References

26. Ashton JL, Burton RAB, Bub G, Smaill BH, Montgomery JM. Synaptic Plasticity in Cardiac Innervation and Its Potential Role in Atrial Fibrillation. Mini Review. *Frontiers in Physiology*. 2018-March-20 2018;9(240)doi:10.3389/fphys.2018.00240
27. Kohl P, Sachs F. Mechanoelectric Feedback in Cardiac Cells. *Philosophical Transactions: Mathematical, Physical and Engineering Sciences*. 2001;359(1783):1173-1185.
28. Debbi L, Drori S, Tzlil S. The Influence of the Timing of Cyclic Load Application on Cardiac Cell Contraction. *Frontiers in physiology*. 2018;9:917. doi:10.3389/fphys.2018.00917
29. Hiroshi K, Masayuki K, Mako O, et al. The effects of mechanical stress on the growth, differentiation, and paracrine factor production of cardiac stem cells. *PLoS ONE*. 2011;6(12). doi:10.1371/journal.pone.0028890
30. Chiung-Zuan C, Bao-Wei W, Kou-Gi S. Effects of cyclic stretch on the molecular regulation of myocardin in rat aortic vascular smooth muscle cells. *Journal of Biomedical Science*. 2013;20(1):50. doi:10.1186/1423-0127-20-50
31. Fu D-g. Cardiac Arrhythmias: Diagnosis, Symptoms, and Treatments. *Cell Biochemistry and Biophysics*. 2015;73(2):291-296. doi:10.1007/s12013-015-0626-4
32. Jonsson MK, Wang QD, Becker B. Impedance-based detection of beating rhythm and proarrhythmic effects of compounds on stem cell-derived cardiomyocytes. *Assay and drug development technologies*. 2011;9(6):589-99. doi:10.1089/adt.2011.0396
33. Osadchii OE. Role of abnormal repolarization in the mechanism of cardiac arrhythmia. *Acta Physiol (Oxf)*. Jul 2017;220 Suppl 712:1-71. doi:10.1111/apha.12902
34. Sidhu S, Marine JE. Evaluating and managing bradycardia. *Trends Cardiovasc Med*. Jul 2020;30(5):265-272. doi:10.1016/j.tcm.2019.07.001
35. van Gorp PRR, Trines SA, Pijnappels DA, de Vries AAF. Multicellular In vitro Models of Cardiac Arrhythmias: Focus on Atrial Fibrillation. *Front Cardiovasc Med*. 2020;7:43. doi:10.3389/fcvm.2020.00043
36. Monnerat G, Alarcon ML, Vasconcellos LR, et al. Macrophage-dependent IL-1beta production induces cardiac arrhythmias in diabetic mice. *Nat Commun*. Nov 24 2016;7:13344. doi:10.1038/ncomms13344
37. Sher AA, Wang K, Wathen A, et al. A local sensitivity analysis method for developing biological models with identifiable parameters: Application to cardiac ionic channel modelling. *Future Generation Computer Systems*. 2013;29(2):591-598. doi:10.1016/j.future.2011.09.006
38. Jonsson MKB, van Veen TAB, Goumans M-J, Vos MA, Duker Gr, Sartipy P. Improvement of cardiac efficacy and safety models in drug discovery by the use of stem cell-derived cardiomyocytes. *Expert Opinion on Drug Discovery*. 2009;4(4):357-372. doi:10.1517/17460440902794912

8. References

39. Davis RP, van den Berg CW, Casini S, Braam SR, Mummery CL. Pluripotent stem cell models of cardiac disease and their implication for drug discovery and development. *Trends in molecular medicine*. 2011;17(9):475-84. doi:10.1016/j.molmed.2011.05.001
40. Ziegler T, Hinkel R, Kupatt C. Induced pluripotent stem cell derived cardiac models: effects of Thymosin β 4. *Expert Opinion on Biological Therapy*. 2018;18(sup1):111-120. doi:10.1080/14712598.2018.1473370
41. White SM, Constantin PE, Claycomb WC. Cardiac physiology at the cellular level: use of cultured HL-1 cardiomyocytes for studies of cardiac muscle cell structure and function. *American journal of physiology Heart and circulatory physiology*. 2004;286(3):823-9.
42. Tsao CJ, Taraballi F, Pandolfi L, et al. Controlled Release of Small Molecules for Cardiac Differentiation of Pluripotent Stem Cells. *Tissue engineering Part A*. 2018;24(23-24):1798-1807. doi:10.1089/ten.TEA.2018.0054
43. Bartosh TJ, Wang Z, Rosales AA, Dimitrijevic SD, Roque RS. 3D-model of adult cardiac stem cells promotes cardiac differentiation and resistance to oxidative stress. *J Cell Biochem*. Oct 1 2008;105(2):612-23. doi:10.1002/jcb.21862
44. Zuppinger C. 3D Cardiac Cell Culture: A Critical Review of Current Technologies and Applications. *Frontiers in Cardiovascular Medicine*. 2019;6doi:10.3389/fcvm.2019.00087
45. Entcheva E, Bub G. All-optical control of cardiac excitation: combined high-resolution optogenetic actuation and optical mapping. *The Journal of physiology*. 2016;594(9):2503-10. doi:10.1113/JP271559
46. Gunkel M, Flottmann B, Heilemann M, Reymann J, Erfle H. Integrated and correlative high-throughput and super-resolution microscopy. *Histochem Cell Biol*. Jun 2014;141(6):597-603. doi:10.1007/s00418-014-1209-y
47. Waters JC, Wittmann T. Concepts in quantitative fluorescence microscopy. *Quantitative Imaging in Cell Biology*. 2014;123:1-18. doi:10.1016/B978-0-12-420138-5.00001-X
48. Yildiz A, Vale RD. Total Internal Reflection Fluorescence Microscopy. *Cold Spring Harbor protocols*. 2015;2015(9):pdb.top086348. doi:10.1101/pdb.top086348
49. Axelrod D. Chapter 7 Total Internal Reflection Fluorescence Microscopy. *Methods in Cell Biology*. Academic Press; 2008:169-221.
50. Coucheron DA, Helle ØI, Øie CI, Dullo FT, Ahluwalia BS. Chip-based nanoscopy: towards integration and high-throughput imaging. International Society for Optics and Photonics; 2017:103500W.
51. Streets AM, Li A, Chen T, Huang Y. Imaging without fluorescence: nonlinear optical microscopy for quantitative cellular imaging. *Analytical chemistry*. 2014;86(17):8506-13. doi:10.1021/ac5013706

8. References

52. So PT, Yew EY, Rowlands C. High-throughput nonlinear optical microscopy. *Biophysical journal*. 2013;105(12):2641-54. doi:10.1016/j.bpj.2013.08.051
53. Helmchen F, Denk W. Deep tissue two-photon microscopy. *Nature Methods*. 2005/12/01 2005;2(12):932-940. doi:10.1038/nmeth818
54. Sanderson MJ, Smith I, Parker I, Bootman MD. Fluorescence Microscopy. *Cold Spring Harbor protocols*. 2014;2014(10):pdb.top071795. doi:10.1101/pdb.top071795
55. Lakowicz JR, Gryczynski I, Gryczynski Z. High Throughput Screening with Multiphoton Excitation. *Journal of Biomolecular Screening*. 1999;4(6):355-361. doi:10.1177/108705719900400610
56. Escobet-Montalbán A, Gasparoli FM, Nylk J, Liu P, Yang Z, Dholakia K. Three-photon light-sheet fluorescence microscopy. *Optics letters*. 2018;43(21):5484-5487. doi:10.1364/OL.43.005484
57. Cutrona MB, Simpson JC. A High-Throughput Automated Confocal Microscopy Platform for Quantitative Phenotyping of Nanoparticle Uptake and Transport in Spheroids. *Small*. 2019;15(37):1902033. doi:<https://doi.org/10.1002/sml.201902033>
58. Thorn K. A quick guide to light microscopy in cell biology. *Molecular Biology of the Cell*. 2016;27(2):219-222. doi:10.1091/mbc.e15-02-0088
59. Zemanová L, Schenk A, Valler MJ, Nienhaus GU, Heilker R. Confocal optics microscopy for biochemical and cellular high-throughput screening. *Drug Discovery Today*. 2003/12/01/ 2003;8(23):1085-1093. doi:[https://doi.org/10.1016/S1359-6446\(03\)02833-2](https://doi.org/10.1016/S1359-6446(03)02833-2)
60. Krmpot AJ, Nikolić SN, Oasa S, et al. Functional Fluorescence Microscopy Imaging: Quantitative Scanning-Free Confocal Fluorescence Microscopy for the Characterization of Fast Dynamic Processes in Live Cells. *Analytical chemistry*. 2019;91(17):11129-11137. doi:10.1021/acs.analchem.9b01813
61. Koike-Tani M, Tani T, Mehta SB, Verma A, Oldenbourg R. Polarized Light Microscopy in Reproductive and Developmental Biology. *Molecular reproduction and development*. 2015;82(7-8):548-562. doi:10.1002/mrd.22221
62. Sugano K, Kato T, Suzuki K, Keiko K, Sujaku T, Mano T. High throughput solubility measurement with automated polarized light microscopy analysis. *Journal of Pharmaceutical Sciences*. 2006;95(10):2115-2122. doi:<https://doi.org/10.1002/jps.20628>
63. Jiang W, Yin Z. Seeing the invisible in differential interference contrast microscopy images. *Med Image Anal*. Dec 2016;34:65-81. doi:10.1016/j.media.2016.04.010
64. Ku Y-s, Shyu D-M, Lin Y-S, Cho C-H. Infrared differential interference contrast microscopy for 3D interconnect overlay metrology. *Optics Express*. 2013/08/12 2013;21(16):18884-18898. doi:10.1364/OE.21.018884

8. References

65. Scientifica. A guide to Differential Interference Contrast (DIC). Company Website. Scientifica. Accessed April 25/2021, 2021. <https://www.scientifica.uk.com/learning-zone/differential-interference-contrast>
66. Piper T, Piper J. Variable multimodal light microscopy with interference contrast and phase contrast; dark or bright field. *Journal of Microscopy*. 2014;255(1):30-41. doi:10.1111/jmi.12134
67. Strasser F, Offtenderinger M, Piestun R, Jesacher A. Spectral image scanning microscopy. *Biomedical Optics Express*. 2019/05/01 2019;10(5):2513-2527. doi:10.1364/BOE.10.002513
68. Cardoso MC. Fluorescence Microscopy: Spectral Imaging vs. Filter-based Imaging. *Encyclopedic Reference of Genomics and Proteomics in Molecular Medicine*. Springer Berlin Heidelberg; 2006:583-586.
69. Farkas DL. Spectral Microscopy for Quantitative Cell and Tissue Imaging. In: Periasamy A, ed. *Methods in Cellular Imaging*. Springer New York; 2001:345-361.
70. Zimmermann T, Rietdorf J, Pepperkok R. Spectral imaging and its applications in live cell microscopy. *FEBS Letters*. 2003/07/03/ 2003;546(1):87-92. doi:[https://doi.org/10.1016/S0014-5793\(03\)00521-0](https://doi.org/10.1016/S0014-5793(03)00521-0)
71. Xiao L, He Y, Yeung ES. High Throughput Single Molecule Spectral Imaging of Photoactivated Luminescent Silver Clusters on Silver Island Films. *The Journal of Physical Chemistry C*. 2009/04/16 2009;113(15):5991-5997. doi:10.1021/jp8102904
72. Periasamy A. Advanced light microscopy. *Methods (San Diego, Calif)*. 2014;66(2):121-3. doi:10.1016/j.ymeth.2014.03.011
73. Weber M, Mickoleit M, Huisken J. Chapter 11 - Light sheet microscopy. In: Waters JC, Wittman T, eds. *Methods in Cell Biology*. Academic Press; 2014:193-215.
74. Elisa Z, Toon B, De Smedt SC, Katrien R, Kristiaan N, Kevin B. Technical implementations of light sheet microscopy. *Microscopy Research and Technique*. 2018;81(9):941-958. doi:<https://doi.org/10.1002/jemt.22981>
75. Santi PA. Light Sheet Fluorescence Microscopy:A Review. *Journal of Histochemistry & Cytochemistry*. 2011;59(2):129-138. doi:10.1369/0022155410394857
76. Schaufele F. Maximizing the quantitative accuracy and reproducibility of Förster resonance energy transfer measurement for screening by high throughput widefield microscopy. *Methods (San Diego, Calif)*. 2014;66(2):188-99. doi:10.1016/j.ymeth.2013.07.040
77. Jares-Erijman EA, Jovin TM. Imaging molecular interactions in living cells by FRET microscopy. *Current Opinion in Chemical Biology*. 2006/10/01/ 2006;10(5):409-416. doi:<https://doi.org/10.1016/j.cbpa.2006.08.021>

8. References

78. Li M, Chen X, Ye Q-Z, Vogt A, Yin X-M. A high-throughput FRET-based assay for determination of Atg4 activity. *Autophagy*. 2012;8(3):401-412.
79. Song Y, Madahar V, Liao J. Development of FRET assay into quantitative and high-throughput screening technology platforms for protein–protein interactions. *Annals of biomedical engineering*. 2011;39(4):1224-1234.
80. Banoth E, Jagannadh VK, Gorthi SS. Single-Cell Optical Absorbance Characterization With High-Throughput Microfluidic Microscopy. *IEEE Journal of Selected Topics in Quantum Electronics*. 2016;22(3)doi:10.1109/JSTQE.2015.2414912
81. Su T-W, Xue L, Ozcan A. High-throughput lensfree 3D tracking of human sperms reveals rare statistics of helical trajectories. *Proceedings of the National Academy of Sciences of the United States of America*. 2012;109(40):16018-16022.
82. Jahan-Tigh RR, Chinn GM, Rapini RP. A Comparative Study Between Smartphone-Based Microscopy and Conventional Light Microscopy in 1021 Dermatopathology Specimens. *Archives of pathology & laboratory medicine*. 2016;140(1):86-90. doi:10.5858/arpa.2014-0593-OA.s1
83. Sala F, Castriotta M, Paiè P, et al. High-throughput 3D imaging of single cells with light-sheet fluorescence microscopy on chip. *Biomedical Optics Express*. 2020/08/01 2020;11(8):4397-4407. doi:10.1364/BOE.393892
84. Ji N. Adaptive optical fluorescence microscopy. *Nature methods*. 2017;14(4):374-380. doi:10.1038/nmeth.4218
85. Ishmukhametov RR, Russell AN, Wheeler RJ, Nord AL, Berry RM. A Simple low-cost device enables four epi-illumination techniques on standard light microscopes. *Scientific Reports*. 2016;6(1)doi:10.1038/srep20729
86. Singh S, Bray MA, Jones TR, Carpenter AE. Pipeline for illumination correction of images for high-throughput microscopy. *Journal of Microscopy*. 2014;256(3):231-236. doi:10.1111/jmi.12178
87. Zhang F, Hancock ER. Graph spectral image smoothing using the heat kernel. *Pattern Recognition*. 2008/11/01/ 2008;41(11):3328-3342. doi:<https://doi.org/10.1016/j.patcog.2008.05.007>
88. Gupta G. Algorithm for image processing using improved median filter and comparison of mean, median and improved median filter. *International Journal of Soft Computing and Engineering*. 2011;1(5):304-311.
89. Portes de Albuquerque M, Esquef IA, Gesualdi Mello AR, Portes de Albuquerque M. Image thresholding using Tsallis entropy. *Pattern Recognition Letters*. 2004/07/02/ 2004;25(9):1059-1065. doi:<https://doi.org/10.1016/j.patrec.2004.03.003>

8. References

90. Riccio D, Brancati N, Frucci M, Gragnaniello D. A New Unsupervised Approach for Segmenting and Counting Cells in High-Throughput Microscopy Image Sets. *IEEE journal of biomedical and health informatics*. 2019;23(1):437-448. doi:10.1109/JBHI.2018.2817485
91. Farooq H, Skinner-Ramos S, Algasham H, Bernussi AA, Grave de Peralta L. Scanning diffracted-light microscopy. *Applied Optics*. 2018;57(25):7329. doi:10.1364/AO.57.007329
92. Plonka G, Potts D, Steidl G, Tasche M. *Numerical Fourier Analysis*. Springer; 2018.
93. Oldenbourg R, Shribak M. Microscopes. 2010:28.1-28.62.
94. Ehler E, Moore-Morris T, Lange S. Isolation and culture of neonatal mouse cardiomyocytes. *Journal of visualized experiments : JoVE*. 2013;(79):50154. doi:10.3791/50154
95. Burton RA, Klimas A, Ambrosi CM, et al. Optical control of excitation waves in cardiac tissue. *Nature photonics*. 2015;9(12):813-816.
96. Napolitano C, Priori SG, Schwartz PJ. Torsade de Pointes. *Drugs*. 1994/01/01 1994;47(1):51-65. doi:10.2165/00003495-199447010-00004
97. Wilders R, Jongsma HJ. Beating irregularity of single pacemaker cells isolated from the rabbit sinoatrial node. *Biophysical Journal*. 1993/12/01/ 1993;65(6):2601-2613. doi:[https://doi.org/10.1016/S0006-3495\(93\)81289-X](https://doi.org/10.1016/S0006-3495(93)81289-X)
98. Vaisberg EA, Lenzi D, Hansen RL, Keon BH, Finer JT. An infrastructure for high-throughput microscopy: instrumentation, informatics, and integration. *Methods Enzymol*. 2006;414:484-512. doi:10.1016/S0076-6879(06)14026-4